Behaviour and design of direct-formed hollow structural section members

by

Kamran Tayyebi

Master of Science, Sharif University of Technology, 2014

A Dissertation Submitted in Partial Fulfillment of the Requirements for the Degree of

DOCTOR OF PHILOSOPHY

in the Department of Civil Engineering

Behaviour and design of direct-formed hollow structural section members

by

Kamran Tayyebi
Master of Science, Sharif University of Technology, 2014

Supervisory Committee

Dr. Min Sun, Supervisor
(Department of Civil Engineering)

Dr. Cheng Lin, Departmental Member
(Department of Civil Engineering)

Dr. Kian Karimi, Outside Member
(Department of Civil Engineering, British Columbia Institute of Technology)

Abstract

In North America, cold-formed square and rectangular hollow sections (collectively referred to as RHS hereinafter) of commonly specified cross-sectional dimensions are produced using either the indirect-forming approach or the direct-forming approach. The indirect-forming approach, as the conventional approach of the two, consists of three steps: (i) roll-forming the coil material progressively into a circular hollow section; (ii) closing the section using electric resistance welding (ERW); and (iii) reshaping the circular section into the final square or rectangular shape. On the other hand, the direct-forming approach, as the new approach of the two, roll-forms the coil material directly into the final square or rectangular shape.

RHS with similar cross-sectional dimensions but different production histories (i.e., different cold-forming approaches and post-production treatments) are expected to have significantly different material and residual stress properties. However, RHS design provisions in the existing North American steel design standards (AISC 360-16 and CSA S16-19) are in general developed based on research on indirect-formed RHS and currently do not differentiate RHS cold-formed by different approaches. Based on the research presented in Chapter 1 of this thesis, comparing to indirect-formed RHS, direct-formed RHS in general contain lower levels of residual stresses around cross sections, since the flat faces are not severely cold worked during production. This in turn affects member behaviours under compressive and flexural loadings. The test results presented in Chapters 2 and 4 show that direct-formed RHS have superior stub column and beam behaviours, comparing to their indirect-formed counterparts. In particular, the stub column and beam testing programs, covering a wide range of cross-section dimensions and two strength grades (nominal yield stresses of 350 and 690 MPa), show that the slenderness limits in the existing North American steel design standards are excessively conservative for direct-formed RHS, resulting in unnecessary penalty and member strength underestimation. As a result, the existing design formulae are not suitable for direct-formed RHS. In response to this, subsequent finite element (FE) parametric investigations are performed and presented in Chapters 3 and 5. Modified stub column and beam design recommendations for direct-formed regular- and high-strength RHS are proposed.

The effects of post-cold-forming hot-dip galvanizing on material properties, residual stresses, stub column behaviours and beam behaviours of direct-formed regular- and high-strength RHS are also studied in Chapters 1-5 of this thesis. Similar to the application of the heat treatment per ASTM A1085 Supplement S1 or the Class H finish per CSA G40.20/G40.21, post-cold-forming galvanizing improves the stub column (Chapter 2) and beam (Chapter 4) behaviours of direct-formed RHS via effective reduction of residual stresses (Chapter 1). Based on subsequent FE parametric investigations, modified stub column and beam design recommendations catering to galvanized direct-formed RHS are proposed in Chapters 3 and 5.

Contents

List of Tables

List of Figures

List of Publications

This thesis is based on the following published or under review manuscripts:

i. Kamran Tayyebi, Min Sun, Kian Karimi, Residual stresses of heat-treated and hot-dip galvanized RHS cold-formed by different methods, J. Constr. Steel Res. 169 (2020) 106071. https://doi.org/10.1016/j.jcsr.2020.106071.

ii. Kamran Tayyebi, Min Sun, Stub column behaviour of heat-treated and galvanized RHS manufactured by different methods, J. Constr. Steel Res. 166 (2020) 105910. https://doi.org/10.1016/j.jcsr.2019.105910.

iii. Kamran Tayyebi, Min Sun, Design of direct-formed square and rectangular hollow section stub columns, J. Constr. Steel Res. 178 (2021) 106499. https://doi.org/https://doi.org/10.1016/j.jcsr.2020.106499.

iv. Kamran Tayyebi, Min Sun, Kian Karimi, Ray Daxon, Brandon Rossi, Experimental investigation of direct-formed square and rectangular hollow section beams, J. Constr. Steel Res. (2021) (under review).

v. Kamran Tayyebi, Min Sun, Kian Karimi, Ray Daxon, Brandon Rossi, Design of direct-formed square and rectangular hollow section beams, Eng. Struct. (2021) (under review).

Acknowledgements

First and foremost, I would like to express my special gratitude to my supervisor, Dr. Min Sun, for his consistent support and guidance throughout this research project. I am extremely grateful for your patience and positive encouragements during the course of my PhD degree.

I would also like to sincerely thank my supervisory committee members: Dr. Kian Karimi, for his invaluable technical inputs and for making the arrangements for me to use the structures laboratory at BCIT, and Dr. Cheng Lin for his insightful comments and suggestions.

My appreciation extends to Dr. Armando Tura (Laboratory Supervisor) and Geoff Burton (Laboratory Technologist) from the University of Victoria, and Ray Daxon (Assistant Instructor) and Brandon Rossi from BCIT, whose assistance in carrying out the experimental tests was most helpful.

This research would not have been possible without the financial support of the University of Victoria, the Natural Sciences and Engineering Research Council of Canada (NSERC), the Canadian Institute of Steel Construction (CISC), the British Columbia Institute of Technology (BCIT) and the Mathematics of Information Technology and Complex Systems (MITACS). Appreciation is extended to Bull Moose Tube, Silver City Galvanizing, McAllister Industries, and Park Derochie for their donation of material and service.

Finally, I would like to profusely thank my sister, Helaleh, and all my friends and colleagues for their endless support and encouragements.

Dedication

This dissertation is dedicated to the memory of my beloved parents, Hengameh and Ahmad

Chapter 1: Residual Stresses of Heat-Treated and Hot-Dip Galvanized RHS Cold-Formed by Different Methods

Kamran Tayyebi, Min Sun, Kian Karimi, *Residual stresses of heat-treated and hot-dip galvanized RHS cold-formed by different methods*, J. Constr. Steel Res. 169 (2020) 106071. https://doi.org/10.1016/j.jcsr.2020.106071.

1.1 Abstract

Rectangular hollow sections (RHS) are produced in diverse locations internationally to various specifications, predominantly by cold-forming. RHS cold-formed by different techniques have different material and residual stress properties. Hot-dip galvanizing and heat treatment are commonly applied post-cold-forming processes. A comprehensive literature review showed that dedicated research on the effects of these processes on the performances of tubular steel members and connections is insufficient. Also, there is no definitive published guidance on this topic from structural steel associations. In particular, further research on the effects of heat treatment at various temperatures for various durations is needed to ensure a fit-for-purpose process (e.g. improvement of compressive member behaviour) which consumes less energy. This paper reports a comprehensive experimental investigation on the residual stress properties of 26 RHS specimens with different grades (nominal yield strengths from 350 to 690 MPa), cold-formed by different techniques, and subsequently subjected to post-production galvanizing and heat treatments to different degrees.

1.2 Introduction

According to a complimentary literature review [1], to this day the implications of using Hollow Structural Section (HSS) materials manufactured by different techniques and subsequently subjected to different post-production processes are not fully appreciated. In particular, further research is needed on the effects of post-production hot-dip galvanizing and heat treatment to different degrees on HSS material [2,3]. This research covers Rectangular Hollow Sections (RHS) cold-formed by two predominant methods.

Hot-dip galvanizing is an efficient method for a reliable protection against corrosion that might affect the service lives of the steel structures. Due to the advantages in structural and economic aspects, galvanized trusses made of hollow sections are being increasingly used in exposed steel structures. Permanent or temporary building solutions are available for a wide range of sectors including aviation, industrial, marine, offshore, oil and gas, as well as sports (see Fig. 1.1 for examples). Based on experimental testing of a limited number of galvanized and ungalvanized hollow section members under axial compression [4–6], it was speculated that for cold-formed HSS, the hot-dip galvanizing process may sometimes effectively reduce the overall level of residual stress contained in the cross section, similar to a heat treatment process described in ASTM A1085 Supplement S1 [7] and CSA G40.20/G40.21 [8]. It should be noted that the intention of the latter is to partially relieve the residual stresses in steel members to improve the compressive member behaviours. This type of heat treatment is typically conducted at a temperature of 450 ºC or higher for a 30-minute holding time, followed by cooling in air. On the other hand, the hot-dipping process of steel members (of commonly specified sizes) in a molten zinc bath (typically maintained at a temperature of 450 ºC) only takes approximately 10 minutes [1,2]. Hence, the fit-for-purpose heat treatment duration (for a partial release of residual stress and improvement of compressive member behaviour) needs to be revisited, via a comprehensive residual stress measurement on hollow sections with different production histories.

(a) Aviation

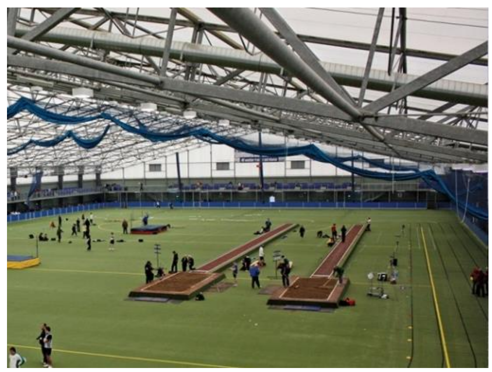

(b) Sports

(c) Transportation

(d) Parking

Figure 1.1 Galvanized tubular steel structures

In North America, RHS materials are predominantly cold-formed by two methods: indirect-forming and direct-forming. RHS materials produced by the two methods can have the same appearances but very different structural behaviours [6]. This research covers North American-produced RHS with different grades and cold-formed by the two predominant methods in order to develop general conclusions on the effects of different post-cold-forming processes. In particular, a new type of high-strength RHS product cold-formed by the direct-forming approach is included in this research. The new material has a nominal yield strength of 690 MPa. Recent research showed that the new RHS material has superior stub column behaviour, comparing to the conventional RHS [6]. In addition, the cross section classification rules in North American steel design standards for elements under axial compression were proven to be unnecessarily conservative for the new RHS product. It was speculated that the superior behaviour was due to an inherently low level of residual stress as a result of the unique manufacturing approach, where the cold-forming is only concentrated at the four corner regions. Since research on direct-formed high-strength RHS is still limited, with the aim of generating design tools to facilitate the application of the new construction material in North America, special attention is given to it in this research. The residual stresses in RHS of similar cross-sectional dimensions with regular strength (nominal yield strength = 350 MPa) and cold-formed by both the direct-forming method and the indirect-forming method were also measured for comparison.

1.3 Background

1.3.1 Galvanizing

The galvanizing process starts with surface preparation (degreasing, pickling, and further cleaning using a flux solution) to ensure a proper chemical reaction between the molten zinc bath and the steel during hot-dipping. The molten zinc bath is typically maintained at a temperature of approximately 450 ºC. The final hot-dipping process during galvanizing of steel members of commonly specified sizes only takes approximately 10 minutes [1,2]. In order to control the reactivity between steel and molten zinc mixture, no significant change can be made to bath temperature or dipping time. Recent research has been performed on the effects of general galvanizing practice and structural details on: (1) the possible changes in material properties, and (2) the thermally-induced stress and strain demands on structural components. A Critical review of the relevant research can be found in [2,3]. The hot dipping process in general does not change the steel microstructure and grain size. However, it is shown that it can reduce residual stresses in cold-formed steels [2,3].

For hot-dip galvanizing of welded tubular steel trusses and girders, holes must be specified at the welded joint location of the connections to allow for filling, venting and drainage. Adequate sizing of the galvanizing holes also minimizes the differential thermal stresses experienced by the structure during the hot-dipping process. Detailed discussions on the effect of such holes on the connection behaviours under static and fatigue loadings can be found in [9–11].

1.3.2 Heat treatment

In North America, two steel product standards, ASTM A1085 [7] and CSA G40.20/40.21 [8], contain heat treatment rules for justification of an improved compressive member behaviour for an HSS member (e.g. the use of a high column curve in the Canadian steel design standard CSA S16-19 [12]). Both ASTM A1085 [7] and CSA G40.20/40.21 [8] specify a furnace temperature of 450 ºC or higher for such process (see Fig. 1.2 for an example). However, neither manufacturing standard specifies the holding time or total duration. Since there is no definitive requirement, in practice heat treaters generally hold the furnace temperature at 450 ºC for 30 minutes [1–3]. Previous research by Sun and Packer [13] found that such heat treatment has negligible effect on the Charpy V-notch impact toughness of cold-formed RHS material, since it does not change the steel microstructure or grain size. Recently, via a comprehensive experimental research on RHS stub columns, Tayyebi and Sun [6] found that the hot-dip galvanizing process can also effectively improve the structural performance of cold-formed RHS under axial compression. Similar observations have been made in the investigations on galvanized CHS column members by Shi et al. [4,5]. Hence, one can deduce that for the 450 ºC post-production heat treatment per [7,8] for improvement of column behaviour, a 30-minute holding time is likely excessive. However, research evidence is needed to support this speculation. Therefore, this investigation measures the residual stresses in galvanized and heat-treated hollow sections cold-formed by different methods. The aim is to find a fit-for-purpose duration for such heat treatment such that it consumes less energy. Another occasionally applied post-production heat treatment option at a temperature of 595 ºC or higher is available with ASTM A143 [14]. The main objective of the 595 ºC heat treatment is to further reduce residual stress, and to recover the loss of material ductility due to severe cold deformation such as cold-bending and roll-forming. This type of heat treatment is also included in the test matrix of this study for comparison.

Figure 1.2 Removal of RHS material from furnace

1.3.3 Cold-forming methods

In North America, RHS of commonly specified cross-sectional dimensions are cold-formed by either direct-forming or indirect-forming. For the direct-forming method, flat rollers (see Fig. 1.3(a)) are used to form the coil strip directly into the desired rectangular cross section (see Fig. 1.3(b)). For the indirect-forming method, the coil strip is first cold-shaped into a circular form using concave rollers (see Fig. 1.3(c)). The circular shape is then further flattened into the desired rectangular shape, as shown in Fig. 1.3(d). Intuitively, one can deduce that the residual stress magnitude in an indirect-formed RHS will be higher comparing to that in its direct-formed counterpart. One can also expect that the increase of yield strength from flat face to corner of a direct-formed RHS will be larger than that of its indirect-formed RHS counterpart, since during the direct-forming process, only the corner regions of the cross section are heavily cold worked (i.e. strain hardened). On the other hand, the level of cold work around the cross section is relatively uniform during the indirect-forming process.

In addition to strain hardening, cold forming is also associated with the generation of residual stresses. In particular, the longitudinal component of residual stress is important for structural stability research. Compression members with high longitudinal residual stress levels are likely to experience early yielding. One can see the significance of longitudinal residual stresses over a cross section by superimposing the applied stress on them. As the loading increases, the summation of the applied and residual stresses causes some portions of the cross section to yield before others, which in return leads to a reduction in stiffness and in turn a loss in load-carrying capacity [6]. On the other hand, a good understanding of transverse residual stresses at corner regions of severely cold-formed RHS members is important for prevention of cracking during hot-dip galvanizing. Experience has shown that when cracking occurs during galvanizing, it usually initiates at the corner regions of the RHS free end. The RHS free end tends to “open” during galvanizing as a result of high residual and thermal stresses in the transverse direction. The risk of cracking can be reduced by welding end plates to the RHS to restrain the expansion of the section [1–3].

In all, although extensive research on the material properties of hollow sections [15–24], the difference among cold-formed, galvanized, lightly heat-treated (at 450ºC), and heavily heat-treated (at 595ºC) hollow sections has been a point of debate to date [1,2]. This paper focuses on their residual stress properties.

(a) Flat rollers used in direct-forming

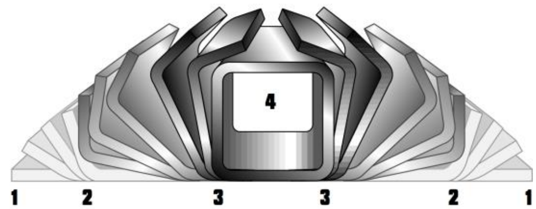

(b) direct-forming sequence

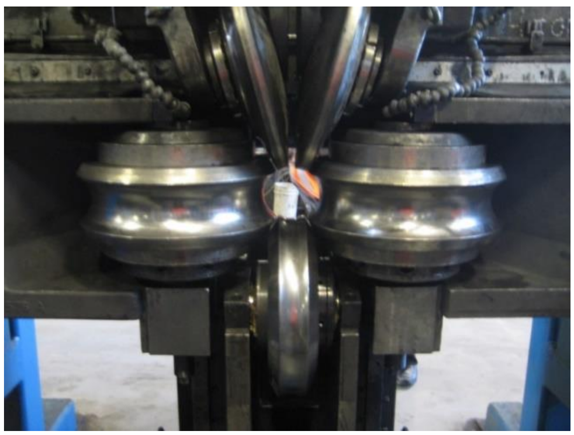

(c) Concave rollers used in indirect-forming

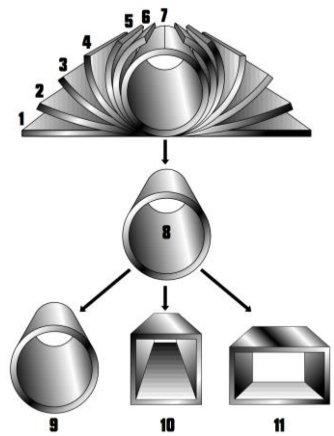

(d) indirect-forming sequence

Figure 1.3 Different cold-forming approaches

1.4 Preparation of RHS specimens

1.4.1 Parent hollow sections

Eleven parent tubes made of steels with different grades and produced by the two predominant cold-forming approaches were used to fabricate a total of 26 RHS specimens in this research. Each parent RHS ID in Table 1.1 contains two components. The first differentiates the material by its nominal yield strength ($\sigma_{y,nom}$) and cold-forming process, where I = regular-strength indirect-formed material ($\sigma_{y,nom}$ = 350 MPa); D = regular-strength direct-formed material ($\sigma_{y,nom}$ = 350 MPa); and DH = high-strength direct-formed material ($\sigma_{y,nom}$ = 690 MPa). The nominal external width, external height and wall thickness (in mm) are used in the second component of the parent RHS ID. The regular-strength materials (D and I) were produced to Gr. 350W Class C of CSA

G40.20/40.21 [8]. The high-strength materials (DH) were produced to ASTM A1112 Class 100 [25]. All direct-formed materials (D and DH) were cold-formed in the same production facility to allow direct comparison and to study individually the effects of different material strengths. The selection of specimens also allows the direct comparisons of residual stresses in RHS over a wide range of cross-sectional dimensions. Prior to tests, the cross-sectional dimensions were carefully measured and are listed in Table 1.1. Table 1.2 shows the chemical compositions of the parent RHS.

1.4.2 Post-cold-forming heat treatment and galvanizing

This research sought to: (1) determine the fit-for-purpose duration and temperature for heat treatment to improve compressive member behaviour of cold-formed RHS; and (2) quantify the effects of hot-dip galvanizing on residual stress properties of cold-formed RHS. Hence, using the 11 parent hollow sections, 26 RHS specimens of different production histories were prepared and are listed in Table 1.1. As shown, a third component was added to the specimen ID, to differentiate the materials by the post-production processes they received. For the third ID component, “U” and “G” represent as-received untreated and galvanized cold-formed RHS, respectively. Neither was subjected to post-cold-forming heat treatment. “450” and “595” represent RHS heat-treated to 450 ºC per [7,8] and 595 ºC per [14], respectively. Similar furnace cycles were applied to all heat-treated specimens (i.e. hold the specified furnace temperature for 30 minutes) for the purpose of direct comparison. As discussed in Section 1.2, the furnace cycles are consistent with the current industrial practice.

Table 1.1 Measured dimensions of parent RHS

Parent RHS ID	B (mm)	H (mm)	t (mm)	r_{i1} (mm)	r_{i2} (mm)	r_{i3} (mm)	r_{i4} (mm)	RHS specimen ID
I-102×102×6.4	102.1	102.2	6.41	7.2	6.6	8.9	9.1	I -102×102×6.4- U I -102×102×6.4- 450 I -102×102×6.4- 595 I -102×102×6.4- G
I-102×102×7.9	101.9	102.1	7.83	11.0	11.9	13.0	10.8	I -102×102×7.9- U I -102×102×7.9- 450 I -102×102×7.9- 595 I -102×102×7.9- G
I-102×102×13	101.6	101.7	12.90	11.8	11.6	11.7	11.9	I -102×102×13- U I -102×102×13- 450 I -102×102×13- 595 I -102×102×13- G
D-76×102×3.2	76.5	101.9	3.03	2.6	2.8	2.1	2.0	D -76×102×3.2- U D -76×102×3.2- G
D-76×102×4.8	76.4	101.9	4.36	2.5	3.4	3.7	4.2	D -76×102×4.8- U D -76×102×4.8- G
D-102×102×4.8	101.6	102.1	4.40	5.6	5.4	4.5	7.1	D -102×102×4.8- U
DH-76×76×4.8	76.3	76.6	4.81	10.2	7.7	8.7	7.3	DH -76×76×4.8- U DH -76×76×4.8- G
DH-76×102×3.2	76.9	102.6	3.02	2.2	2.7	2.9	2.6	DH -76×102×3.2- U DH -76×102×3.2- G
DH-76×102×4.1	76.3	101.8	4.06	5.2	5.6	3.9	4.3	DH -76×102×4.1- U
DH-76×102×4.8	76.6	102.0	4.82	9.2	9.2	8.5	8.5	DH -76×102×4.8- U DH -76×102×4.8- G
DH-76×152×4.1	77.2	153.1	4.04	6.3	4.4	5.0	4.6	DH -76×152×4.1- U DH -76×152×4.1- G

Table 1.2 Chemical compositions of parent RHS

Parent RHS ID	C	Si	Mn	Cu	Ni	Cr	Mo	V	Ti	CE
I-102×102×6.4	0.140	0.240	0.870	0.010	0.050	0.003	0.000	0.003	N/A	0.29
I-102×102×7.9	0.140	0.230	0.860	0.010	0.050	0.040	0.000	0.013	N/A	0.30
I-102×102×13	0.200	0.023	0.750	0.020	0.008	0.026	0.002	0.002	0.002	0.33
D-76×102×3.2	0.180	0.020	0.390	0.140	0.060	0.080	0.020	0.001	0.001	0.28
D-76×102×4.8	0.040	0.040	0.710	0.120	0.040	0.060	0.000	0.002	0.000	0.18
D-102×102×4.8	0.061	0.029	0.610	0.014	0.010	0.020	0.002	0.001	0.002	0.17
DH-76×76×4.8	0.061	0.020	1.650	0.010	0.030	0.030	0.000	0.010	0.000	0.35
DH-76×102×3.2	0.072	0.020	1.350	0.010	0.040	0.020	0.000	0.010	0.120	0.31
DH-76×102×4.1	0.078	0.020	1.340	0.010	0.030	0.030	0.000	0.010	0.110	0.31
DH-76×102×4.8	0.061	0.020	1.690	0.010	0.030	0.020	0.000	0.010	0.080	0.35
DH-76×152×4.1	0.080	0.020	1.330	0.010	0.040	0.030	0.010	0.010	0.110	0.32

Cast analysis (%)

Note: carbon equivalent $\mathrm{CE} = \mathrm{C} + \frac{\mathrm{Mn}}{6} + \frac{\mathrm{Cr} + \mathrm{Mo} + \mathrm{V}}{5} + \frac{\mathrm{Ni} + \mathrm{Cu}}{15}$

1.5 Tensile coupon test

1.5.1 Test procedures

For all 26 RHS specimens, the material properties were determined via tensile coupon tests following the requirements in ASTM E8 [26]. The tensile coupons were cut from the flat faces and the corners of the cross sections (see Fig. 1.4). An extensometer and a pair of strain gauges were installed on the coupon to determine the strains. Representative stress-strain curves are shown in Figs. 1.5 to 1.8. Tables 1.3 and 1.4 list the key tensile coupon test results.

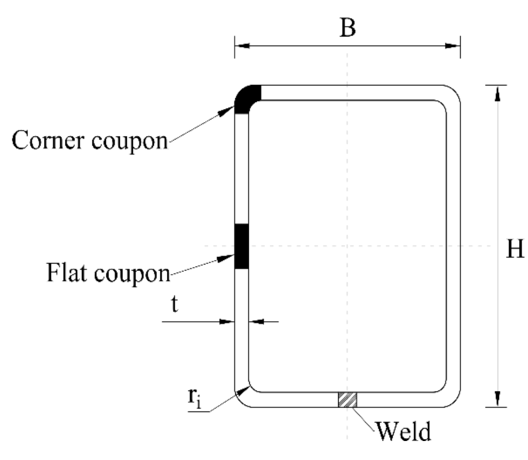

Figure 1.4 Locations of tensile coupons

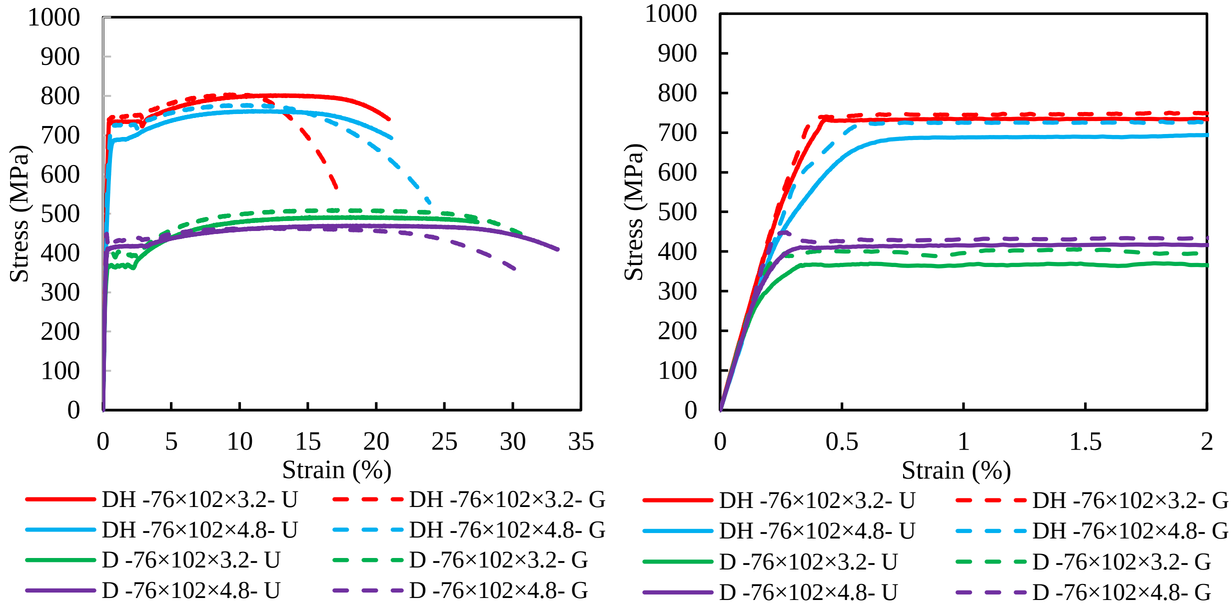

(a) Full curves

(b) Initial portions

Figure 1.5 Representative tensile stress-strain relationships of flat coupons from direct-formed RHS

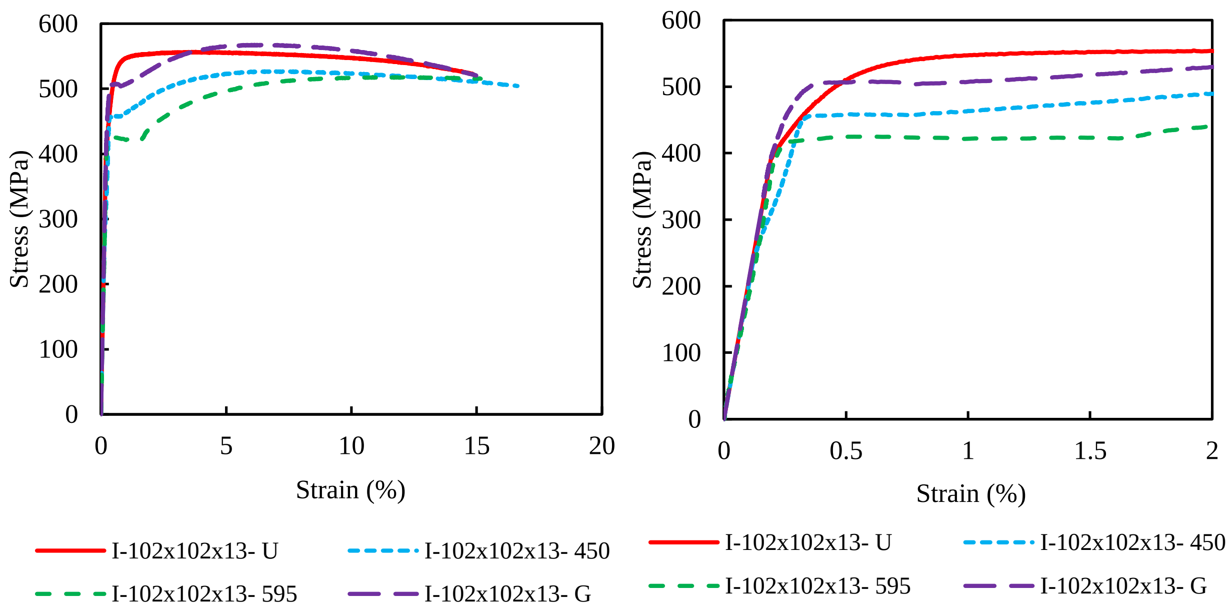

(a) Full curves

(b) Initial portions

Figure 1.6 Representative tensile stress-strain relationships of flat coupons from indirect-formed RHS

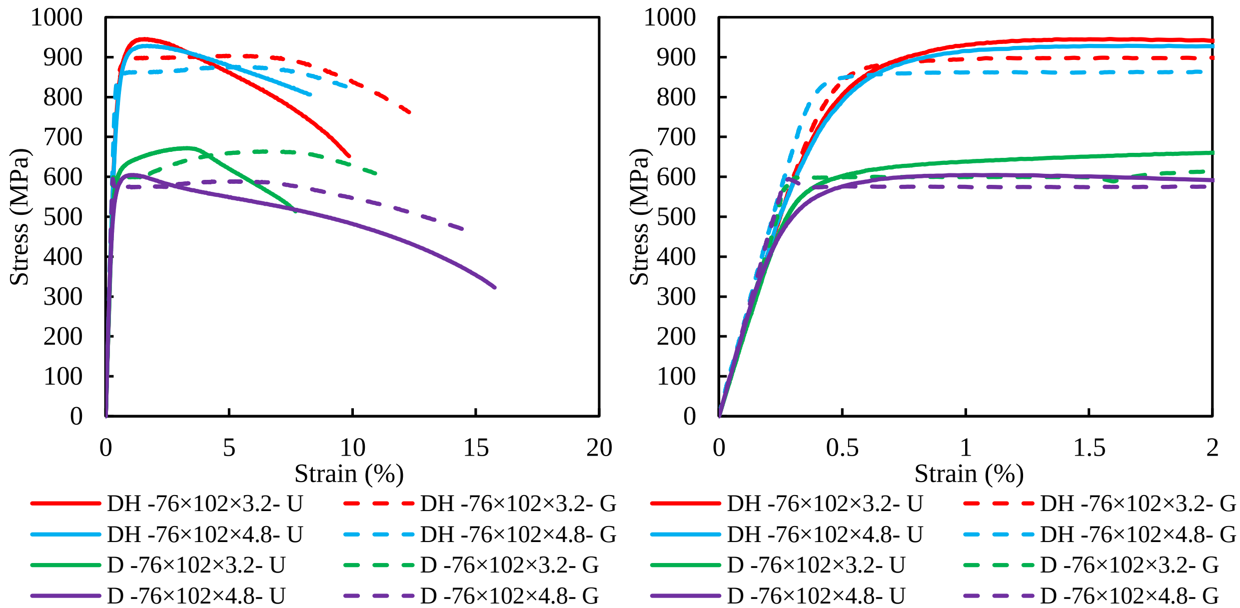

(a) Full curves

(b) Initial portions

Figure 1.7 Representative tensile stress-strain relationships of corner coupons from direct-formed RHS

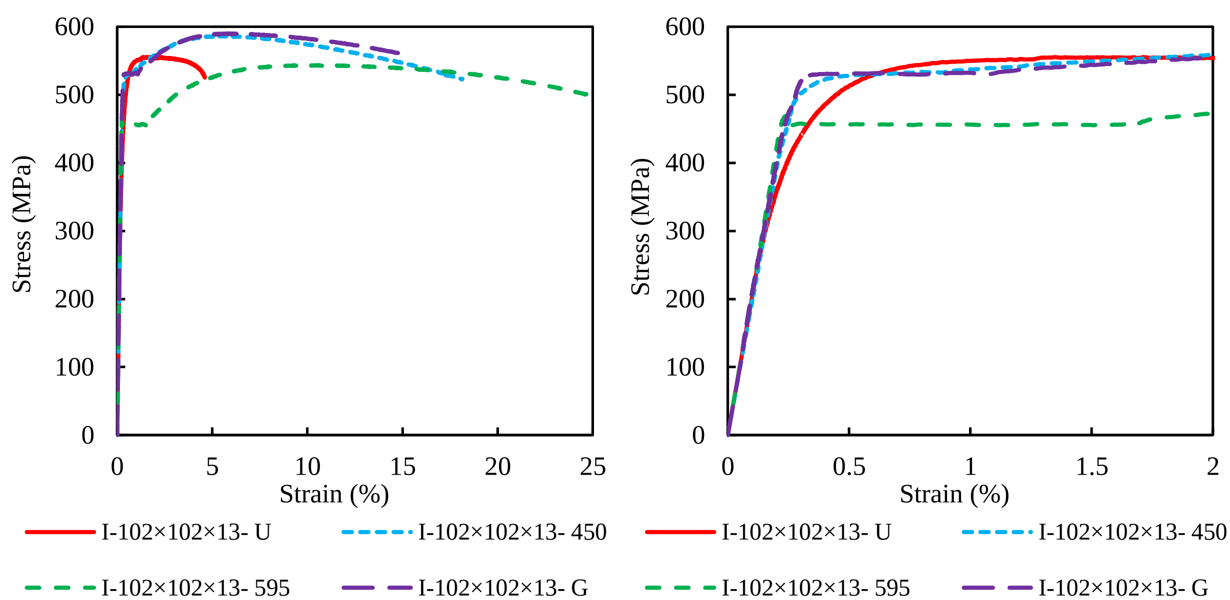

(a) Full curves

(b) Initial portions

Figure 1.8 Representative tensile stress-strain relationships of corner coupons of indirect-formed RHS

Table 1.3 Flat coupon test results

Specimen ID	E (GPa)	σ_y (MPa)	σ_u (MPa)	ε_u (%)	ε_r (%)	σ_u/σ_y	$\varepsilon_u/(\sigma_y/E)$
I-102×102×6.4-U	199	415	482	16.0	30	1.16	76.7
I-102×102×6.4-450	201	427	505	12.5	31	1.18	58.8
I-102×102×6.4-595	200	384	486	15.2	33	1.27	79.2
I-102×102×6.4-G	203	445	509	10.1	27	1.14	46.1
I-102×102×7.9-U	198	458	509	9.5	25	1.11	41.1
I-102×102×7.9-450	208	468	539	8.6	26	1.15	38.2
I-102×102×7.9-595	206	409	505	13	31	1.23	65.5
I-102×102×7.9-G	194	478	530	6.8	22	1.11	27.6
I-102×102×13-U	201	483	549	4.4	22	1.14	18.3
I-102×102×13-450	201	480	566	5.6	25	1.18	23.5
I-102×102×13-595	196	433	527	10.5	30	1.22	47.5
I-102×102×13-G	207	493	555	6.3	25	1.13	26.5
D-76×102×3.2-U	203	367	492	15.1	34	1.34	83.5
D-76×102×3.2-G	211	400	509	17.3	32	1.27	91.3
D-76×102×4.8-U	200	409	470	19.5	39	1.15	95.4
D-76×102×4.8-G	204	424	463	10.3	36	1.09	49.6
D-102×102×4.8-U	205	399	487	12.9	38	1.22	66.3
DH-76×76×4.8-U	199	638	767	10	27	1.20	31.2
DH-76×76×4.8-G	203	743	786	9.8	28	1.06	26.8
DH-76×102×3.2-U	217	730	802	12.6	27	1.10	37.5
DH-76×102×3.2-G	217	742	803	9.3	20	1.08	27.2
DH-76×102×4.1-U	202	692	776	11.8	26	1.12	34.4
DH-76×102×4.8-U	194	651	761	10.9	29	1.17	32.5
DH-76×102×4.8-G	191	720	777	9.5	26	1.08	25.2
DH-76×152×4.1-U	198	713	815	13.9	30	1.14	38.6
DH-76×152×4.1-G	208	744	819	12.1	28	1.10	33.8

Table 1.4 Corner coupon test results

Specimen ID	E (GPa)	σ_y (MPa)	σ_u (MPa)	ε_u (%)	ε_r (%)	σ_u/σ_y	$\varepsilon_u/(\sigma_y/E)$
I-102×102×6.4-U	198	496	544	1.4	14	1.10	5.6
I-102×102×6.4-450	199	550	610	6.7	21	1.11	24.2
I-102×102×6.4-595	198	434	502	9.8	26	1.16	44.7
I-102×102×6.4-G	200	508	554	4.8	16	1.09	18.9
I-102×102×7.9-U	201	539	577	1.3	14	1.07	4.8
I-102×102×7.9-450	205	566	629	6.3	21	1.11	22.8
I-102×102×7.9-595	202	485	559	9.0	25	1.15	37.5
I-102×102×7.9-G	201	539	590	5.6	17	1.09	20.9
I-102×102×13-U	198	506	563	1.6	14	1.11	6.3
I-102×102×13-450	201	528	592	5.3	19	1.12	20.2
I-102×102×13-595	204	459	546	9.7	26	1.19	43.1
I-102×102×13-G	206	538	596	5.8	17	1.11	22.2
D-76×102×3.2-U	200	601	672	3.3	14	1.12	11.0
D-76×102×3.2-G	208	599	664	6.4	16	1.11	22.2
D-76×102×4.8-U	217	568	605	1.1	18	1.07	4.2
D-76×102×4.8-G	225	574	595	4.6	20	1.04	18.0
D-102×102×4.8-U	206	574	618	1.2	18	1.08	4.3
DH-76×76×4.8-U	190	789	863	1.4	19	1.09	3.4
DH-76×76×4.8-G	229	878	893	5.6	22	1.02	14.6
DH-76×102×3.2-U	206	862	945	1.6	12	1.10	3.8
DH-76×102×3.2-G	207	876	904	5.1	14	1.03	12.1
DH-76×102×4.1-U	211	879	960	1.3	12	1.09	3.1
DH-76×102×4.8-U	206	849	928	1.8	16	1.09	4.4
DH-76×102×4.8-G	225	816	876	5.3	20	1.07	14.6
DH-76×152×4.1-U	204	930	1054	1.8	14	1.13	3.9
DH-76×152×4.1-G	222	918	949	5.2	16	1.03	12.6

1.5.2 Discussions of tensile coupon test results

1.5.2.1 Effects of cold-forming methods

Using the data in Tables 1.3 and 1.4, for the untreated specimens (i.e. 3rd ID component = U), the changes of yield strength, ultimate strength and rupture strain from the flat face to the corner region of the cross sections are shown in Fig. 1.9. As discussed in Section 1.3.3, for direct-formed RHS, only the corner regions are heavily cold worked, while for the indirect-formed RHS, the entire cross section is heavily cold worked. According to Fig. 1.9(a), the yield strength increases from flat face to corner of the direct-formed RHS (D and DH) are larger than those of the indirect-formed RHS (I), which is consistent with the speculations based on the comparison between the two cold-forming approaches. For the three indirect-formed RHS, the increase in yield strength decreases as the wall thickness increases, since the degree of cold working over the perimeter of the cross section becomes more uniform as the width-to-thickness ratio increases. Similar observations can be made in Fig. 1.9(b) for the ultimate strength. Since steel producers often aim at rolling RHS with large “flat width” dimensions, the overall amount of cold working and in turn the residual stress level in the cross section of an indirect-formed RHS should in theory be much higher than that in its direct-formed counterpart. This speculation is substantiated in Section 1.6.

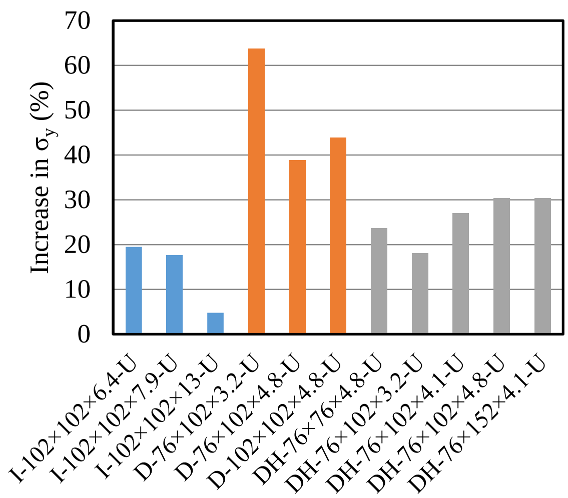

(a) Increase of yield strength

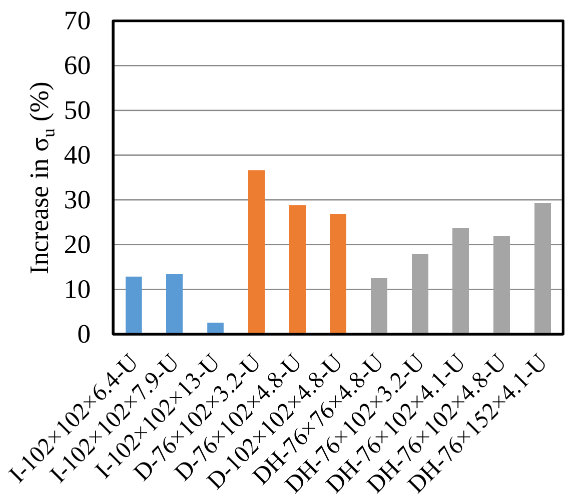

(b) Increase of ultimate strength

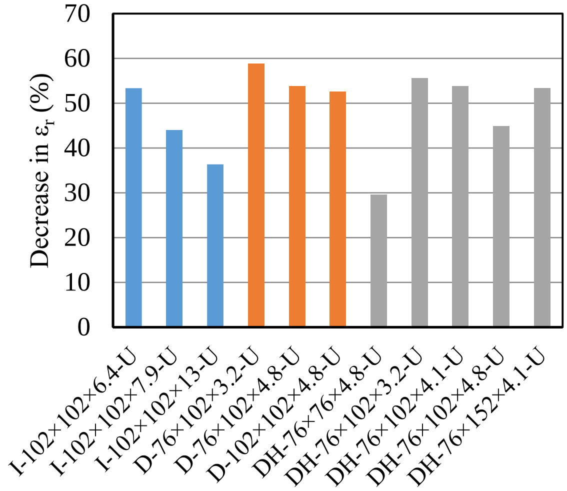

(c) Decrease of rupture strain

Figure 1.9 Changes of material properties from flat face to corner region

1.5.2.2 Effects of galvanizing and heat treatment

Using the data in Tables 1.3 and 1.4, the effects of the 450 ºC heat treatment, the 595 ºC heat treatment and the hot-dip galvanizing process on the material yield and ultimate strengths are compared in Fig. 1.10. As shown, both the 450 ºC heat treatment per [7,8] and galvanizing had minor effect on the strength properties of materials from different locations of the cross sections. On the other hand, the 595 ºC heat treatment per ASTM A143 [14] led to significant reduction in yield strength, and in some cases significant reduction in ultimate strength.

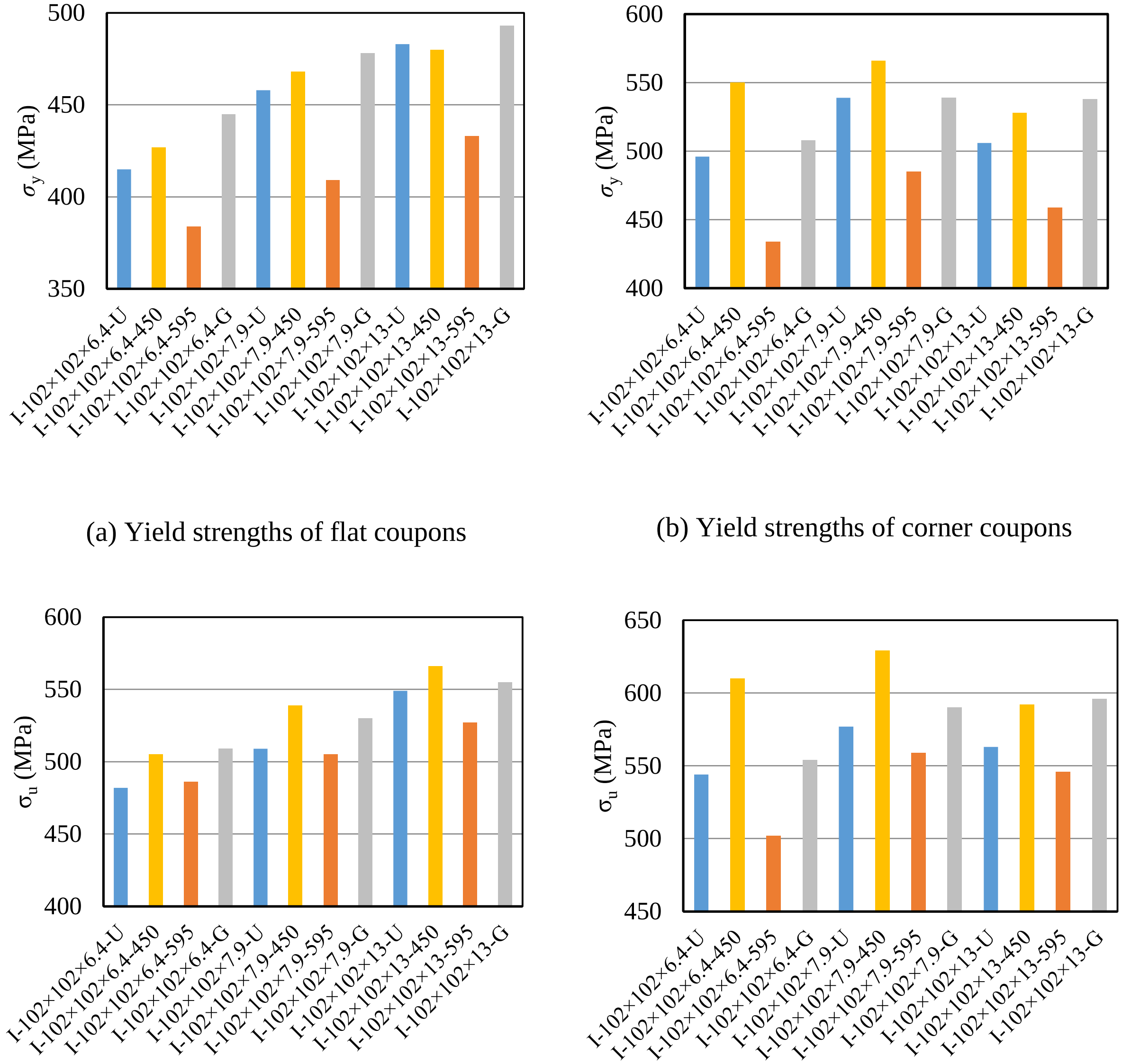

(a) Yield strengths of flat coupons

(b) Yield strengths of corner coupons

(c) Ultimate strengths of flat coupons

(d) Ultimate strengths of corner coupons

Figure 1.10 Yield and ultimate strengths of RHS materials subjected to different post-cold-forming processes

In both EN 1993-1-1:2005 [27] and EN 1993-1-12:2007 [28], the minimum ductility required for design is expressed in terms of limits for: (1) the ratio of the specified minimum tensile strength to the specified minim yield strength; (2) the rupture strain at the test region of a tensile coupon; and (3) the ratio of the ultimate strain to the yield strain of a tensile coupon. The requirements are listed in Table 1.5.

Table 1.5 Ductility requirement in Eurocode 3

EN 1993-1-1:2005 [27]	EN 1993-1-12:2007 [28]
$\sigma_u/\sigma_y \geq 1.10$ $\varepsilon_r \geq 15\%$ $\varepsilon_u/(\sigma_y/E) \geq 15$	$\sigma_u/\sigma_y \geq 1.05$ $\varepsilon_r \geq 10\%$ $\varepsilon_u/(\sigma_y/E) \geq 15$

In AISC 360-16 [29] the minimum ductility required for design is expressed in a similar manner. Structural steel material conforming to one of the listed ASTM or CSA standards is approved for use under AISC 360-16. For cold-formed HSS, ASTM A500 [30], ASTM A1085 [7], and CSA G40.20/40.21 [8] are included in AISC 360-16 [29]. The minimum ductility in these steel product standards are similar to those in Eurocode [27,28] and are shown in Table 1.6. As discussed in Section 1.4.1, the high-strength materials (DH) in this research were produced to ASTM A1112 Class 100 [25]. The ductility requirements from ASTM A1112 are also listed in Table 1.6.

Table 1.6 Ductility requirements in ASTM and CSA standards approved for use under AISC 360-16

Standard	Grade	Minimum specified ε_r (%)	Minimum specified σ_y (MPa)	Minimum specified σ_u (MPa)	σ_u/σ_y
ASTM A500 [39]	C	21	345	425	1.23
ASTM A1085 [7]	A	21	345	450	1.30
CSA-G40.20/G40.21 [8]	350W	22	350	450	1.29
ASTM A1112 [34]	100	12	690	760	1.10

Using the same criteria in the above standards and the data in Tables 1.3 and 1.4, the effects of galvanizing and heat treatments to different degrees on the material ductility (expressed in terms of the measured values of ε_r and σ_u/σ_y) are shown in Fig. 1.11. As shown, both galvanizing and heat treatment at 450 ºC per [7,8] had minor effect on the ductility of the flat and corner coupons. On the other hand, the 595 ºC heat treatment per ASTM A143 [14] led to significant reduction material ductility. However, the trade-off between ductility and strength must be taken in to consideration by the designers and fabricators when specifying the ASTM A143 [14] heat treatment.

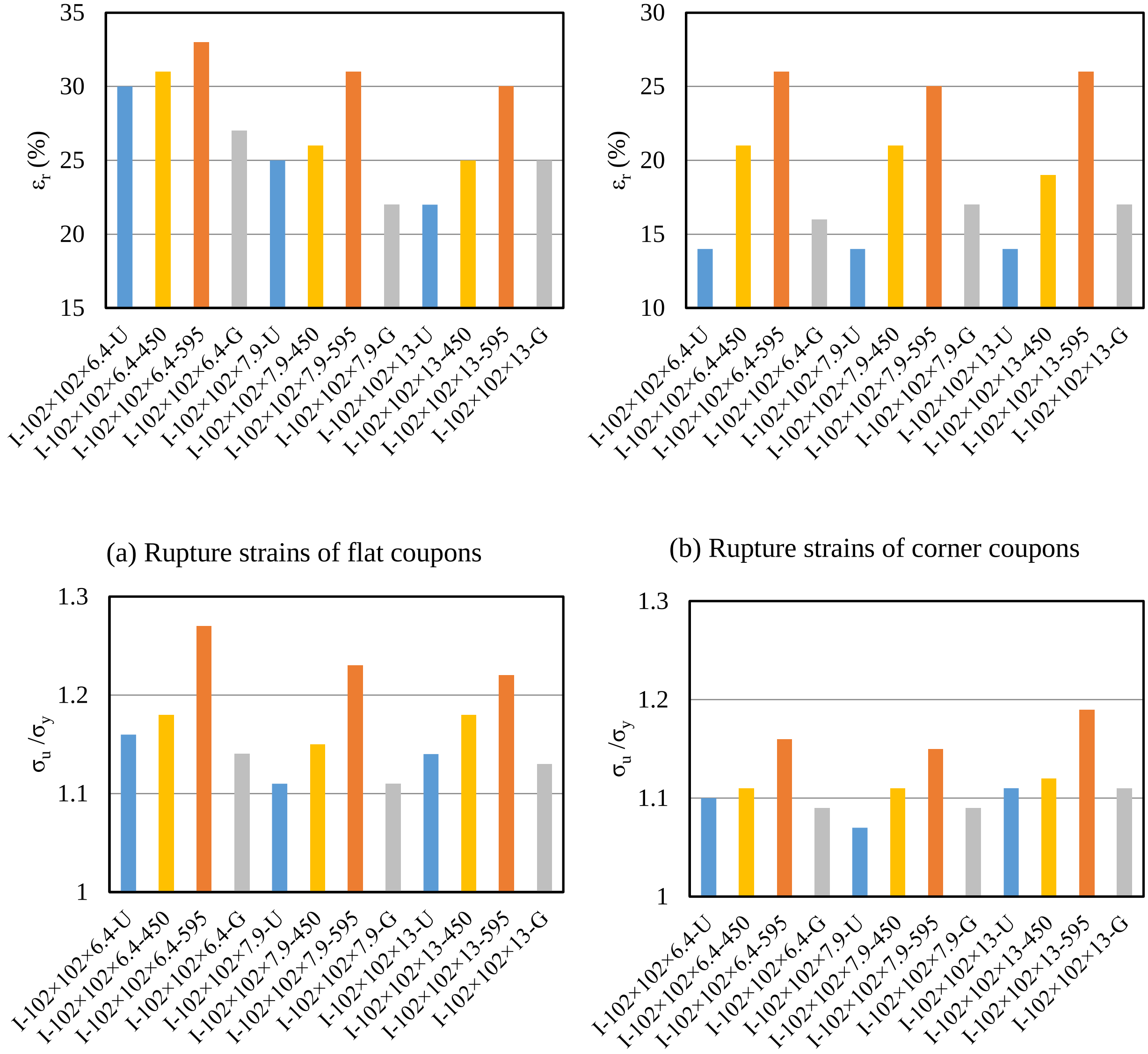

(a) Rupture strains of flat coupons

(b) Rupture strains of corner coupons

(c) σ_u / σ_y-values of flat coupons

(d) σ_u / σ_y-values of corner coupons

Figure 1.11 Ductility of RHS materials subjected to different post-cold-forming processes

1.6 Residual stress measurement

In this research, the sectioning technique recommended by the Structural Stability Research Council (SSRC) [31] was applied to measure the residual stresses in the longitudinal direction. A total of 342 strips were carefully machined from the 26 RHS specimens. Following the same approach used by [5,32–35], mechanical gauges were used to measure strip deformations for calculation of the in-situ residual stresses. A typical test piece (D-76×102×4.8-U) is illustrated in

Fig. 1.12. Following the requirements in the SSRC guide [31], all test pieces were cut from a location at least three times the largest cross-sectional dimension away from the ends of the parent tubes. The width of each strip was 10 mm. Through-thickness gauge holes were drilled prior to sectioning. For each RHS test piece, after measuring the initial distances between the gauge holes, the cross section was cut open using a horizontal band saw. The sectioning setup is shown in Fig. 1.13. Liquid coolant was used throughout the process to minimize the heat input from cutting. After cutting, all strips were cooled to ambient temperature before measurements of the final distances between the gauge holes. Both the initial and the final gauge length measurements were repeated three times, and the average values were used in the residual stress calculations.

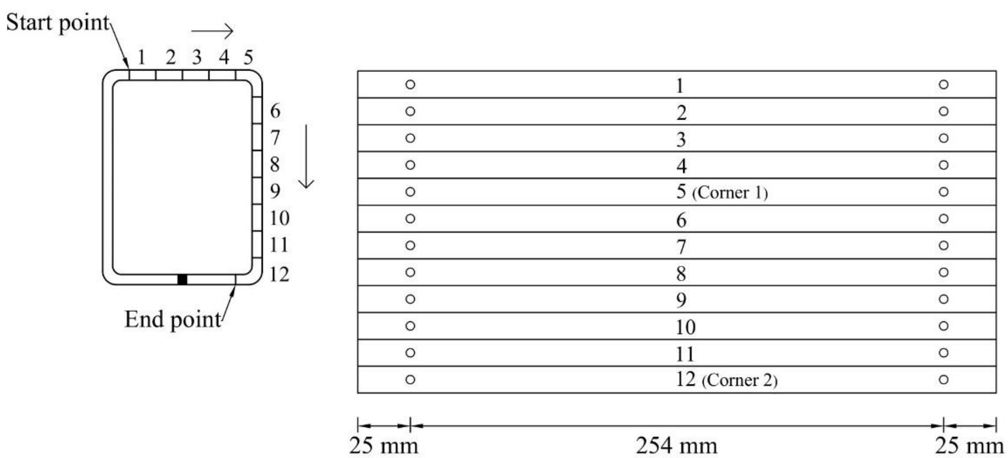

Figure 1.12 Arrangement of strips around a typical RHS specimen (D-76×102×4.8-U)

Figure 1.13 RHS specimen during sectioning

Before calculation, the deformed shapes of the strips from RHS with different production histories were compared. The deformed strips from typical RHS are shown in Figs. 1.14 and 1.15. In general, the strips from the untreated test pieces (Figs. 1.14(a), 1.15(a) and 1.15(c)) were heavily deformed. The deformations of the strips from RHS subjected to galvanizing (Figs. 1.14(b), 1.15(b) and 1.15(d)) and heat treatment at 450 ºC for a holding time of 30 minutes (Fig. 1.14(c)) are similar and a lot smaller. This very clearly indicated similar amounts of reduction in residual stress from the two very different post-production processes. It should be noted that the 450 ºC heat treatment in this case is much more onerous comparing to hot-dip galvanizing, as discussed in Section 1.3.2. The heat treatment at 595 ºC for a holding time of 30 minutes released almost all residual stresses since the strips remained straight after sectioning (Fig. 1.14(d)).

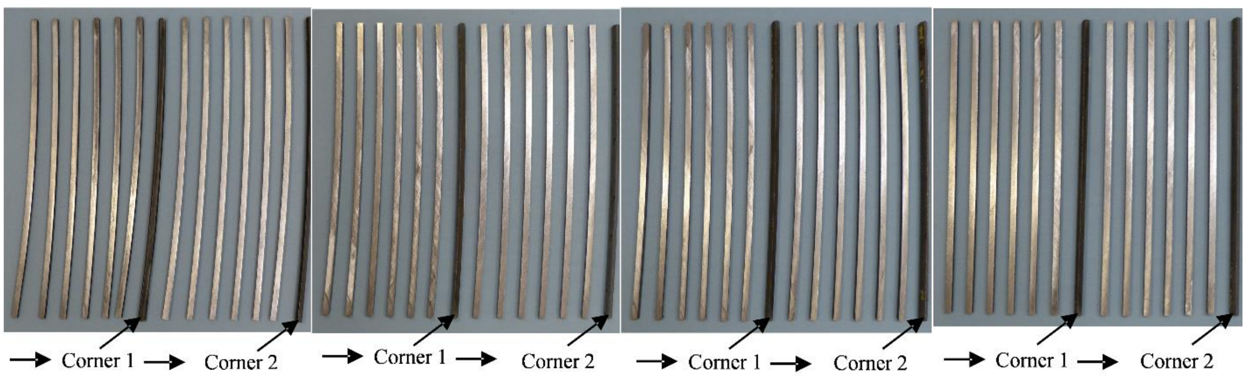

(a) I-102×102×6.4-U (b) I-102×102×6.4-G (c) I-102×102×6.4-450 (d) I-102×102×6.4-595

Figure 1.14 Deformed strips from indirect-formed RHS subject to different post-cold-forming processes

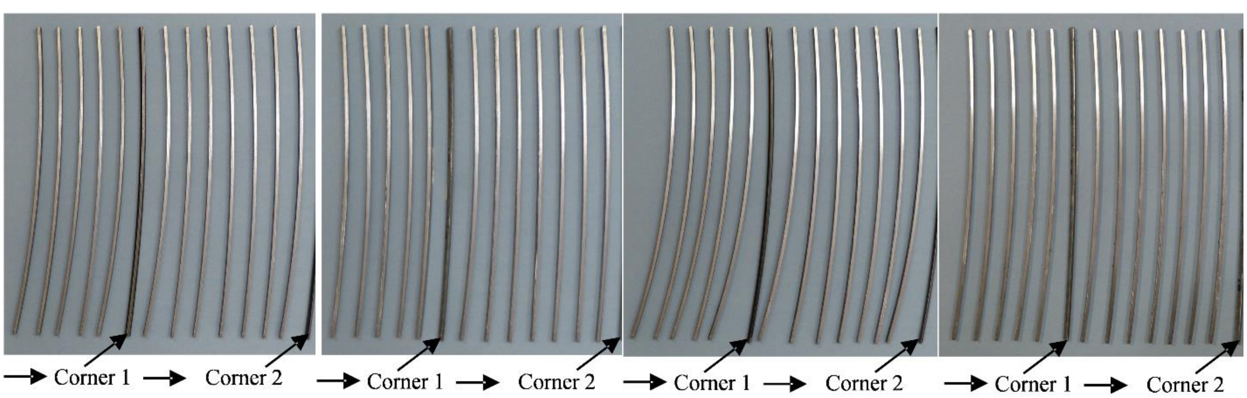

(a) D-76×102×3.2-U (b) D-76×102×3.2-G (c) DH-76×102×3.2-U (d) DH-76×102×3.2-G

Figure 1.15 Deformed strips from untreated and galvanized direct-formed RHS

1.6.1 Calculation of residual stresses

For measurement of the relaxation of strains resulting from removal of material, this research applied the standard procedures and the standard mechanical gauges recommended by the SSRC guide [31]. The same approach has been used in previous research on cold-formed steel members [5,32–35]. As illustrated in Fig. 1.16, the sectioning method in the SSRC guide [31] assumes a linear though-thickness distribution of residual stress, which can be determined by measuring the elastic spring back upon removal of strips from the cross section. In Fig. 1.16, σ_{in} and σ_{out} are the total longitudinal residual stresses on the inside and outside surfaces of the strip, respectively. The membrane residual stress (σ_m) is the mean of σ_{in} and σ_{out}. The bending residual stress (σ_b) is the deviation of the total from the membrane component. A Whittemore gauge with an accuracy of 0.00254 mm over a gauge length of 254 mm was employed to measure the change in length of the strips (axial deformations). The bending deformation of each strip was determined by measuring the deflections at various locations by using a Mitutoyo digital height gauge with an accuracy of 0.01 mm. Since all measurements were performed in a lab space (with temperature control), the effect of temperature change on the readings was considered negligible. The bending and membrane residual stresses were calculated by applying the same procedures used by Gardner and Cruise [35] as well as Yuan et al. [33].

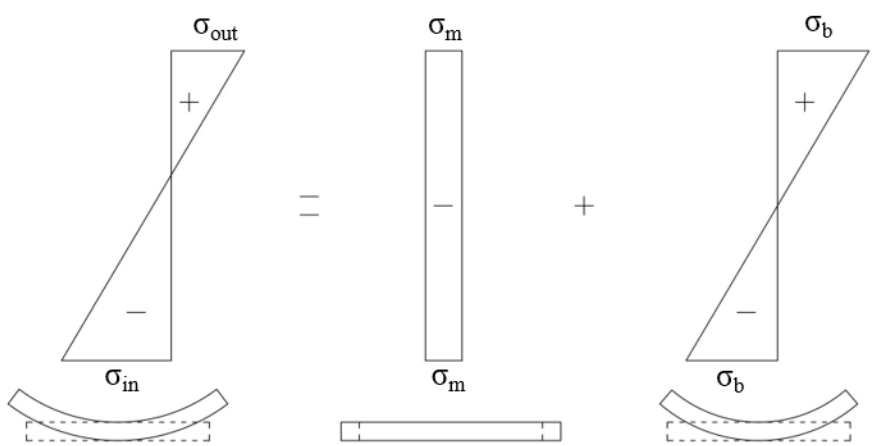

Total through-thickness residual stress | Membrane component | Bending component

Figure 1.16 Bending and membrane residual stress components

1.6.2 Discussions of residual stress measurement results

The membrane and bending residual stress distributions in the longitudinal direction of the 26 RHS specimens are shown in Figs. 1.17 and 1.18, respectively. In these figures, the residuals stresses at the flat face and corner regions are normalized by the measured yield stress (σ_y) of tensile coupon at the corresponding location. The start and end points in Figs. 1.17 and 1.18 are consistent with Fig. 1.12. In Figs. 1.17 and 1.18, compressive residual stresses are shown as negative values and tensile residual stresses as positive values. Fig. 1.18 shows only the bending residual stresses on the external surfaces of the RHS specimens. The averages of the normalized values for different regions over the cross sections are listed in Table 1.7. The overall cross-sectional values in Table 1.7 are calculated using a weighted average method (i.e. residual stress × tributary area in Fig. 1.12 / total cross-sectional area). The overall cross-sectional values are especially useful for comparison of residual stresses in RHS with different production histories. In particular, compression members made with RHS with large overall cross-sectional residual stresses are likely to experience early yielding, which in return leads to a reduction in stiffness and in turn a loss in load-carrying capacity.

As shown by the results in Figs 1.17 and 1.18 as well as Table 1.7, the membrane components can be compressive or tensile depending on the location of measurement. For the bending components, all strips from all test pieces curved outward after sectioning, indicating compressive stresses on the inner surface of the RHS and tensile on the outer surface. The maximum residual stresses in general occur in the near corner regions. Similar observations have been made in the relevant research in the past [15,24,36,37]. Since the bending components (σ_b) are in general significantly larger than the membrane components (σ_m), the following discussions will focus on the former.

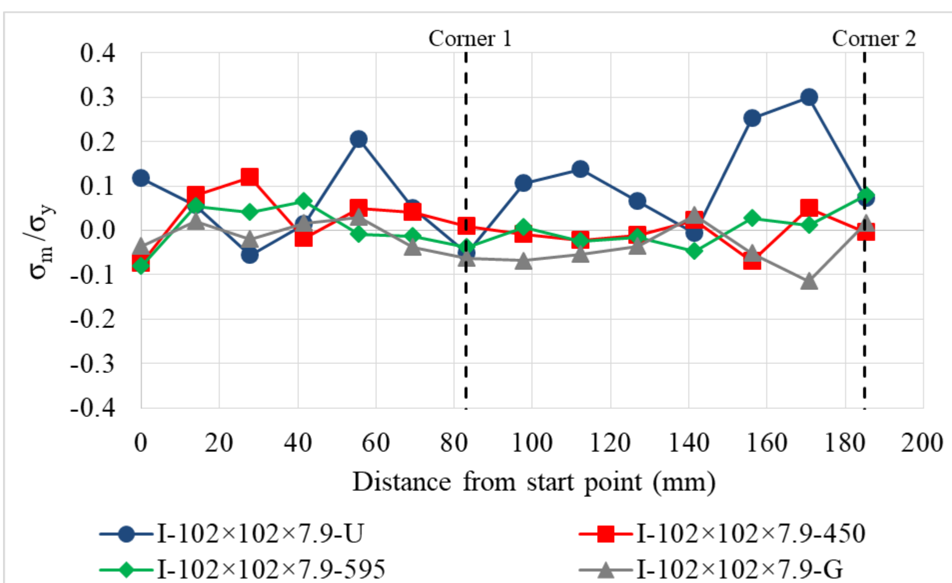

(a) Indirect-formed RHS

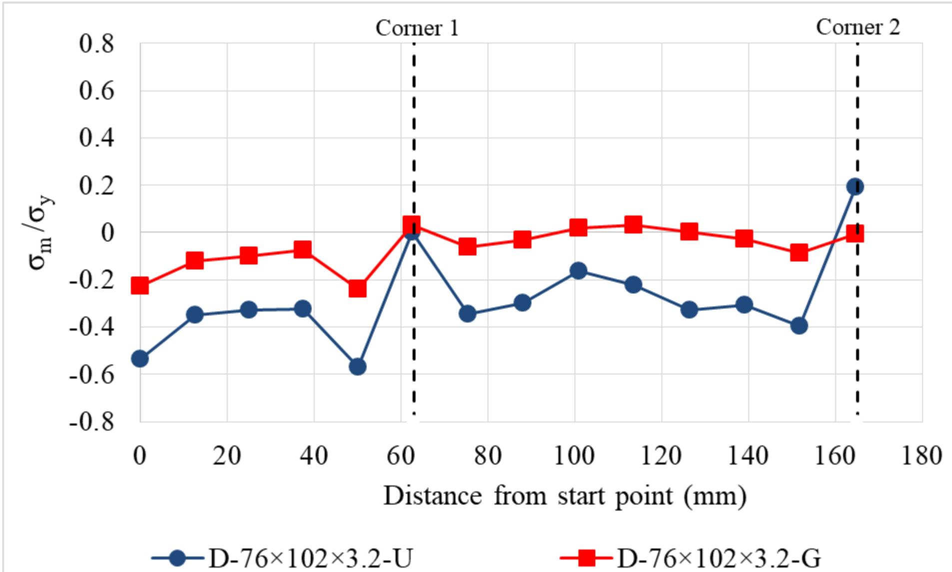

(b) Direct-formed RHS

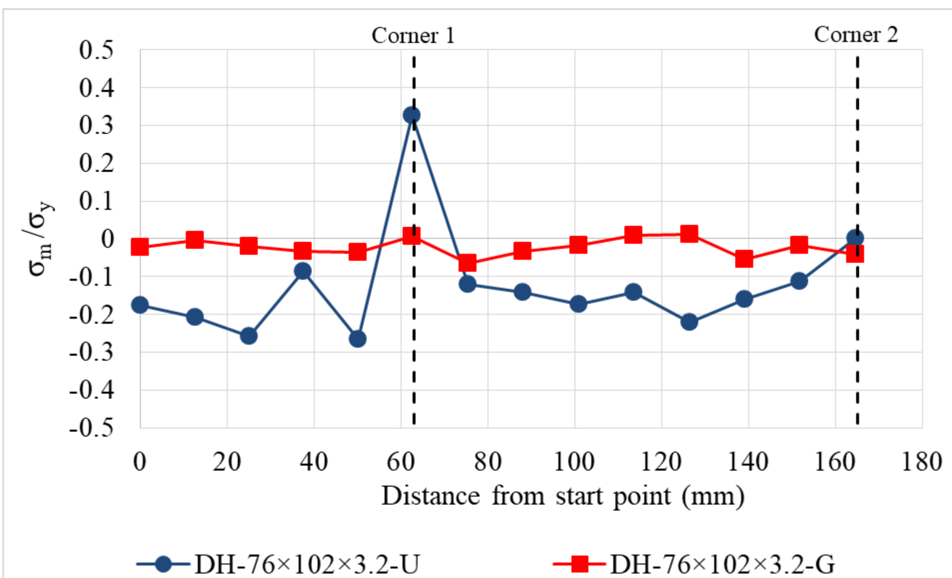

(c) Direct-formed high-strength RHS

Figure 1.17 Typical membrane residual stress distributions in RHS specimens

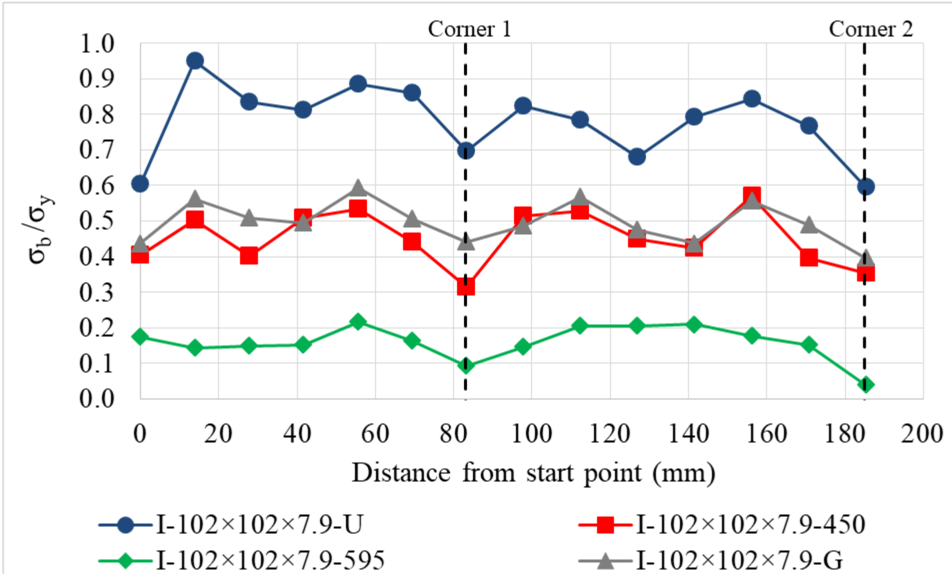

(a) Indirect-formed RHS

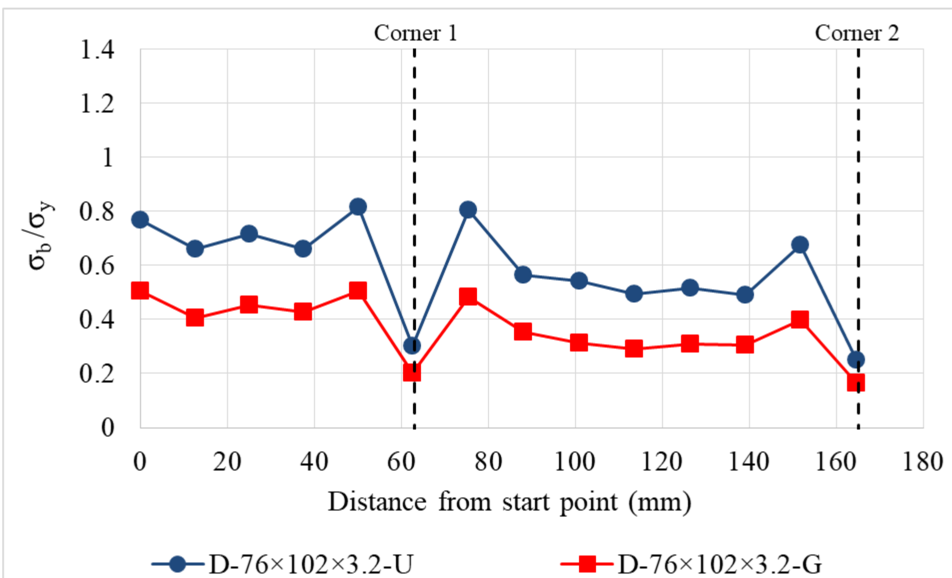

(b) Direct-formed RHS

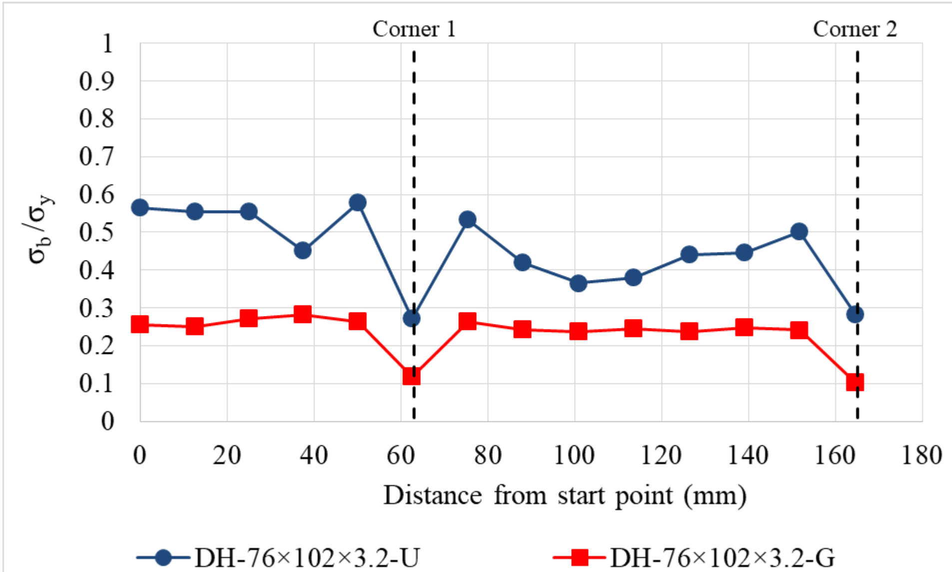

(c) Direct-formed high-strength RHS

Figure 1.18 Typical bending residual stress distributions in RHS specimens

Table 1.7 Averages of normalized residual stresses in RHS specimens

Specimen ID	Flat		Corner		Overall	
	σ_b/σ_y (%)	σ_m/σ_y (%)	σ_b/σ_y (%)	σ_m/σ_y (%)	σ_b/σ_y (%)	σ_m/σ_y (%)
I-102×102×6.4-U	82	-7	67	-2	80	-6
I-102×102×6.4-450	41	-1	24	3	39	0
I-102×102×6.4-595	13	-4	5	-3	12	-4
I-102×102×6.4-G	45	2	37	-3	44	2
I-102×102×7.9-U	80	10	65	1	78	9
I-102×102×7.9-450	47	1	33	0	45	1
I-102×102×7.9-595	17	0	7	2	16	0
I-102×102×7.9-G	51	-3	42	-2	50	-3
I-102×102×13-U	99	1	87	10	97	2
I-102×102×13-450	58	2	37	11	55	3
I-102×102×13-595	11	-2	7	-1	10	-2
I-102×102×13-G	49	-2	52	-14	49	-4
D-76×102×3.2-U	64	-35	45	16	62	-27
D-76×102×3.2-G	40	-8	27	2	38	-6
D-76×102×4.8-U	62	-6	29	11	56	-3
D-76×102×4.8-G	37	-10	12	3	33	-8
D-102×102×4.8-U	88	-9	40	8	81	-7
DH-76×76×4.8-U	77	-5	35	11	69	-2
DH-76×76×4.8-G	41	-12	18	0	37	-10
DH-76×102×3.2-U	48	-17	33	19	46	-12
DH-76×102×3.2-G	25	-2	13	-2	24	-2
DH-76×102×4.1-U	54	-4	24	12	49	-2
DH-76×102×4.8-U	76	0	24	2	67	0
DH-76×102×4.8-G	37	-2	18	-3	34	-2
DH-76×152×4.1-U	52	-9	25	7	49	-7
DH-76×152×4.1-G	30	-10	10	6	27	-8
Average D-U	71	-17	38	12	66	-12
Average D-G	39	-9	20	3	36	-7
Average DH-U	61	-7	28	10	56	-5
Average DH-G	33	-7	15	0	31	-6
Average I-U	87	1	73	3	85	2
Average I-G	48	-1	44	-6	48	-2
Average I-450	49	1	31	5	46	1
Average I-595	14	-2	6	-1	13	-2

1.6.2.1 Effects of cold-forming methods

As discussed in Section 1.4.1, the selection of the RHS specimens allows direct comparisons of residual stresses in untreated RHS cold-formed using different methods and coil materials of different grades. For each of the three groups (i.e. untreated direct-formed regular-strength RHS (D-U), untreated direct-formed high-strength RHS (DH-U), and untreated indirect-formed regular-strength RHS (I-U)), the average values of the overall cross-sectional bending residual stresses are calculated and listed in Table 1.7. The values are $0.66\sigma_y$, $0.56\sigma_y$ and $0.85\sigma_y$, respectively. It can be seen that the direct-forming approach introduces a much lower level of residual stresses in the final RHS product, comparing to the indirect-forming approach. In particular, since the residual stress is a function of the cold-bending curvature rather than the strength of the coil material, the direct-formed high-strength RHS contains the lowest level of residual stress of all. This is consistent with its superior stub column behaviour reported by Tayyebi and Sun [6].

1.6.2.2 Effects of galvanizing and heat treatment

For the groups of galvanized direct-formed regular-strength RHS (D-G), galvanized high-strength direct-formed RHS (DH-G), and galvanized indirect-formed regular-strength RHS (I-G), the average values of the overall cross-sectional bending residual stresses are calculated and listed in Table 1.7. The values are $0.36\sigma_y$, $0.31\sigma_y$ and $0.48\sigma_y$, respectively. By comparing the values to those discussed in Section 1.6.2, it can be seen that the 10-minute hot-dipping process is already very efficient in lowering the residual stresses. For the indirect-formed regular-strength RHS specimens heat treated to 450 ºC (I-450) according to ASTM A1085 [7] or CSA G40.20/G40.21 [8] for a holding time of 30 minutes, the average value of the overall cross-sectional bending residual stresses is $0.46\sigma_y$, which is similar to the average value of the galvanized counterparts. This is consistent with results of the experimental research on galvanized and heat-treated RHS stub columns reported by Tayyebi and Sun [6]. Hence, one can speculate that the 30-minute holding time used in the current industrial practice is excessively long. It should be noted that the aim of the ASTM A1085 [7] and the CSA G40.20/G40.21 [8] heat treatment is to provide a partial relief of residual stress throughout the cross section for better compressive member behaviour. In Canada, such heat treatment justifies the use of a higher column curve in the steel design standard CSA S16-19 [12]. According to the experimental findings of this research, a 10-minute holding time for a heat treatment at 450 ºC serves the purpose already. Hence, the current industrial practice for such heat treatment needs to be revisited. On the other hand, for the indirect-formed regular-strength RHS specimens heat treated to 595 ºC (I-595) according to ASTM A143 [14], the average value of the overall cross-sectional bending residual stresses is only $0.13\sigma_y$. However, when specifying such heat treatment, the trade-off among residual stress, material ductility and strength must be taken into consideration by the designers and fabricators.

1.7 Conclusions

This paper reports the tensile coupon test results of 26 rectangular hollow section (RHS) specimens with different grades (nominal yield strengths from 350 to 690 MPa), produced by different cold-forming techniques (indirect-forming versus direct-forming), and subjected to various post-production heat-treatment and galvanizing processes. Using the sectioning method, a total of 342 strips were carefully machined from the 26 RHS specimens for a comprehensive residual stress measurement.

Based on the residual stress data presented in this paper, and the column test results reported by Tayyebi and Sun [6] as well as Shi et al. [4,5], it can be concluded that the current North American industrial practice for hot-dip galvanizing can effectively reduce the residual stress level in cold-formed HSS (rectangular and circular), similar to a heat treatment process described in ASTM A1085 Supplement S1 [7], and CSA G40.20/G40.21 [8]. This in turn can improve the column behaviour. The holding time of 30 minutes used in the current industrial practice for heat treatment to an ASTM A1085 [7] or CSA G40.20/G40.21 [8] finish might be excessively long. A holding time of 10 minutes for such heat treatment might be sufficient already.

The direct-forming approach introduces a much lower level of residual stresses in the final RHS product, comparing to the indirect-forming approach. In addition, since the residual stress is primarily a function of the cold-bending curvature rather than the strength of the coil material, the direct-formed high-strength RHS contains the lowest level of normalized residual stress.

Nomenclature

B	Measured width
D	Chord length
E	Young's modulus
H	Measured depth
r_i	Inner corner radius
t	Measured thickness
ε	Measured strain
ε_r	Rupture strain of coupons
ε_u	Strain at ultimate stress of coupons
σ_b	Bending residual stress
σ_{in}	Total residual stress on inner surface of RHS in longitudinal direction
σ_m	Membrane residual stress
σ_{out}	Total residual stress on outer surface of RHS in longitudinal direction
σ_u	Measured ultimate stress
σ_y	Measured yield stress
$\sigma_{y,nom}$	Nominal yield stress

Chapter 2: Stub Column Behaviour of Heat-Treated and Galvanized RHS Manufactured by Different Methods

Kamran Tayyebi, Min Sun, *Stub column behaviour of heat-treated and galvanized RHS manufactured by different methods*, J. Constr. Steel Res. 166 (2020) 105910. https://doi.org/10.1016/j.jcsr.2019.105910.

2.1 Abstract

A complementary study showed that hot-dip galvanizing can sometimes significantly change the residual stress properties of cold-formed rectangular hollow sections (RHS). Hot dipping the RHS specimens in a molten zinc bath maintained at 450 ºC for 10 minutes provided a partial residual stress relief comparable to the onerous heat treatment specified in ASTM A1085 and CSA G40.20/G40.21. Hence, further research is needed to: (1) quantify the effects of galvanizing, and (2) determine the optimized heat treatment duration for a partial residual stress relief for improvement of column behaviour. This paper presents a comprehensive experimental investigation including 36 stub column tests. The RHS specimens were manufactured by two dominant cold-forming methods: indirect-forming and direct-forming. The nominal yield stresses of the materials ranged from 350 to 690 MPa. The stub column test matrix included also galvanizing and different degrees of heat treatments. The experimental results, particularly those from the direct-formed high-strength RHS, are compared against the design strengths calculated based on various steel design standards. The compactness criteria in the standards are also evaluated.

2.2 Introduction

The application of galvanized tubular steel structures in bridges, highways, transmission towers, and industrial plants has expanded over the years [2]. Since the service life of the zinc coating is in general longer than the design life of the structure it protects, galvanized steel structures are often maintenance-free [38]. To support the sustainable development agenda, recent investigations [3–5] have been performed on galvanized hollow structural sections (HSS) to further facilitate their applications. It was found that the hot-dipping process can sometimes significantly lower the residual stress level and in turn improve the column behaviour. However, these investigations did not cover a wide range of cross-sectional shapes, dimensions or material grades. The implications of using materials cold-formed by different approaches were not appreciated either. Nevertheless, these investigations concluded that the potential benefits of the hot-dip galvanizing process on material properties should not be neglected, other than the improvement on the durability of structures.

In North America, square and rectangular hollow sections (collectively referred to as RHS herein) of commonly specified sizes are produced as cold-formed members by two methods: (i) indirect-forming, where the coil material is initially cold-formed into a circular section, and subsequently cold-shaped into a rectangular section; or (ii) direct-forming, where the coil material is directly cold-formed into a rectangular shape. Indirect-formed RHS is subjected to high degrees of cold-forming over the entire cross-section. For direct-formed RHS, the cold-forming is only concentrated at the corner regions. Although the appearances of the sections can be similar, the material and structural behaviours of RHS produced by the two methods can sometimes be significantly different [13,15,16,24,39]. It should also be noted that the new generation of direct-formed high-strength RHS products with a nominal yield stress of 690 MPa are now readily available in the North American market. The new high-strength product contains inherently a low level of residual stress as a result of the unique manufacturing process [13,24,39]. Hence, its application can reduce the weight of the structure and save the cost of heat treatment. However, existing design specifications (e.g. [12,29]) do not distinguish the new products from the conventional hollow sections, hindering their widespread application in construction. Recent research efforts [18,21,40–44] have been made to study the structural performances of cold-formed tubular members manufactured from high-strength steel coils with nominal yield stresses in the range of 460 to 1100 MPa [18,20,21,40–43]. It can be concluded from these investigations that the relevant provisions in the existing design standards are in general not directly applicable to high-strength tubular steel members. However, the above research focused only on indirect-formed RHS members. Hence, a comprehensive study on the effects of the direct-forming process on the structural behaviour of regular- and high-strength RHS is deemed necessary.

Associated with cold-forming is the generation of residual stress. In practice, the column behaviour can be improved by specification of a post-cold-forming heat treatment per ASTM A1085 Supplement S1 [7], or for a Class H finish per CSA G40.20/G40.21 [8]. Both standards describe identical heat treatment, at a temperature of 450 ºC or higher, followed by cooling in air. Due to the lack of definitive provisions in ASTM A1085 or CSA G40.20/G40.21, producers typically specify a holding time of 30 minutes once the furnace temperature is stable at 450°C [2,3]. However, it was deduced by Sun and Ma [3] that 30 minutes may be excessive for a partial relief of residual stress (i.e. the improvement of column behaviour can be marginal after 10 minutes). Hence, further research is needed to determine the optimized duration, so that the heat treatment is fit-for-purpose and energy efficient.

In this research, a total of 36 stub columns and 112 tensile coupons were tested to comprehensively investigate the effects of: (1) galvanizing; (2) different cold-forming approaches on coil materials of different strength grades; and (3) heat treatments to different degrees. The stub column test results were compared to the design strengths calculated using various design standards. In particular, the test results from the slender cross sections subjected to different post-cold-forming treatments were used to examine the compactness criteria in the design standards.

2.3 RHS specimens

In this study, a total of 13 cold-formed and untreated parent RHS (direct-formed or indirect-formed) were used to produce 36 RHS specimens subjected to different post-cold-forming treatments (untreated, galvanized, or heat treated to a carefully controlled degree). Eight of the 13 parent RHS are regular-strength, and are manufactured to CSA G40.20/40.21 Gr. 350W Class C [8]. The other five parent RHS are high-strength and direct-formed. The 36 RHS specimens were then used to produce a total of 36 stub columns and 112 tensile coupons. The stub column specimens are listed in Table 2.1. As shown, the nominal external dimensions of the specimens varied from 76 to 152 mm, and the nominal wall thicknesses varied from 3.2 to 13 mm. Hence, the selected RHS covered a wide range of external dimension-to-thickness ratios, corresponding to a wide range of overall (cross-sectional) degrees of cold-working. Each stub column specimen in Table 2.1 is assigned an ID consisted of three components. The first component distinguishes the material by its cold-forming method and strength grade, where DH represents direct-formed high-strength RHS with a nominal yield stress of 690 MPa, while D and C represents direct-formed and indirect-formed RHS with a nominal yield stress of 350 MPa, respectively. The second component shows the nominal dimensions of the parent tube (width×height×wall thickness in mm). The third component indicates the type of post-cold-forming treatment applied to the specimens, where U = as-received untreated cold-formed RHS; G = hot-dip galvanizing at 450 ºC for a duration of 10 minutes; 450 = heat treatment at 450 ºC according to CAN/CSA G40.20/G40.21 for a Class H finish [8] or ASTM A1085 by specifying Supplement S1 [7]; and 595 = heat treatment at an annealing temperature of 595 ºC per ASTM A143 [14]. It should be noted that the heat treatment at both 450 and 595 ºC temperatures had a holding time of 30 minutes in furnace based on the current industrial practice. Prior to the experimental program, the cross-sectional dimensions of all sections were carefully measured using the approach adopted by [3,24] and are summarized in Table 2.1. The nominal dimensions, as indicated by a subscript “n”, are used to calculate the external dimension-to-thickness ratios. As can be seen from Table 2.1, the effects of galvanizing and heat treatment to different degrees can be directly studied. Moreover, with the carefully selected specimens, the effect of different coil material grades can be directly studied [e.g. DH-76×102×3.2 (U and G) vs. D-76×102×3.2 (U and G); and DH-76×102×4.8 (U and G) vs. D-76×102×4.8 (U and G)]. Also, the effect of different cold-forming processes can be directly studied using specimens with similar cross-sectional dimensions [e.g. D-102×102×4.8 (U and G) vs. C-102×102×6.4 (U and G)].

Table 2.1 Dimensions of RHS Stub column specimens

Stub column ID	B (mm)	H (mm)	t (mm)	r (mm)	L (mm)	A (mm^2)	B_n/t_n	H_n/t_n
DH-76×76×4.8-U DH-76×76×4.8-G	76.3	76.6	4.81	8.5	352	1303	16	16
DH-76×102×3.2-U DH-76×102×3.2-G DH-76×102×3.2-U* DH-76×102×3.2-G*	76.9	102.6	3.02	2.6	403	961	24	32
DH-76×102×4.1-U DH-76×102×4.1-G	76.3	101.8	4.06	4.8	402	1252	19	25
DH-76×102×4.8-U DH-76×102×4.8-G	76.6	102.0	4.82	8.9	402	1471	16	21
DH-76×152×4.1-U DH-76×152×4.1-G DH-76×152×4.1-U* DH-76×152×4.1-G*	77.2	153.1	4.04	5.1	503	1639	19	37
D-76×102×3.2-U D-76×102×3.2-G	76.5	101.9	3.03	2.4	402	994	24	32
D-76×102×4.8-U D-76×102×4.8-G	76.4	101.9	4.36	3.4	404	1445	16	21
D-102×102×3.2-U D-102×102×3.2-G	101.1	101.9	3.03	3.4	402	1142	32	32
D-102×102×4.8-U D-102×102×4.8-G	101.6	102.1	4.40	5.6	403	1671	21	21
D-127×127×4.8-U D-127×127×4.8-G	127.0	127.6	4.40	6.6	403	2123	26	26
C-102×102×6.4-U C-102×102×6.4-450 C-102×102×6.4-595 C-102×102×6.4-G	102.1	102.2	6.41	8.0	350	2253	16	16
C-102×102×7.9-U C-102×102×7.9-450 C-102×102×7.9-595 C-102×102×7.9-G	101.9	102.1	7.83	11.7	350	2735	13	13
C-102×102×13-U C-102×102×13-450 C-102×102×13-595 C-102×102×13-G	101.6	101.7	12.90	11.8	350	4180	8	8

* indicates repeated test.

2.4 Material properties

2.4.1 Tensile coupon tests

The material properties of the 36 RHS specimens were obtained via a total of 112 tensile coupon tests. For each direct-formed RHS specimen, one flat coupon and one corner coupon were machined from the cross section. For each in-formed RHS specimen, two flat and four corner coupons were machined and tested to study the effects of the two-step forming process (circular to rectangular) on the tensile stress-strain behaviours at different locations around the cross section. The locations of the tensile coupons are shown in Fig. 2.1. The dimensions of the flat coupons and the testing procedures adopted were in compliance with ASTM E8 [26]. An MTS 810 testing machine with a capacity of 250 KN was used. For testing of the corner coupons, based on the approach suggested by [36,45,46], a pair of pin-loaded connectors were employed. Holes were drilled in the grips of the curved coupons, and tensile loading was applied from the MTS machine to the coupon via the connector (See Fig. 2.2). The loading was applied at a displacement rate of 0.1 mm/min. An extensometer was used to record the elongation of the testing region of the coupons. Strain gauges were also employed to cross reference the extensometer readings. The readings agree well. Hence, credence was given to the accuracy of the tensile coupon test results. An overview of the test setup is shown in Fig. 2.2.

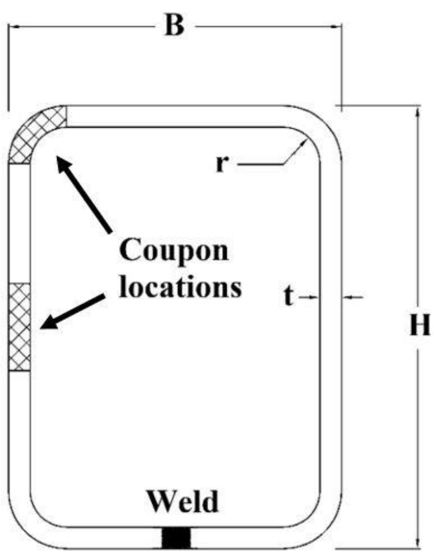

(a) Direct-formed RHS

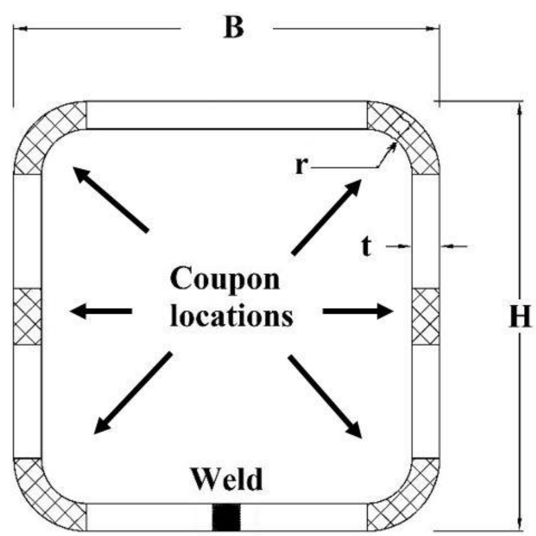

(b) indirect-formed RHS

Figure 2.1 Locations of tensile coupons

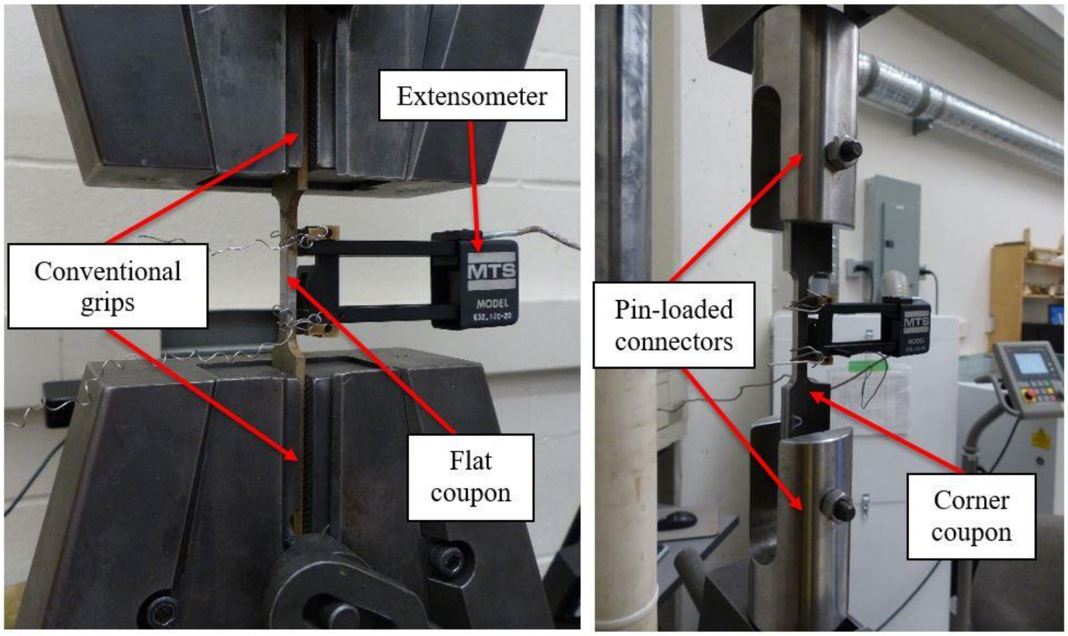

Figure 2.2 Test setup for the flat and corner coupons

2.4.2 Discussion of tensile test results

Typical tensile stress-strain curves of the direct- and indirect-formed RHS materials are shown in Figs. 2.3 and 2.4, respectively. As shown, the corner coupons of the cold-formed and untreated RHS, whether direct-formed or indirect-formed, had rounded stress-strain responses with no sharply defined yield point. Similar responses were observed for the flat coupons of the indirect-cold-formed and untreated RHS, since the flat face materials were also heavily cold-worked during the two-step rolling process. On the other hand, the curves for the flat faces of the direct-cold-formed RHS are less rounded and in general have much higher proportional limits, indicating a much lower level of cold-working at these locations. Since tube manufacturers in general emphasize on achieving a reliably large flat width dimension, it can be deduced that a direct-formed RHS contains a much lower overall (cross-sectional) level of residual stress than its indirect-formed counterpart.

One important finding of the tensile coupon tests is that the hot-dip galvanizing process is very effective in reducing the residual stress levels. As shown in Figs. 2.3 and 2.4, the curves for the coupons machined from the galvanized RHS specimens in general showed clear yield plateaus. Another important finding, as clearly shown in Fig. 2.4, is that the effect of hot-dipping, with a ten-minute duration, is very similar to the onerous heat treatment specified in ASTM A1085 S1 [7] and CSA G40.20/40.21 [8], which includes: (i) increasing the furnace containing the cold-formed hollow section materials to 450 ºC or higher; (ii) holding the furnace temperature for 30 minutes; and (iii) cooling the materials to ambient temperature. The same phenomenon was observed in the stub column tests, which will be discussed in Section 2.6. Hence, comprehensive research is needed in this regard to optimize the current practice for post-cold-forming heat treatment (for improvement of column behaviour) so that it is fit-for-purpose and energy efficient. On the other hand, a clear trade-off between yield strength and residual stress level can be observed by comparing the materials heat treated to 595 ºC to their untreated counterparts.

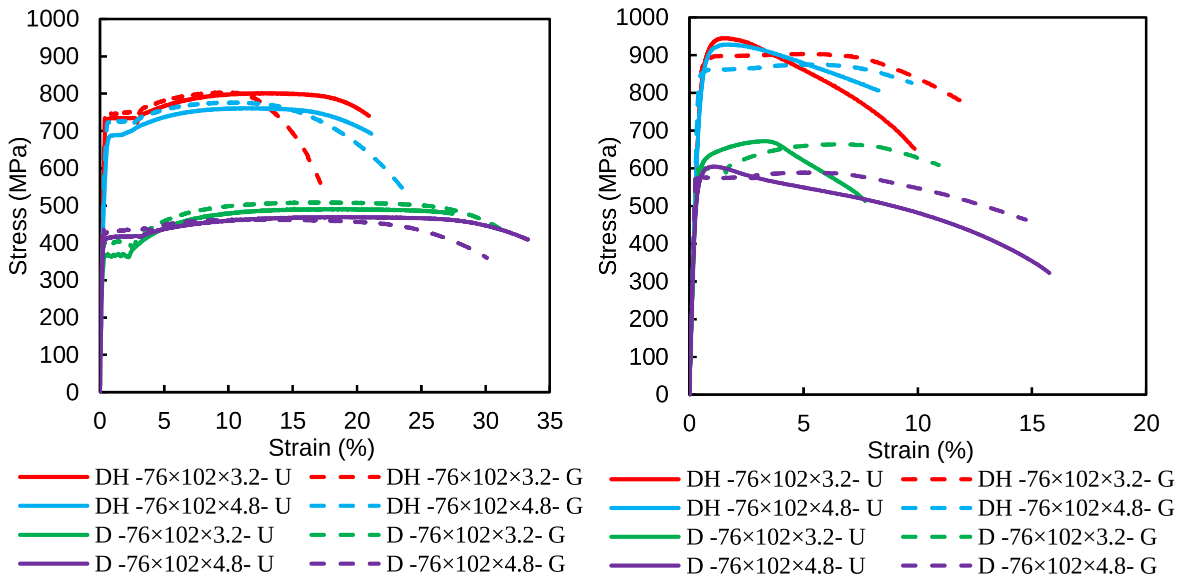

(a) Flat coupon (b) Corner coupon

Figure 2.3 Typical tensile stress-strain curves of direct-formed regular- and high-strength RHS

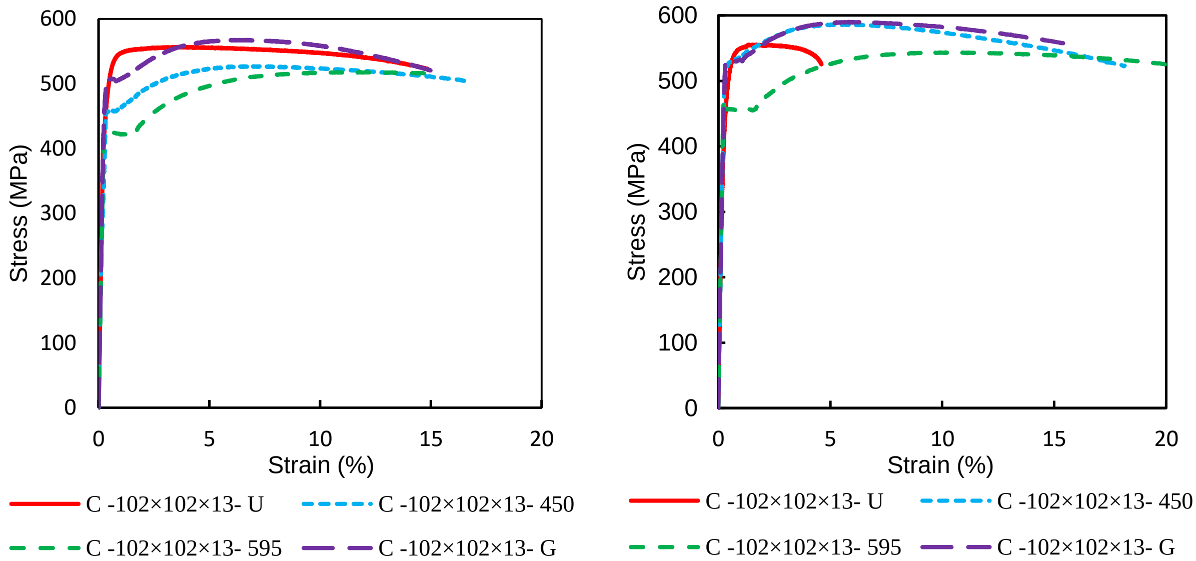

(a) Flat coupon

(b) Corner coupon

Figure 2.4 Typical stress-strain curves of indirect-formed regular-strength RHS

All of the above conclusions are further substantiated by analysing the average values of the key test results of all tensile coupons in Table 2.2, including the yield stress (σ_y), ultimate stress (σ_u), and rupture strain (ε_r). Subscripts "f" and "c" were added to the labels to differentiate the flat and corner coupons. The yield stress was determined using the 0.2% strain offset method. Similar to the commonly applied post-cold-forming heat treatment at 450 ºC for partial residual stress relieving (e.g. for a Class H finish per [8]), the application of hot-dip galvanizing in general has minor effects on (slightly increased) the yield and ultimate strengths of the cold-formed and untreated materials, regardless of the strength grades. On the other hand, for the 595 ºC heat treatment, the trade-off between strength and ductility should be considered by the engineers and fabricators when specifying this post-cold-forming heat treatment.

As discussed previously, the cross-sectional dimensions of the RHS were carefully selected so that direct comparisons among the specimens could be made. All indirect-formed RHS have the same external dimensions but different wall thickness. As shown in Table 2.2, for the three indirect-cold-formed and untreated RHS specimens, as the wall thickness increases, the $\sigma_{y,c}$ / $\sigma_{y,f}$ - ratio decreases and the $\varepsilon_{y,c}$ / $\varepsilon_{y,f}$ - ratio increases. This shows that, as the external dimension-to-thickness ratios increases, the amount of cold-working over different regions of an indirect-cold-formed cross section becomes more uniform. On the other hand, for the direct-formed RHS specimens, high $\sigma_{y,c}$ / $\sigma_{y,f}$ - ratios and low $\varepsilon_{y,c}$ / $\varepsilon_{y,f}$ - ratios were observed for all cross sections with different external dimension-to-thickness ratios, which shows that the cold-working is only concentrated at the corner regions. Hence, it can be concluded that the overall ductility of the entire cross section of a direct-formed RHS is better than its indirect-formed counterpart.

Table 2.2 Average tensile coupon test results

Specimen ID	Corner coupons				Flat coupons				Comparison	
	$\sigma_{p,c}$ (MPa)	$\sigma_{y,c}$ (MPa)	$\sigma_{u,c}$ (MPa)	$\varepsilon_{r,c}$ (%)	$\sigma_{p,f}$ (MPa)	$\sigma_{y,f}$ (MPa)	$\sigma_{u,f}$ (MPa)	$\varepsilon_{r,f}$ (%)	$\frac{\sigma_{y,c}}{\sigma_{y,f}}$	$\frac{\varepsilon_{r,c}}{\varepsilon_{r,f}}$
DH-76×76×4.8-U	360	789	863	19	330	638	767	27	1.24	0.70
DH-76×76×4.8-G	420	878	893	22	450	743	786	28	1.18	0.79
DH-76×102×3.2-U	520	862	945	12	340	730	802	27	1.18	0.44
DH-76×102×3.2-G	680	876	904	14	580	742	803	20	1.18	0.70
DH-76×102×4.1-U	430	879	960	12	350	692	776	26	1.27	0.46
DH-76×102×4.1-G	760	901	909	17	420	711	792	26	1.27	0.65
DH-76×102×4.8-U	560	849	928	16	350	651	761	29	1.30	0.55
DH-76×102×4.8-G	670	816	876	20	520	720	777	26	1.13	0.77
DH-76×152×4.1-U	420	930	1054	14	300	713	815	30	1.30	0.47
DH-76×152×4.1-G	730	918	949	16	460	744	819	28	1.23	0.57
D-76×102×3.2-U	360	601	672	14	175	367	492	34	1.64	0.41
D-76×102×3.2-G	500	599	664	16	280	400	509	32	1.50	0.50
D-76×102×4.8-U	320	568	605	18	225	409	470	39	1.39	0.46
D-76×102×4.8-G	510	574	595	20	280	424	463	36	1.35	0.56
D-102×102×3.2-U	230	567	623	15	220	344	469	32	1.65	0.47
D-102×102×3.2-G	320	536	638	15	310	380	497	32	1.41	0.47
D-102×102×4.8-U	300	574	618	18	260	399	487	38	1.44	0.47
D-102×102×4.8-G	550	596	620	20	320	470	515	30	1.27	0.67
D-127×127×4.8-U	220	553	588	16	190	395	457	40	1.40	0.40
D-127×127×4.8-G	460	574	603	22	310	427	468	37	1.34	0.59
C-102×102×6.4-U	180	496	544	14	170	415	482	30	1.2	0.47
C-102×102×6.4-450	510	550	610	21	350	427	505	31	1.29	0.68
C-102×102×6.4-595	360	434	502	26	350	384	486	33	1.13	0.79
C-102×102×6.4-G	390	508	554	16	360	445	509	27	1.14	0.59
C-102×102×7.9-U	260	539	577	14	210	458	509	25	1.18	0.56
C-102×102×7.9-450	485	566	629	21	420	468	539	26	1.21	0.81
C-102×102×7.9-595	460	485	559	25	390	409	505	31	1.19	0.81
C-102×102×7.9-G	440	539	590	17	400	478	530	22	1.13	0.77
C-102×102×13-U	240	506	563	14	150	483	549	22	1.05	0.64
C-102×102×13-450	390	528	592	19	250	480	566	25	1.10	0.76
C-102×102×13-595	425	459	546	26	380	433	527	30	1.06	0.87
C-102×102×13-G	405	538	596	17	360	493	555	25	1.09	0.81

2.5 Geometric imperfections

As a result of the manufacturing processes such as roll forming, most structural steel members have initial geometric imperfections, including local and global out-of-straightness in the perpendicular directions to the member surfaces [12,29]. The buckling response and load carrying capacity of a steel member under compression is influenced by its geometric imperfections. In this study, the magnitude and distribution of the initial imperfections of all four faces of sections cold-formed by different methods were determined using the seven representative RHS stub column specimens listed in Table 2.3. The measurements were performed on all three sizes of the indirect-formed RHS, and four direct-formed RHS to cover a wide range of external dimension-to-thickness ratios. As shown in Fig. 2.5, the setup consisted of a milling machine worktable on which the specimens were firmly clamped. The worktable provided a flat reference surface for the measurements. A digital Linearly Varying Displacement Transducer (LVDT), with an accuracy of 0.002 mm, was mounted to the head of the milling machine to measure the imperfections, as recommended by [41,42,47–49]. To exclude the possible local distortions due to cold sawing at the ends of the specimens, the starting and finishing points for the measurements were selected to be 30 mm away from the ends [41]. The worktable and the RHS specimen moved together in the longitudinal direction, which allowed the stationary LVDT to capture the imperfections along the 12 lines of interest shown in Fig. 2.6. On each face of an RHS, two of the lines were located near the corners, and a third one at the centreline of the flat face. The difference between the centreline reading (δ_1) and the average of the two near- the-corner readings (δ_1 and δ_3) was calculated and taken as the imperfection. This procedure, which recurred at every 5 mm, was repeated on all four faces, and the overall maximum magnitudes were obtained.

Table 2.3 Results of geometric imperfection measurements

Specimen ID	δ_{max}	Section slenderness ratio $\alpha = (H - 2R)/t$	$\lvert\delta_{max}/ t\rvert$ (%)	$\lvert\delta_{max}/ \alpha\rvert$ (mm)	$\lvert(\delta_{max}/ \alpha)\rvert_{avg}$ (mm)
DH -76×76×4.8- U	0.356	10.4	7.4	0.034	0.023
DH -76×152×4.1- U	0.376	33.4	9.3	0.011	
D -76×102×4.8- U	-0.172	19.8	3.9	0.009	0.014
D -102×102×3.2- U	0.602	29.4	20.0	0.020	
C -102×102×6.4- U	0.314	11.4	4.9	0.027	0.090
C -102×102×7.9- U	0.294	8.1	3.7	0.036	
C -102×102×13- U	0.836	4.0	6.5	0.206	

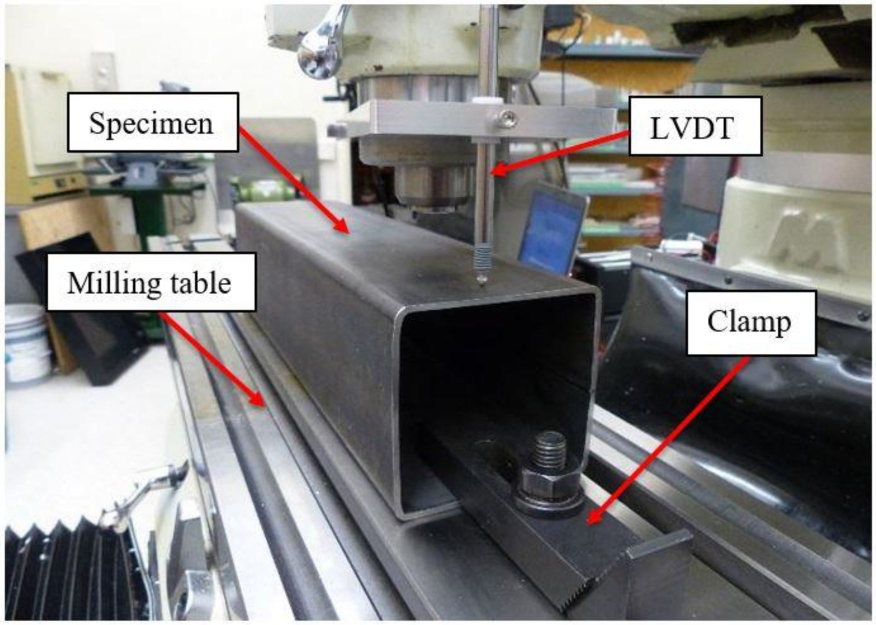

Figure 2.5 Test setup for geometric imperfection measurements

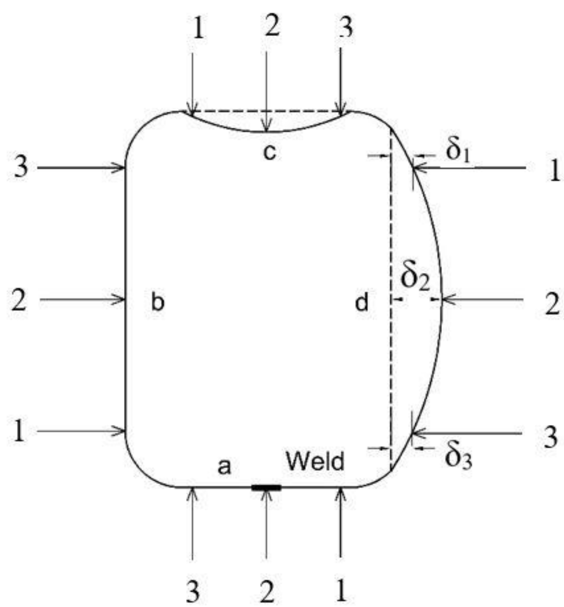

Figure 2.6 Locations of geometric imperfection measurements

Table 2.3 summarizes the key values of the measured magnitudes of the initial imperfections of the seven representative RHS specimens. The geometric imperfection profiles along the lengths of three representative RHS specimens are shown in Figs. 2.7 to 2.9, including one indirect-formed, one direct-formed and one direct-formed high-strength RHS of similar cross-sectional dimensions.

Faces a to d in these graphs are consistent with those shown in Fig. 2.6. In Figs. 2.7 to 2.9, a positive value represents a convex deformation, whereas a negative value represents a concave deformation. It can be seen from the figures that the initial geometric imperfections of the three representative RHS specimens are in general in the same order, regardless of the cold-forming approach used. The maximum local imperfect (δ_{max}) of the seven RHS specimens are listed in Table 2.3. The δ_{max}/t-ratios were also tabulated. Previous research [41,42,47–50] suggested that δ_{max} is also proportional to the cross section slenderness. Hence the δ_{max} values were also normalized in Table 2.3 by $\alpha = (H - 2R)/t$, where H and R are the depth and the outside corner radius of the corresponding RHS. These correlations can easily be used in finite element modelling of the stub columns.

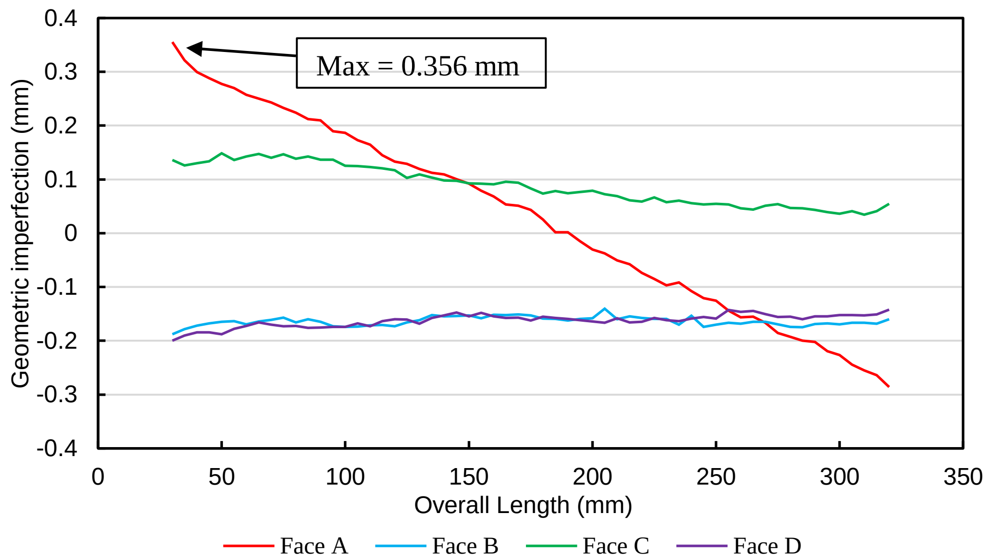

Figure 2.7 Local geometric imperfection profiles of DH-76×76×4.8-U

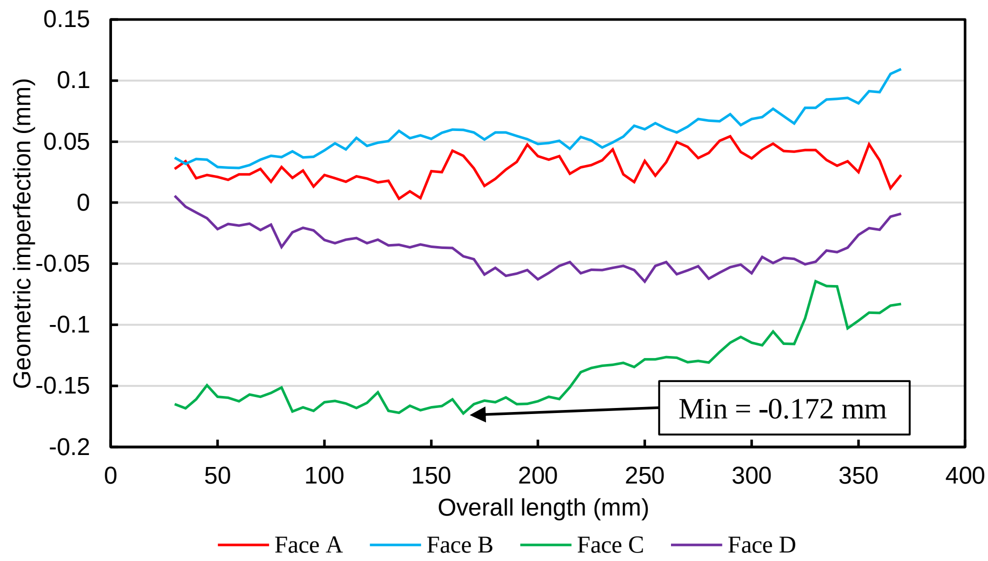

Figure 2.8 Local geometric imperfection profiles of D-76×102×4.8-U

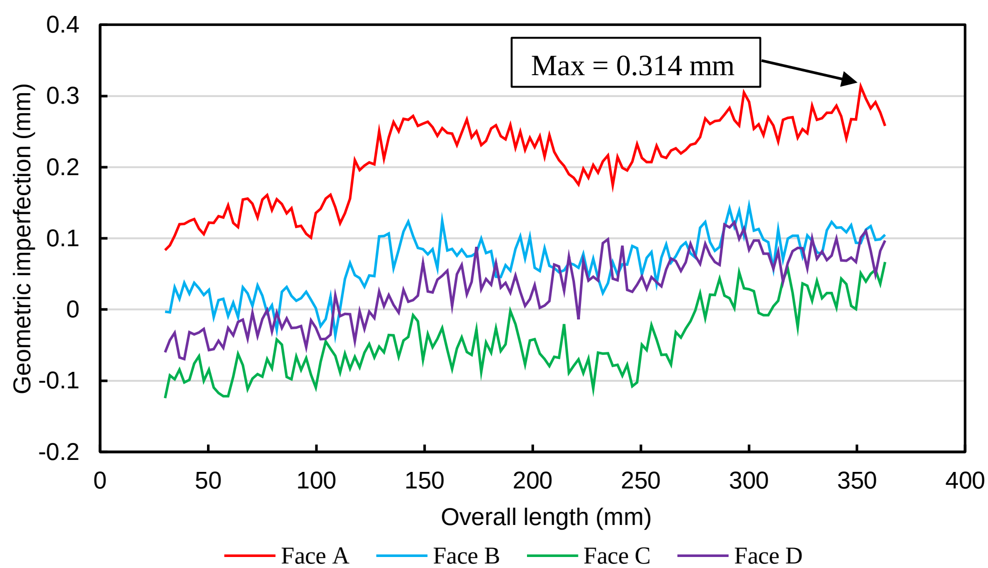

Figure 2.9 Local geometric imperfection profiles of C-102×102×6.4-U

2.6 Stub column tests

The 36 stub column specimens in Table 2.1 were prepared and tested following the widely accepted recommendations documented in the Structural Stability Research Council (SSRC) guide [31]. The lengths of the stub columns were selected to be at least three times the larger external dimension, but no more than 20 times the smaller radius of gyration. This ensures a realistic inclusion of the initial geometric imperfections and residual stresses, while minimizing the likelihood of global buckling. After cutting a stub column into the desired length, both ends were machined flat and normal to the tube's longitudinal axis. Compression tests were conducted using an MTS universal testing machine with a force capacity of 2000 kN. A spherical bearing was installed under the bottom bearing platen to ensure alignment, and to remove any gap between the bearing platens and the specimen ends. Fig. 2.10 shows the stub column test setup. Quasi-static displacement-controlled loading was applied at a rate of 0.5 mm/min. Four LVDTs were arranged next to each flat face to determine the average end shortening. Strain gauges were installed on all faces of all stub columns. An HBM data acquisition system and the CATMAN software package were used to record and log the strain gauge readings at one-second intervals. The strain gauge readings were monitored in real time to ensure alignment of the stub column specimens, and also to determine the onset of local buckling.

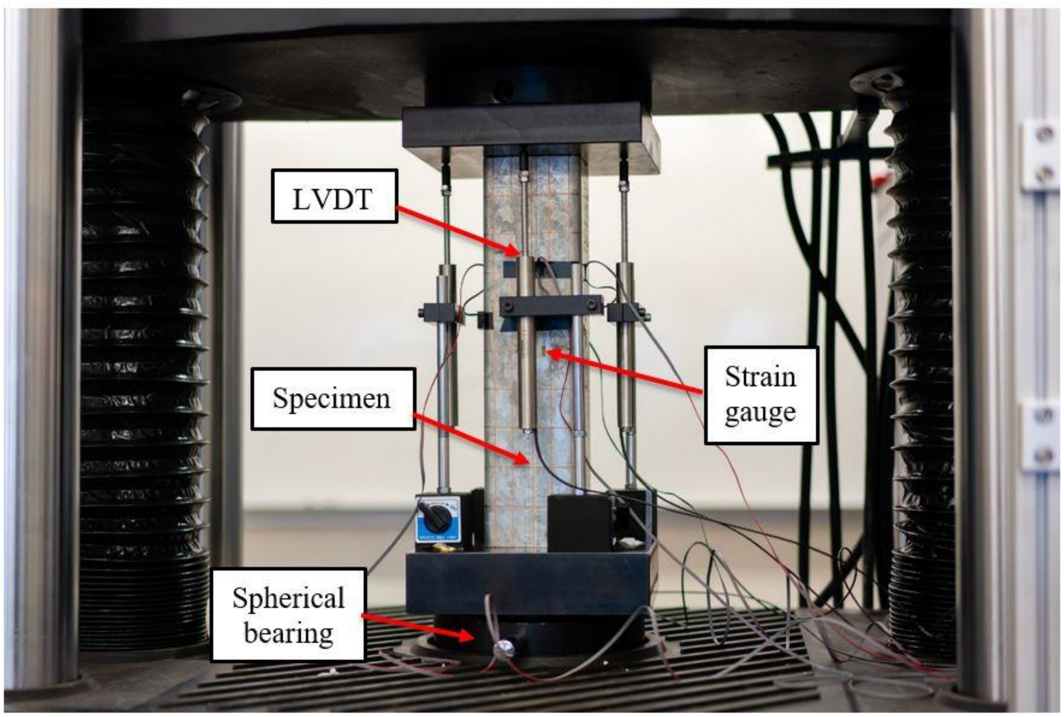

Figure 2.10 Stub column test setup

Representative stub column test results are shown in Fig. 2.11. The compressive stress was determined by dividing the axial load by the cross-sectional area. The cross-sectional area was measured through dividing the weight of each specimen by its length and the density of steel (taken as 7850 kg/m^3 [12]). The axial strain was calculated by dividing the average end shortening based on the LVDT readings by the initial length of the specimen. According to the stress-strain curves, nonslender sections in general reached cross-sectional yielding (CY in Table 2.4) and exhibited pronounced strain hardening responses. On the other hand, responses of slender sections showed early initiation of local buckling (LB in Table 2.4), followed by rapid loss of load carrying capacity. Similar to the findings from the tensile coupon tests, the stub column results herein further substantiated that both hot-dip galvanizing and heat treatment can effectively reduce residual stresses, and increase the uniformity of material properties around the section [3–5,24]. A shown in Figs. 2.11(c) and (d), the compressive stress-strain curves of the hot-dip galvanized specimens and the specimens heat-treated at 450 ºC are comparable. The key results of the stub column tests are summarized in Table 2.4. The cross-sectional compressive yield stress was measured using the 0.2% strain offset method. The Young's modulus was determined based on the average strain gauge data in the linear elastic range. In Table 2.4, the cross-sectional compressive yield and ultimate stresses were compared to their corresponding tensile yield and ultimate stresses of the flat tensile coupons ($\sigma_{y,f}$ and $\sigma_{u,f}$). As shown by the comparisons, due to the strength enhancement at the corner regions, the cross-sectional compressive yield and ultimate stresses are in general higher for the nonslender sections. Four of the indirect-formed specimens with a 13-mm nominal wall thickness had squash loads higher than the capacity of the MTS machine (2000 kN). In these cases, attempts were made to determine the proportional limits of the four specimens.

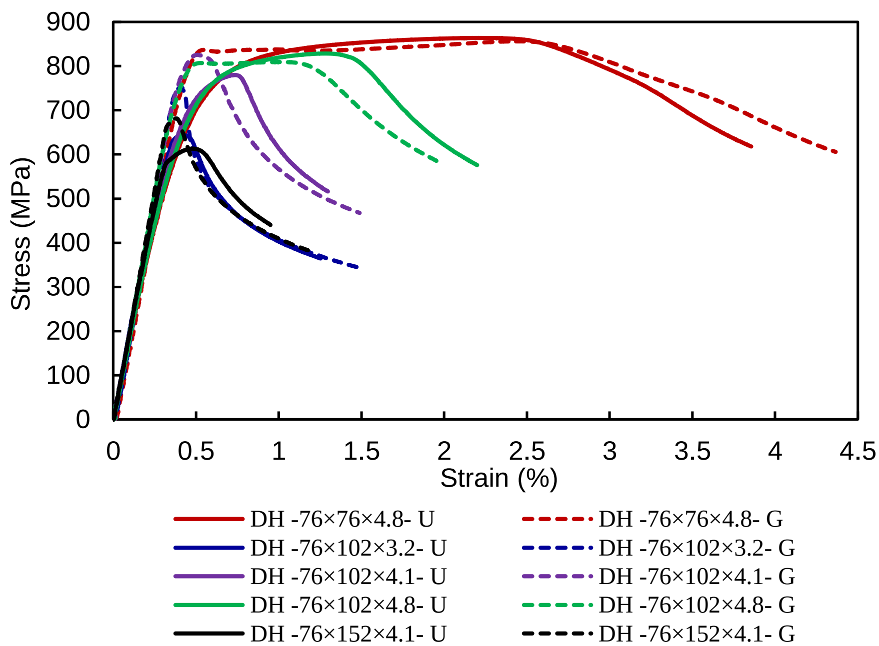

(a) Untreated and galvanized direct-formed high-strength RHS specimens

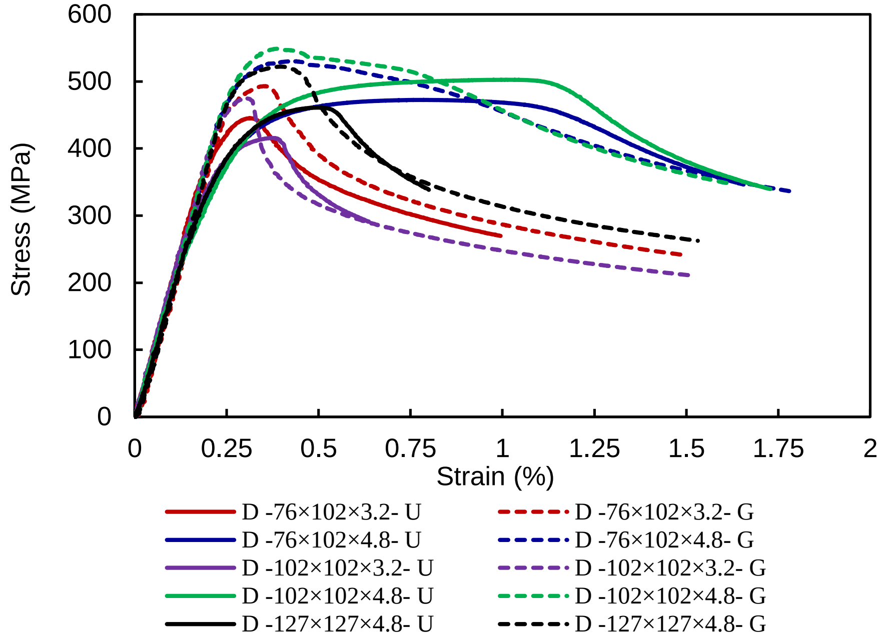

(b) Untreated and galvanized direct-formed regular-strength RHS specimens

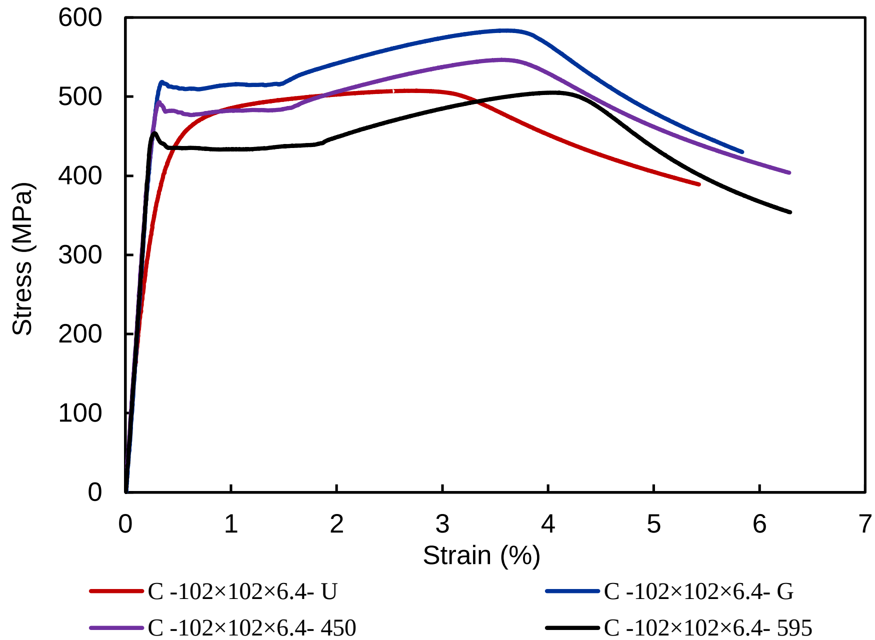

(c) Untreated, galvanized, and heat-treated indirect-formed regular-strength RHS 102×102×6.4

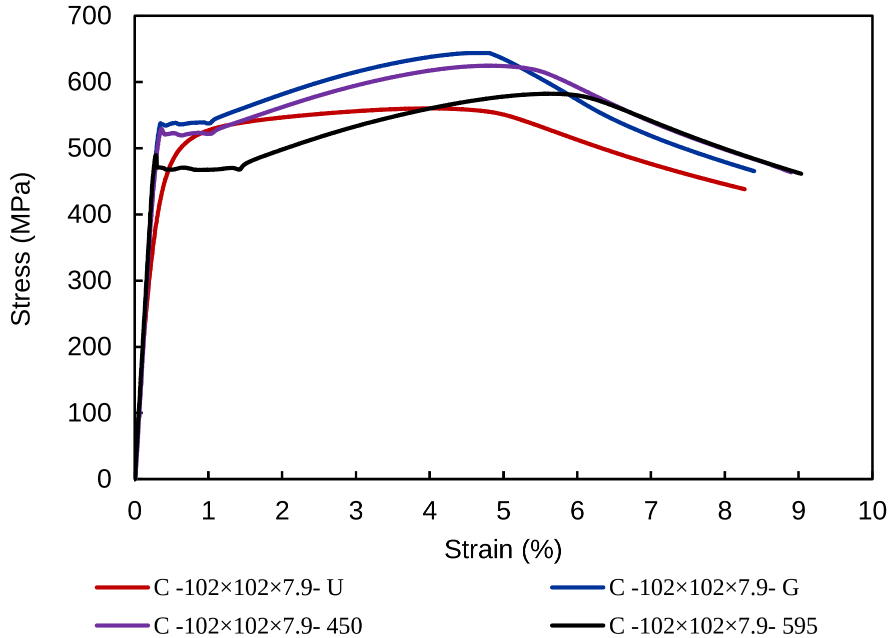

(d) Untreated, galvanized, and heat-treated indirect-formed regular-strength RHS 102×102×7.9

Figure 2.11 Representative stub column test results

Table 2.4 Key stub column test results

Specimen ID	E (GPa)	σ_y (MPa)	σ_u (MPa)	σ_p (MPa)	σ_{lb} (MPa)	Failure mode	$\sigma_y/\sigma_{y,f}$	$\sigma_u/\sigma_{u,f}$	$\sigma_{lb}/\sigma_{y,f}$	$\sigma_p/\sigma_{y,f}$
DH -76×76×4.8- U	202	754	864	320	N/A	CY	1.18	1.13	N/A	0.50
DH -76×76×4.8- G	217	833	856	650	N/A	CY	1.12	1.09	N/A	0.87
DH -76×102×3.2- U	209	643	643	310	625	LB	0.88	0.80	0.86	0.42
DH -76×102×3.2- G	228	755	755	620	N/A	CY	1.02	0.94	N/A	0.84
DH -76×102×3.2- U*	213	661	661	310	640	LB	0.91	0.82	0.88	0.42
DH -76×102×3.2- G*	225	765	765	670	N/A	CY	1.03	0.95	N/A	0.90
DH -76×102×4.1- U	205	757	780	350	N/A	CY	1.09	1.01	N/A	0.51
DH -76×102×4.1- G	223	829	829	660	N/A	CY	1.17	1.05	N/A	0.93
DH -76×102×4.8- U	209	756	828	325	N/A	CY	1.16	1.09	N/A	0.50
DH -76×102×4.8- G	220	806	811	600	N/A	CY	1.12	1.04	N/A	0.83
DH -76×152×4.1- U	209	613	613	325	570	LB	0.86	0.75	0.80	0.46
DH -76×152×4.1- G	221	687	687	650	660	LB	0.92	0.84	0.89	0.87
DH -76×152×4.1- U*	219	618	618	345	600	LB	0.87	0.76	0.84	0.48
DH -76×152×4.1- G*	224	698	698	640	685	LB	0.94	0.85	0.92	0.86
D -76×102×3.2- U	212	445	445	330	N/A	CY	1.21	0.90	N/A	0.90
D -76×102×3.2- G	212	496	496	420	N/A	CY	1.24	0.97	N/A	1.05
D -76×102×4.8- U	210	459	472	150	N/A	CY	1.12	1.00	N/A	0.37
D -76×102×4.8- G	215	529	532	430	N/A	CY	1.25	1.15	N/A	1.01
D -102×102×3.2- U	212	416	416	255	N/A	CY	1.21	0.89	N/A	0.74
D -102×102×3.2- G	216	477	477	380	N/A	CY	1.26	0.96	N/A	1.00
D -102×102×4.8- U	206	473	503	170	N/A	CY	1.19	1.03	N/A	0.43
D -102×102×4.8- G	220	537	551	450	N/A	CY	1.14	1.07	N/A	0.96
D -127×127×4.8- U	205	457	461	245	N/A	CY	1.16	1.01	N/A	0.62
D -127×127×4.8- G	217	523	523	410	N/A	CY	1.22	1.12	N/A	0.96
C -102×102×6.4- U	196	430	507	140	N/A	CY	1.04	1.05	N/A	0.34
C -102×102×6.4- 450	192	480	546	360	N/A	CY	1.12	1.08	N/A	0.84
C -102×102×6.4- 595	193	440	505	410	N/A	CY	1.15	1.04	N/A	1.07
C -102×102×6.4- G	192	510	583	370	N/A	CY	1.15	1.15	N/A	0.83
C -102×102×7.9- U	201	470	560	175	N/A	CY	1.03	1.10	N/A	0.38
C -102×102×7.9- 450	190	525	625	350	N/A	CY	1.12	1.16	N/A	0.75
C -102×102×7.9- 595	191	470	582	425	N/A	CY	1.15	1.15	N/A	1.04
C -102×102×7.9- G	197	535	644	350	N/A	CY	1.12	1.22	N/A	0.73
C -102×102×13- U	171	N/A	N/A	150	N/A	N/A	N/A	N/A	N/A	0.31
C -102×102×13- 450	194	N/A	N/A	360	N/A	N/A	N/A	N/A	N/A	0.75
C -102×102×13- 450	195	N/A	N/A	N/A	N/A	N/A	N/A	N/A	N/A	0.75
C -102×102×13- G	193	N/A	N/A	380	N/A	N/A	N/A	N/A	N/A	0.77

* indicates a repeated test.

2.6.1 Stub column strengths

By comparing the stub column test results of the 15 untreated RHS specimens (including RHS cold-formed by different methods and the repeated tests) with their 15 galvanized counterparts in Table 2.4, it was found that the hot-dipping process (with a duration of 10 minutes) increased on average the cross-sectional yield stress by 13%. This is consistent with the experimental observations by [3,5]. As shown by the experimental evidence discussed in Section 2.4.2, the galvanizing process had minor effects on the material yield stress based on the tensile coupon test results. Hence, the increase in the stub column load carrying capacity (i.e. the increase in the cross-sectional yield stress) is mainly due to the effective reduction of residual stress levels. Due to the same reason, the galvanizing process increased on average the cross-sectional ultimate stress by 11% based on the results in Table 2.4. Similar to hot-dip galvanizing, heat treatment at 450 ºC (with a holding time of 30 minutes based on the current practice) on average increased the cross-sectional yield and ultimate stresses of the untreated Class C indirect-formed RHS by 12% and 10%, respectively. Hence, the holding time used in the current practice for an ASTM A1085 S1 finish [7], or a CSA G40.20/40.21 Class H finish [8] may be excessively long. In other words, the improvement on column behaviour may be very marginal after a ten-minute holding time.

On the other hand, heat treatment at 595 ºC was shown to have a negligible influence on the load carrying capacities of the stub column specimens. This is because, although the 595 ºC heat treatment is very effective in lowering the residual stress levels, such improvement is offset by the reduction in material yield and ultimate stresses. This is consistent with the findings from the tensile coupon tests. Hence, the 595 ºC heat treatment per ASTM A143 [14], which consumes more energy than the 450 ºC heat treatment per [7,8], should not be specified for improvement of column behaviour.

2.6.2 Local buckling behaviour

Among the 36 stub column tests, six specimens failed by local buckling (LB in Table 2.4). To determine the local buckling stresses (σ_{lb}), the vertical tangent method, suggested by Roorda and Venkataramaiah [51], was adopted. For this purpose, the strain gauge readings were used to establish the compressive stress-strain relationships of all four faces of an RHS stub column (see Fig. 2.12 for an example). As shown, the stress-strain curves of the faces subjected to local plate buckling showed a reduction in the compressive strains. For each of the plate elements that failed by local buckling, the stress at the maximum compressive strain was determined as the local buckling stress. Fig. 2.12 illustrates the determination of the local buckling stress of DH-76×102×3.2-U. Since the location at which the local buckling initiates may not coincide with where the strain gauges are installed, this method provides an upper bound approximation. The local buckling stresses were normalized by the yield stresses of the corresponding tensile coupons from the flat faces in Table 2.4. It can be noticed from Fig. 2.12 that the webs of DH-76×102×3.2-U (faces 1 and 3) experienced local buckling almost simultaneously. This not only indicates a symmetrical distribution of strength and residual stress properties about the transverse axis, but also substantiates the proper alignment of the stub column within the loading frame. The σ_{lb}-values for the six specimens failed by local buckling are listed in Table 2.4.

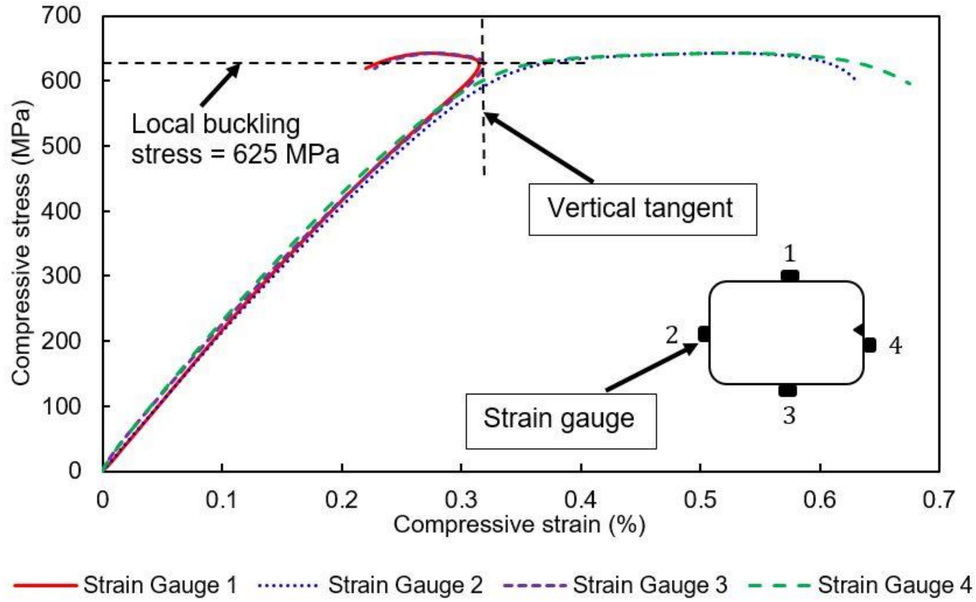

Figure 2.12 Vertical tangent method to determine the local buckling stress of DH-76×102×3.2-U

As shown in Table 2.4, stub column specimen DH-76×102×3.2-U failed by local buckling during the test. On the other hand, after the application of hot-dip galvanizing, DH-76×102×3.2-G exhibited compact section behaviour and exceeded its corresponding squash load ($A\sigma_{y,f}$). The cross-sectional yield stress of DH-76×102×3.2-G was 17% higher than that of DH-76×102×3.2-U. To further substantiate this experimental evidence, two repeated tests was performed (DH-76×102×3.2-U* vs. DH-76×102×3.2-G* in Table 2.4), where after galvanizing the failure mode also changed from local buckling to cross-sectional yielding, and a 16% strength increase was observed. Similar responses were observed when testing: (i) DH-76×152×4.1-U vs. DH-76×152×4.1-G, and (ii) DH-76×152×4.1-U* vs. DH-76×152×4.1-G*. The hot-dipping process raised on average the local buckling stress by 15%, and an average strength increase of 13% was found. Hence, the application of hot-dip galvanizing, similar to heat treatment, is effective in increasing stub column capacity, delaying local buckling, and can potentially convert a slender cross section to a compact one. The effects of galvanizing on the slender sections under compression will be further discussed by examining the compactness criteria in various design standards in Section 2.7.

2.6.3 Proportional limits

One can see the significance of residual stresses over a cross section by superimposing the applied stress on them. As the loading increases, the summation of the applied and residual stresses causes some portions of the cross section to yield before others. The resulting behaviour can be analysed using the "effective section" concept [24]. Portions of the cross-section that have yielded no longer contribute to the stiffness of the cross section, but still carry their portion of the applied load. Hence, proportional limit is an indicator of the maximum compressive residual stress within a cross section. The proportional limits (σ_p) of all stub columns are listed in Table 2.4. Representative curves and values are shown in Figs. 2.13 and 2.14.

As shown in Table 2.4, the proportional limits of the direct-formed RHS stub columns are in general much higher than their indirect-formed counterparts. As shown in Figs. 2.13 and 2.14, the effects of hot-dip galvanizing and the 450 ºC heat treatment per [7,8] on raising the proportional limit are nearly the same. The 595 ºC heat treatment per [14] is the most effective among the three in raising the proportional limits. Hence, it may be more suitable for prevention of corner cracking in thick-walled RHS during welding and galvanizing [3].

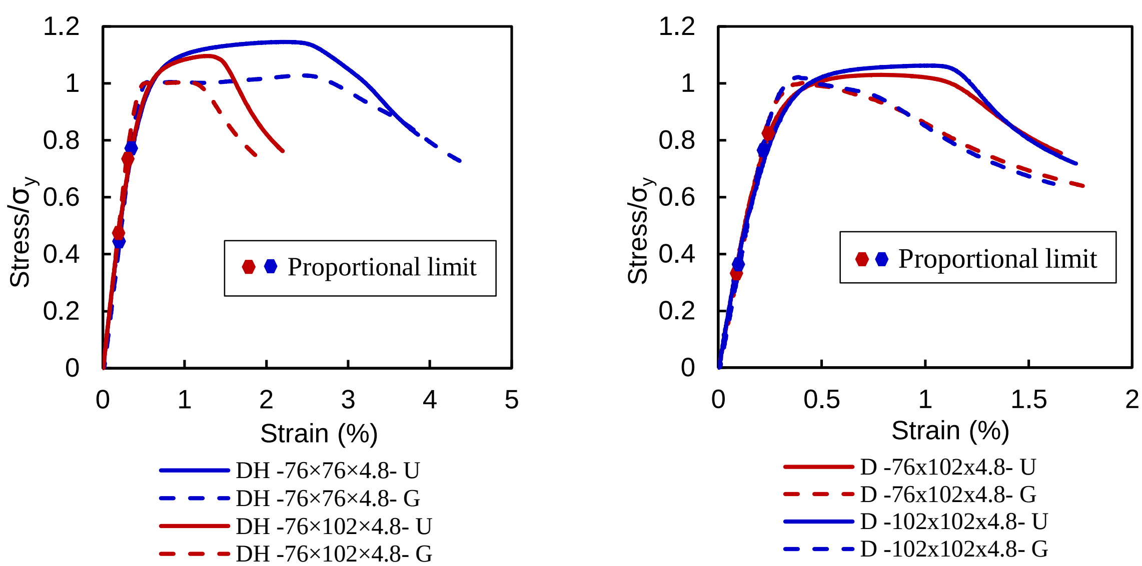

(a) Direct-formed high-strength RHS

(b) Direct-formed regular-strength RHS

Figure 2.13 Normalized stress-strain responses of direct-formed RHS

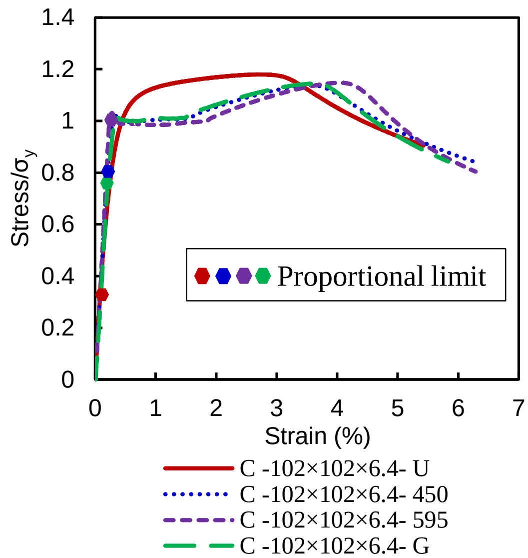

(a) C -102×102×6.4

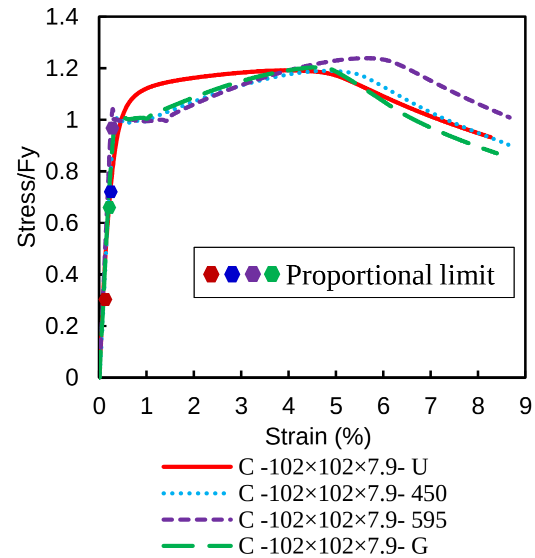

(b) C-102×102×7.9

Figure 2.14 Normalized stress-strain responses of indirect-formed regular-strength RHS

2.7 Evaluation of relevant design provisions

2.7.1 Design strengths

One objective of this research is to compare the stub column test results of the direct-formed regular- and high-strength RHS with the predicted values using various design standards. For the 24 direct-formed RHS specimens, the unfactored axial compressive resistances based on CSA S16-19 [12], ANSI/AISC 360-16 [29], EN-1993-1-1 [27] and the Direct Strength Method in AISI S100-16 [52] were calculated and shown in Table 2.5. The mean values and coefficients of variation for high-strength specimens failed in cross-sectional yielding (DH-CY), high-strength specimens failed in local buckling (DH-LB), and regular-strength specimens failed in cross-sectional yielding (D-CY) are also listed in Table 2.5. As shown, the predictions from various design standards are very conservative for all direct-formed specimens, regardless of the failure modes or the strength grades. In Canada, the steel design standard CSA S16-19 [12] uses two column curves and assigns heat-treated HSS to the upper curve and cold-formed HSS to the lower curve. The former needs to be heat treated to 450 ºC or higher for a Class H finish per CSA G40.20/40.21 [8]. Previous research suggested that the column behaviour of a direct-formed RHS is similar to that of an indirect-formed and heat treated Class H RHS. However, further research is need to develop column design provisions suitable for direct-formed RHS with different strength grades, external dimension-to-thickness ratios, and subjected to different post-cold-forming treatments.

Table 2.5 Comparison of experimental stub column test results with the predicted design values

Specimen ID	P_{exp} (KN)	Failure mode	P_{exp}/P_y*	P_{exp}/P_{CSA}	P_{exp}/P_{EC3}	P_{exp}/P_{AISC}	P_{exp}/P_{DSM}
DH-76×76×4.8-C-U	1116	CY	1.29	1.36	1.35	1.37	1.37
DH-76×76×4.8-C-G	1116	CY	1.12	1.17	1.17	1.18	1.18
DH-76×102×3.2-C-U	666	LB	0.95	1.07	1.09	1.07	1.11
DH-76×102×3.2-C-G	773	CY	0.96	1.22	1.24	1.21	1.24
DH-76×102×3.2-C-U**	678	LB	1.08	1.09	1.11	1.09	1.13
DH-76×102×3.2-C-G**	784	CY	1.09	1.24	1.26	1.22	1.25
DH-76×102×4.1-C-U	1052	CY	1.17	1.23	1.24	1.24	1.24
DH-76×102×4.1-C-G	1109	CY	1.20	1.27	1.27	1.28	1.28
DH-76×102×4.8-C-U	1276	CY	1.30	1.35	1.36	1.36	1.36
DH-76×102×4.8-C-G	1241	CY	1.16	1.19	1.20	1.20	1.20
DH-76×152×4.1-C-U	1043	LB	0.88	1.11	1.12	1.09	1.13
DH-76×152×4.1-C-G	1169	LB	0.89	1.20	1.22	1.17	1.20
DH-76×152×4.1-C-U**	1052	LB	0.95	1.11	1.13	1.10	1.14
DH-76×152×4.1-C-G**	1189	LB	0.97	1.22	1.24	1.19	1.22
D-76×102×3.2-C-U	459	CY	1.21	1.27	1.26	1.27	1.27
D-76×102×3.2-C-G	507	CY	1.24	1.28	1.28	1.29	1.29
D-76×102×4.8-C-U	679	CY	1.09	1.16	1.15	1.17	1.17
D-76×102×4.8-C-G	757	CY	1.18	1.25	1.24	1.25	1.25
D-102×102×3.2-C-U	478	CY	1.18	1.22	1.22	1.23	1.23
D-102×102×3.2-C-G	539	CY	1.22	1.25	1.24	1.25	1.25
D-102×102×4.8-C-U	839	CY	1.20	1.26	1.26	1.27	1.27
D-102×102×4.8-C-G	913	CY	1.13	1.17	1.16	1.17	1.17
D-127×127×4.8-C-U	969	CY	1.12	1.16	1.16	1.16	1.16
D-127×127×4.8-C-G	1091	CY	1.17	1.21	1.20	1.21	1.21
Mean $^{DH\text{-}CY}$				1.26	1.27	1.27	1.27
COV $^{DH\text{-}CY}$				0.058	0.057	0.058	0.058
Mean $^{DH\text{-}LB}$				1.16	1.18	1.14	1.18
COV $^{DH\text{-}LB}$				0.057	0.055	0.049	0.046
Mean $^{D\text{-}CY}$				1.22	1.22	1.23	1.23
COV $^{D\text{-}CY}$				0.037	0.036	0.037	0.037

* $P_y = A_c \times \sigma_{y,c} + A_f \times \sigma_{y,f}$; $A_f = 2\,[(H - 4t)t + (B - 4t)t]$, $A_c = A - A_f$

** indicates a repeated test.

2.7.2 Yield slenderness limits

Another objective of this research is to examine the compactness criteria in various design standards for the direct-formed RHS. The slenderness limits in various steel design standards are in general established based on the elastic critical local buckling stress of a plate element under consideration. To account for the cross-sectional deterioration due to the existence of compressive residual stress, design standards generally specify limits stricter (i.e., lower) than the theoretical values by imposing a conservative empirical reduction to the latter [24]. Cross-section classification and column design rules in existing steel design standards do not differentiate RHS produced by different cold-forming methods. However, previous research [13,24,39] showed that the variation in residual stress levels and other mechanical properties in RHS produced by different cold-forming methods can sometimes be significantly different. The direct-forming method, which is the predominant cold-forming method in China and is also used in North America, generally produces lower residual stress. In this section, the experimental results of the direct-formed high-strength RHS (untreated and galvanized) are used to examine the slenderness limits in CSA S16-19 [12] and AISC 360-16 [29] well as the theoretical elastic critical local buckling stress of a plate element under compression [53].

The slenderness limits in various steel design specifications are based on the elastic plate buckling stress [53]. The critical buckling stress (σ_{cr}) of a plate is written as:

$$\sigma_{cr} = \frac{\pi^2 E}{12(1-\nu^2)} \cdot \frac{k}{(b/t)^2} \qquad (2.1)$$

Where,
E = Young's modulus = 200,000 MPa;
υ = Poisson's ratio = 0.3;
k = elastic boundary coefficient based on the boundary condition of the plate element;
b = width of the stiffened compression element; and
t = thickness of the plate element.

The b/t limits for RHS under uniform compression in CSA S16-19 [12] and AISC 360-16 [29] are based on [53,54]. It was suggested by [54] that the behaviour of a flat face is similar to a simply supported steel plate under uniform edge compression where k can be taken as 4.0. To standardize the slenderness limits from various references, the width-to-thickness ratios can be normalized into the following format:

$$\lambda = \frac{b}{t\sqrt{\frac{E_f}{\sigma_{y,f}}}} \qquad (2.2)$$

To prevent elastic local buckling from occurring before steel yields, the theoretical normalized slenderness limit, λ = 1.90 (see Table 2.6), can be obtained by replacing σ_{cr} in Eq. 2.1 with σ_y. The formulae for cross section classification for RHS member under compression from CSA S16-19 [12] and AISC 360-16 [29] are shown in Table 2.6. The two formulae are modified using Eq. 2.2 to calculate the normalized slenderness limits (λ). It can be seen from Table 6 that, to account for the effects of residual stress and initial geometric imperfection, the λ-values for the design standards [12,29] are lower than the theoretical value of 1.90. It should be noted that the relevant provisions in [12,29] were developed based on testing of indirect-formed RHS. Since the overall levels of residual stresses in the direct-formed (regular- or high-strength) RHS are often considerably lower than their indirect-formed counterparts, the slenderness limit should be closer to 1.90. To assess the performance of the direct-formed high-strength RHS against the yield slenderness limits set out in the design standards, the normalized stub column strengths are plotted against λ in Fig. 2.15. It can be seen from the figure that:

(1) The application of galvanizing in some cases converted slender sections into compact sections.

(2) According to the linear trend lines, the slenderness limits in CSA S16-19 [12] and AISC 360-16 [29] are excessively conservative for direct-formed high-strength RHS (both untreated and galvanized). Hence, the existing slenderness limits have the tendency to misjudge a nonslender direct-formed section as a slender section, resulting in unnecessary penalty, member strength underestimation and more importantly waste of material.

Hence, further research needs to be conducted to generate more data and to propose realistic slenderness limits for direct-formed RHS (both untreated and galvanized).

Table 2.6 Yield slenderness limits

Reference	Formula	Normalized yield slenderness limit
CSA S16-19 [12]	$\frac{b}{t} \leq \frac{670}{\sqrt{\sigma_y}}$	$\lambda = 1.50$
AISC 360-16 [29]	$\frac{b}{t} \leq 1.40\sqrt{\frac{E}{\sigma_y}}$	$\lambda = 1.40$
Elastic plate buckling [53,54]	$\frac{b}{t} \leq \sqrt{\frac{k\pi^2 E}{12(1-\nu^2)\sigma_y}}$ where $k = 4$ and $\nu = 0.3$	$\lambda = 1.90$

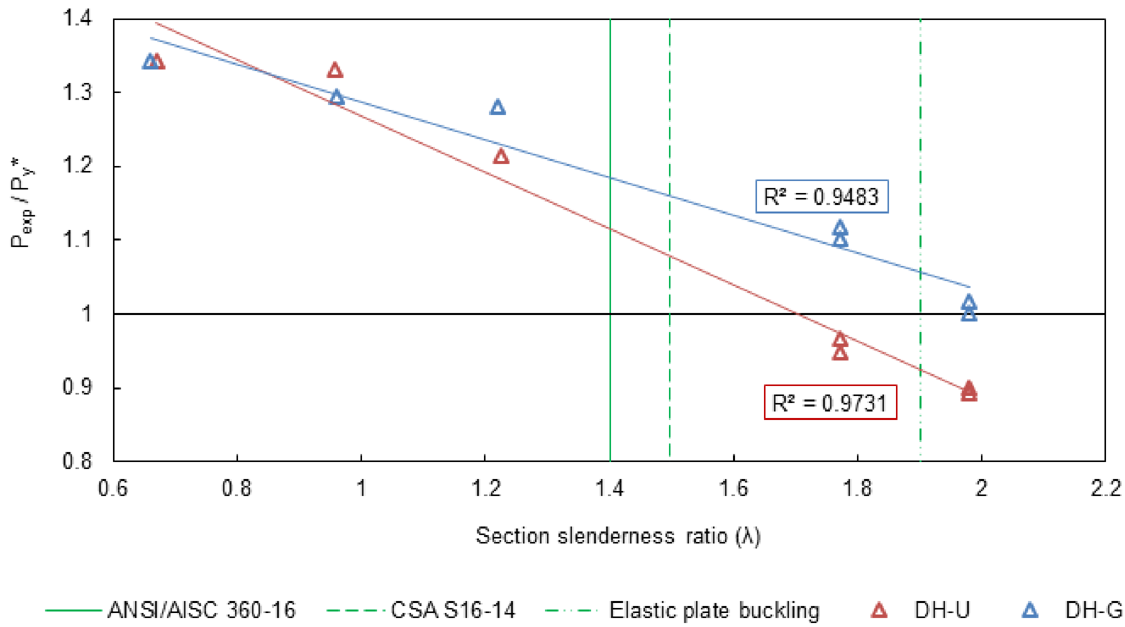

Figure 2.15 Comparison of stub column test results for direct-formed high-strength RHS to slenderness limits

2.8 Conclusions

The main objectives of this research are to: (1) quantify the effects of galvanizing, and (2) examine the current industrial practice on heat treatment for a partial residual stress relief for improvement of column behaviour. A total of 112 tensile coupons and 36 stub columns were tested. The specimens were prepared from RHS materials cold-formed by different methods (indirect-forming versus direct-forming), using coil materials with different strength grades. The nominal yield stresses of the materials ranged from 350 to 690 MPa. The test matrix included also galvanizing and different degrees of heat treatments. The slenderness limits and compression member design rules in various design standards are evaluated using the experimental data. It can be concluded based on the available data from this research that:

(1) Direct-formed RHS generally contain a lower overall (cross-sectional) level of residual stress than its indirect-formed counterpart.

(2) The overall ductility of the entire cross section of a direct-formed RHS is generally better than its indirect-formed counterpart.

(3) For justification of the use of a higher column curve in CSA S16-19 [12], a post-cold-forming heat treatment to 450 ºC or higher for an ASTM A1085 S1 finish [7], or a CSA G40.20/40.21 Class H finish [8] needs to be performed. According to the experimental evidence in this research, the 30-minute holding time used in the current industrial practice may be excessively

long. The improvement on column behaviour may be very marginal after a ten-minute holding time.

(4) The 595 ºC heat treatment per ASTM A143 [14], which consumes more energy than the 450 ºC heat treatment per [7,8], has very minor effect on the load carrying capacity of the stub columns, due to the trade-off between residual stress and material strength. Such heat treatment should not be specified for improvement of column behaviour.

(5) Base on the stub column test data in this research, the effects of galvanizing and post-cold-forming heat treatment to 450 ºC or higher for a 30 minutes holding time are similar. Both can be effective in increasing stub column capacity, delaying local buckling, and can potentially convert a slender cross section to a compact one.

(6) The predicted strengths based on various design standards are very conservative for all direct-formed stub column specimens, regardless of the failure modes and the strength grades. The column behaviour of a direct-formed RHS can be similar to that of an indirect-formed and heat treated Class H RHS. However, further research is need to develop column design rules suitable for direct-formed RHS with different strength grades, external dimension-to-thickness ratios, and subjected to different post-cold-forming treatments.

(7) The slenderness limits in CSA S16-19 [12] and AISC 360-16 [29] are excessively conservative for direct-formed high-strength RHS (both untreated and galvanized). Hence, the existing slenderness limits have the tendency to misjudge a nonslender direct-formed section as a slender section, resulting in unnecessary penalty, member strength underestimation and more importantly waste of material. Further research needs to be conducted to generate more data and to propose realistic slenderness limits for direct-formed RHS.

Nomenclature

A	Cross-sectional area of stub column
b	Width of stiffened compression element
B	Measured width of RHS
B_n	Nominal width of RHS
E	Young's modulus
E_c	Young's modulus obtained from testing of corner coupon
E_f	Young's modulus obtained from testing of flat coupon
P_{AISC}	Unfactored design strength from ANSI/AISC 360-16
P_{CSA}	Unfactored design strength from CSA S16-14
P_{DSM}	Unfactored design strength from direct strength method
P_{EC3}	Unfactored design strength from EN 1993-1-1
P_{exp}	Experimental ultimate load for stub column
P_y	Theoretical squash load of stub column ($A\sigma_{y,f}$)
H_n	Nominal depth of RHS
H	Measured depth of RHS
k	Plate buckling coefficient
L	Length of stub column
r	Inside corner radius of RHS
R	Outside corner radius of RHS
t	Measured wall thickness
t_n	Nominal wall thickness
α	Slenderness ratio
$\varepsilon_{r,c}$	Rupture strain of corner coupon
$\varepsilon_{r,f}$	Rupture strain of flat coupon
λ	Normalized slenderness limit
δ_1, δ_2, δ_3	Local geometric imperfection
δ_{max}	Maximum geometric imperfection
σ_{cr}	Elastic critical buckling stress
σ_p	Proportional limit stress
σ_{lb}	Local buckling stress
σ_u	Ultimate stress

$\sigma_{u,c}$	Ultimate stress of corner coupon
$\sigma_{u,f}$	Ultimate stress of flat coupon
σ_y	Yield stress
$\sigma_{y,c}$	Yield stress of corner coupon
$\sigma_{y,f}$	Yield stress of flat coupon

Chapter 3: Design of Direct-Formed Square and Rectangular Hollow Section Stub Columns

Kamran Tayyebi, Min Sun, *Design of direct-formed square and rectangular hollow section stub columns*, J. Constr. Steel Res. 178 (2021) 106499.
https://doi.org/https://doi.org/10.1016/j.jcsr.2020.106499.

3.1 Abstract

Provisions in the current steel design standards do not differentiate square and rectangular hollow sections (SHS and RHS) members cold-formed by different approaches. Research on the effect of post-cold-forming hot-dip galvanizing on residual stress and stub column behaviour is also insufficient. Complementary experimental studies showed that: (1) the stub column behaviour of a direct-formed SHS/RHS (regular-strength or high-strength) is superior to its indirect-formed counterpart; (2) the current codified slenderness limits and the effective width method tend to misjudge a nonslender direct-formed section as a slender section, resulting in an unnecessary penalty and member strength underestimation; and (3) post-cold-forming galvanizing can effectively relieve residual stress and improve the stub column behaviour of a direct-formed SHS/RHS. This research presents a finite element (FE) study with models developed using previously measured residual stresses, strength properties and geometric imperfections in direct-formed SHS/RHS. The modelling approach was validated against previous experimental data from 24 stub column tests. The stub column behaviour of direct-formed regular- and high-strength SHS/RHS (untreated and galvanized) was studied via an FE parametric study, including 624 models to cover a wide range of cross-sectional dimensions and material properties. The relevant provisions in the current design standards were examined. The experimental and FE data justifies the use of higher design curves for direct-formed SHS/RHS (untreated and galvanized). Modifications to the existing design rules for SHS/RHS stub columns against cross-sectional yielding or local buckling were proposed.

3.2 Introduction

Square and rectangular hollow sections (SHS and RHS) in North America are manufactured predominantly by two approaches:

(1) Direct-forming: cold-forming the coil material directly to a square or rectangular shape, and closing the section using ERW. The direct-forming sequence is demonstrated in Fig. 1.3(b).

(2) Indirect forming: cold-forming the coil material into a circular shape initially, followed by closing the section using electric resistance welding (ERW), and finally cold-shaping the circular shape into a square or rectangular shape. The indirect-forming sequence is shown in Fig. 1.3(d).

Recent investigations (e.g. [18,20,21,40–43]) have been conducted on indirect-formed SHS/RHS with nominal yield stresses from 460 to 1100 MPa. Literature reviews in [6,55] pointed out that dedicated research on the effects of direct forming and the post-production processes (e.g. galvanizing and heat treatment to different degrees) on member behaviour is still insufficient.
Design rules in the existing steel standards do not differentiate SHS/RHS members cold-formed by different approaches. Based on a comprehensive experimental research program [6,55] consisting of tensile coupon tests, stub column tests, residual stress measurements and geometric imperfection measurements, it was found that direct-formed SHS/RHS (with nominal yield strengths of 350 MPa and 690 MPa) have superior stub column behaviour than their indirect-formed counterpart, primarily due to an inherently low level of residual stress.

In practice, by performing a heat treatment to a CSA G40.20/G40.21 Class H finish [8], or an ASTM A1085 Supplement S1 finish [7], a higher column curve in the Canadian steel design standard [12] can be used. Producers typically specify a 30-minute holding time once the furnace temperature is stable at 450°C or higher [2,3]. Such heat treatment can effectively relieve the residual stress from cold forming and improve the column behaviour. Since the direct forming approach only cold work the corners of an SHS/RHS cross-section, it was found by [6,55] that the stub column behaviour of direct-formed SHS/RHS can sometimes be comparable to indirect-formed and subsequently heat-treated sections. For a total of 12 untreated direct-formed RHS stub columns (with nominal yield strengths of 350 MPa and 690 MPa), the experimentally obtained capacities were compared to the nominal cross-sectional strengths calculated from CSA S16-19 [12], ANSI/AISC 360-10 [29], EN-1993-1-1 [27] and the Direct Strength Method (DSM) in AISI S100-16 [52]. In all cases, the code predictions were excessively conservative. In addition, according to a linear regression of the experimental data, the existing slenderness limits in [12,27,29] were proven to be overly conservative for high-strength direct-formed SHS/RHS. As a result, the effective width method based on the existing slenderness limits caused significant strength underestimation due to unnecessary penalties on the effective cross-sectional area. In this research, a parametric study is performed using FE models that incorporated the measured residual stresses, strength properties and geometric imperfections from [6,55], and subsequently validated using the stub column test data in [6]. The aim is to generate sufficient data for accurate evaluations of the existing design rules, and if necessary, to propose modifications to the current design rules for SHS/RHS stub columns against cross-sectional yielding or local buckling.

In practice, hot-dip galvanizing of hollow section members of commonly specified sizes in a 450 ºC molten zinc bath takes approximately 10 minutes. Based on a comprehensive comparison on a total of 36 stub columns with different production histories, it was also found in the complementary experimental studies by [6,55] that the effects of galvanizing and post-cold-forming heat treatment to 450 ºC for a 30-minutes holding time per [7,8] were comparable. It was speculated that, for hollow section members of commonly specified sizes, hot-dip galvanizing could also effectively relieve residual stress and delay local buckling. In this research, this speculation is also examined via an FE parametric study.

3.3 Finite element analysis

3.3.1 Elements, meshing and boundary conditions

A literature survey was performed on previous FE research on tubular stub columns. The modelling approaches therein were found to be consistent. Therefore, in this study, the method used by [20] was followed. The finite element software package ABAQUS [56] was used to conduct the numerical simulation. A four-node shell element with reduced integration (S4R) from the ABAQUS element library was used to model the SHS/RHS stub columns. Based on a mesh sensitivity analysis, a mesh size of (H+B)/25 mm was selected for the FE analyses, where H and B are the external depth and the width of the SHS/RHS, respectively. All nodes at each end of the stub column were tied to a restrained rigid body reference point. The top end could freely move in the axial direction to allow the application of displacement increments to simulate the axial compression force.

3.3.2 Material properties

In this research, the SHS/RHS are given IDs with multiple components to differentiate material type, post-cold-forming process, and cross-sectional sizes. For the first component, D = direct-formed RHS (nominal yield stress = 350 MPa), and DH = direct-formed high-strength RHS (nominal yield stress = 690 MPa). For the second component, U = untreated, and G = galvanized. Where applicable, the third component gives the nominal width, depth, and thickness of the cross-section (in mm). Using the experimental data and the constitutive equations proposed by [57,58], the engineering stress-strain relationships were developed and subsequently converted to true stress-strain relationships for use in ABAQUS [56] for the parametric study.

As shown in Fig. 2.3(b), cold working is concentrated at the corner regions of an SHS/RHS during direct forming. By testing tensile coupons machined from the flat faces of the untreated direct-formed SHS/RHS, clear yield plateaus and large proportional stress-over-yield stress ratios were observed. Typical flat face stress-strain curves of two untreated direct-formed RHS are shown in Fig. 3.1a. As also shown in [6], the proportional stress-over-yield stress ratios in the galvanized sections increased in all cases due to an effective residual stress reduction from the galvanizing process. Typical engineering stress-strain curves of the flat face materials of two galvanized direct-formed RHS are shown in Fig. 3.1b. In both figures, the curves are similar to those of hot-rolled steels. Therefore, for the flat face materials, the quad-linear model proposed by Yun and Gardner [57] for hot-rolled steels (reproduced as Eqs. 3.1-3.3 herein) was applied to simulate the stress-strain relationship in FE analysis. As shown in Fig. 1, Eqs. 3.1-3.3 can generate curves that fit well with the experimental data in all cases. The average values of the key material characteristics of the flat face tensile coupons from the untreated and the galvanized SHS/RHS (regular- and high-strength) in [6] were used in Eqs. 3.1-3.3 to generate the engineering stress-strain relationship (D-U-Flat, DH-U-Flat, D-G-Flat and DH-G-Flat). These values are listed in Table 3.1.

$$f(\varepsilon)=\begin{cases} E\varepsilon & \varepsilon<\varepsilon_{\mathrm{y}} \\ f_{\mathrm{y}} & \varepsilon_{\mathrm{y}}<\varepsilon\leq\varepsilon_{\mathrm{sh}} \\ f_{\mathrm{y}}+E_{\mathrm{sh}}(\varepsilon-\varepsilon_{\mathrm{sh}}) & \varepsilon_{\mathrm{sh}}<\varepsilon\leq C_1\varepsilon_{\mathrm{u}} \\ f_{C_1\varepsilon_{\mathrm{u}}}+\dfrac{f_u-f_{C_1\varepsilon_u}}{\varepsilon_{\mathrm{u}}-C_1\varepsilon_{\mathrm{u}}}(\varepsilon-C_1\varepsilon_{\mathrm{u}}) & C_1\varepsilon_{\mathrm{u}}<\varepsilon\leq\varepsilon_{\mathrm{u}} \end{cases} \tag{3.1}$$

$$C_1=\frac{\varepsilon_{\mathrm{sh}}+0.25(\varepsilon_{\mathrm{u}}-\varepsilon_{\mathrm{sh}})}{\varepsilon_{\mathrm{u}}} \tag{3.2}$$

$$E_{\mathrm{sh}}=\frac{f_{\mathrm{u}}-f_{\mathrm{y}}}{0.4(\varepsilon_{\mathrm{u}}-\varepsilon_{\mathrm{sh}})} \tag{3.3}$$

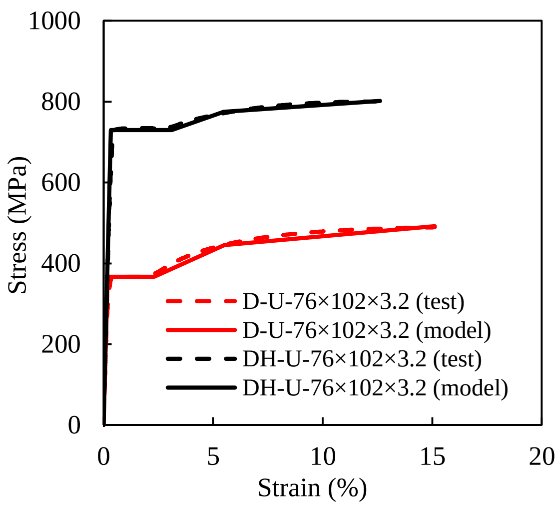

(a) Untreated RHS

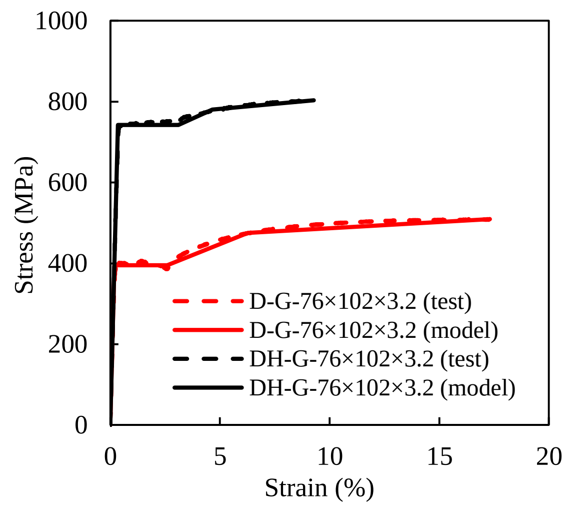

(b) Galvanized RHS

Figure 3.1 Typical engineering stress-strain curves of flat faces of untreated and galvanized RHS

Table 3.1 Parameters for quad-linear stress-strain models

Material ID	E (MPa)	f_y (MPa)	f_u (MPa)	ε_u	ε_y	ε_{sh}	E_{sh} (MPa)	C_1	$C_1\varepsilon_u$	$f_{C_1\varepsilon_u}$ (MPa)
D-U-Flat	202500	383	475	0.1621	0.0019	0.0258	1686	0.369	0.0599	444
DH-U-Flat	202000	708	784	0.1184	0.0035	0.0244	2013	0.405	0.0479	754
D-G-Flat	206400	421	490	0.1402	0.0020	0.0332	1617	0.428	0.0599	469
DH-G-Flat	204200	732	792	0.1036	0.0036	0.0304	2056	0.470	0.0487	767
D-G-Corner	219400	585	622	0.0577	0.0027	0.0218	2576	0.533	0.0308	604
DH-G-Corner	222000	894	906	0.0531	0.0040	-	-	-	-	-

Different from the flat face materials, rounded tensile stress-strain curves were obtained in [6] for the corners of the untreated SHS/RHS due to cold working. Typical curves are shown in Fig. 3.2. The material model proposed by Gardner and Yun [58] for cold-formed steels (reproduced as Eqs. 3.4-3.7 herein) was applied to simulate the engineering stress-strain relationship. Fig. 3.2 shows that Eqs. 3.4-3.7 can generate curves that fit well with the experimental data in both cases. The average values of the key material characteristics of the corner tensile coupons from the untreated SHS/RHS (regular- and high-strength) in [6] were used in Eqs. 3.4-3.7 to generate the engineering stress-strain relationships (D-U-Corner and DH-U-Corner). These characteristic values are listed in Table 3.2. The yield stress (f_y) in Table 3.2 was determined using the 0.2% proof stress method.

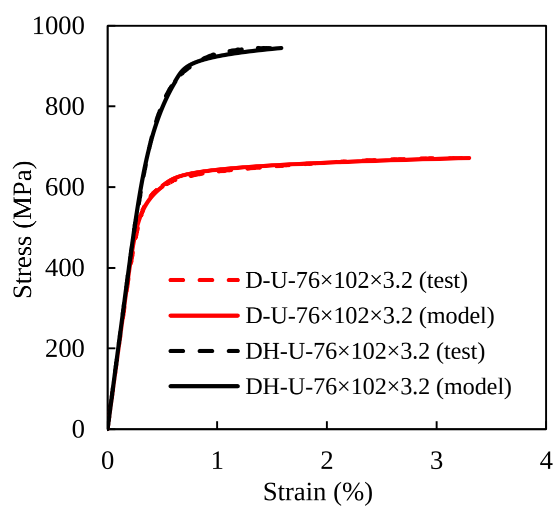

Figure 3.2 Typical engineering stress-strain curves of corner regions of untreated RHS

$$\varepsilon = \begin{cases} \frac{f}{E} + 0.002\left(\frac{f}{f_y}\right)^n & f \le f_y \\ \frac{f - f_y}{E_{0.2}} + \left(\varepsilon_u - \varepsilon_{0.2} - \frac{f_u - f_y}{E_{0.2}}\right)\left(\frac{f - f_y}{f_u - f_y}\right)^m + \varepsilon_{0.2} & f_y < f \le f_u \end{cases} \tag{3.4}$$

$$n = \frac{\ln(4)}{\ln\left(f_y/\sigma_{0.05}\right)} \tag{3.5}$$

$$E_{0.2} = \frac{\mathrm{E}}{1 + 0.002\mathrm{n}\frac{E}{f_y}} \tag{3.6}$$

$$m = 1 + 1.33\frac{f_y}{f_u} \tag{3.7}$$

Table 3.2 Parameters for stress-strain models for corner regions of untreated RHS

Material ID	E (MPa)	f_y (MPa)	f_u (MPa)	$\sigma_{0.05}$	ε_u	$\varepsilon_{0.2}$	$E_{0.2}$ (MPa)	n	m
D-U-Corner	211200	573	621	471	0.0174	0.0047	33994	7.07	4.04
DH-U-Corner	203400	862	950	700	0.0159	0.0062	48997	6.68	3.99

As discussed earlier, previous research [6,55] found that for hollow section members of commonly specified sizes, hot-dip galvanizing can effectively relieve residual stresses. This observation was substantiated by comparing the corner coupon test results from the untreated and galvanized SHS/RHS specimens. In all cases, the stress-strain curves of the corner coupons from the galvanized SHS/RHS showed clear yield plateaus. Typical curves are shown in Fig. 3.3. Noticeable differences can be seen by comparing Figs. 3.2 and 3.3. Therefore, using the average key tensile coupon test results in Table 3.1, Eqs. 3.1-3.3 were applied to generate the engineering stress-strain relationships for the corner regions of the galvanized RHS (D-G-Corner and DH-G-Corner). For the corner regions of the galvanized high-strength SHS/RHS (DH-G-Corner in Table 3.1), the experimentally obtained stress-strain relationship was nearly bilinear (see Fig. 3.3). Such behaviour was modelled by assigning zero values to the strain hardening parameters in Eqs. 3.1-3.3.

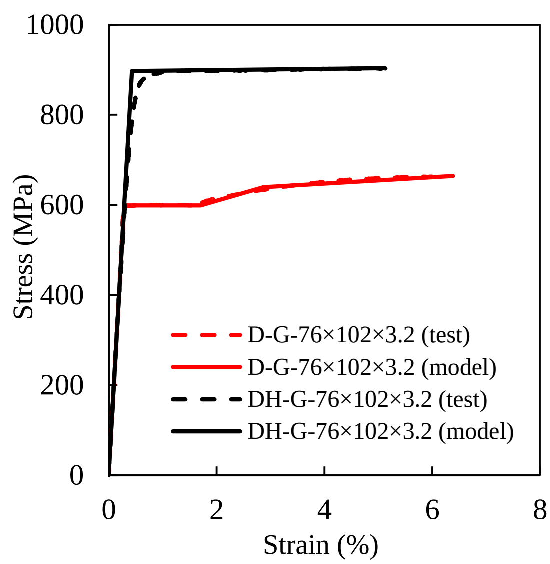

Figure 3.3 Typical engineering stress-strain curves of corner regions of galvanized RHS

The engineering stress-strain relationships developed using Eqs. 3.1-3.7 were subsequently converted to true stress-strain relationships for use in ABAQUS for the parametric study. Due to severe cold working, the materials at the corner and the adjacent regions, in general, have larger yield and ultimate stresses than the flat faces [6,20,55,59]. Similar to the approach used by [20,59], for FE modelling in this study, the experimentally obtained corner material properties were assigned to the corner regions and the adjacent regions (Fig. 3.4). [20] used an extended width of two times the wall thickness (2*t*). [59] used 1*t*, 2*t* and 3*t*, and found on average a 4% stub column strength difference. In this study, the extended corner regions have a width of 3*t* as the FE results match the experimental results the best in this case, which will be further discussed in the following sections.

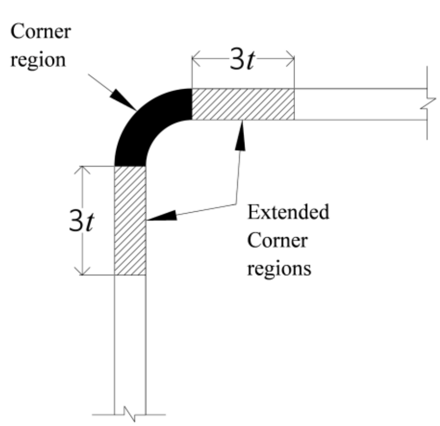

Figure 3.4 Extension of corner material properties to adjacent flat faces

3.3.3 Residual stresses

The inclusion of longitudinal residual stress in FE analysis is critical for simulation of steel members under axial compression [20,47]. In an earlier investigation complementary to this research, Tayyebi et al. [55] experimentally measured the longitudinal residual stresses in 26 SHS/RHS specimens with different production histories (indirect-formed, direct-formed, heat-treated, and galvanized) and with various material properties (nominal yield strengths of 350 and 690 MPa). The procedures suggested by [5,32–35] were adopted for the calculation of residual stresses. As shown in Fig. 2.16, the through-thickness residual stress was resolved into a membrane component and a bending component.

The average values of the normalized membrane and bending residual stresses in direct-formed SHS/RHS are listed in Table 3.3, where the tensile membrane residual stresses are reported as positive values, and the compressive membrane residual stresses are reported as negative values. The tabulated bending residual stresses are the tensile residual stresses from the external surfaces of the SHS/RHS specimens. It is evident in Table 3.3 that the current practice of post-cold-forming hot-dip galvanizing can effectively reduce residual stresses. Tayyebi and Sun [6] showed that post-cold-forming galvanizing can improve the stub column behaviour of cold-formed hollow sections. This study will implement the measured residual stresses in an FE parametric study to quantify such improvement over a wide range of cross-sectional sizes.

Table 3.3 Average values of longitudinal residual stresses from [55]

Specimen ID	Center of flat face		Corner	
	Membrane	Bending	Membrane	Bending
D-U	$-0.06f_y$	$0.39f_y$	$0.08f_y$	$0.25f_y$
D-G	$-0.07f_y$	$0.27f_y$	$0.02f_y$	$0.14f_y$
DH-U	$-0.03f_y$	$0.50f_y$	$0.08f_y$	$0.22f_y$
DH-G	$-0.05f_y$	$0.29f_y$	$0.01f_y$	$0.13f_y$

The approach suggested by [20,59] was adopted in this study to incorporate the measured residual stresses in the FE analyses in ABAQUS. Five integration points were considered through the thickness of each element to ensure the accurate application of the residual stress distribution. Subroutine SIGINI was used to apply the stress magnitude at each integration point.

For the corner region of the untreated SHS/RHS, rounded tensile stress-strain curves shown in Fig. 3.2 were obtained from tensile coupon tests (i.e. relatively small proportional limit-over-yield stress ratio due to the existence of bending residual stress) [41]. As discussed in Section 3.3.2, the tensile stress-strain relationship can be modelled accurately by Eqs. 3.4-3.7. Following the approach in [20,59], since the tensile coupons were clamped in the universal testing machine to the in-situ straight state before testing, the bending residual stresses were already included in the FE models by incorporating the rounded stress-strain curves. The membrane residual stresses were manually added to the FE models using the “initial conditions” function in ABAQUS.

As discussed in Section 3.3.2, although residual stresses were measured at the corner regions of galvanized SHS/RHS and the flat faces of all SHS/RHS [55], as shown in Figs. 3.1 and 3.3, the linear stress-strain relationship described by Eqs. 3.1-3.3 provided the best fit of the experimentally obtained stress-strain curves. However, the direct incorporation of such a relationship in FE modelling does not account for the bending residual stress. Therefore, for the corner regions of galvanized SHS/RHS and the flat faces of all SHS/RHS, both bending residual stresses and membrane residual stresses were added manually in the FE models.

Using the approaches in [20,59], as shown in Fig. 3.4, an extension of the corner region was considered to account for the cold forming effect. The measured residual stresses at corners were applied to the corner regions and the extended flat zones. The measured flat face residual stresses were added to the remaining areas of the cross-sections.

3.3.4 Initial geometric imperfections

Only local geometric imperfections are considered herein since this study is focused on the stub column behaviour. To include the effect of local geometric imperfections in FE analysis, the lowest eigenmode shape is typically chosen as the local geometric imperfection profile [41]. The maximum magnitude over the entire profile can be obtained from experimental measurements. For this numerical research, the geometric imperfections measured over four representative stub column specimens in the complementary study by Tayyebi and Sun [6] were adopted. The average values of the imperfections (δ) for the direct-formed regular- and high-strength RHS were 0.387 and 0.366 mm, respectively. By correlating the measured values to the SHS/RHS wall thicknesses (t), these correspond to $0.12t$ and $0.08t$ for the direct-formed regular- and high-strength SHS/RHS, respectively. On the other hand, Ma et al. [20] suggested that for FE analysis, the measured imperfections can be correlated to the width-to-thickness ratio of flat elements $\alpha = (B - 4t) / t$, where B is the external width. In this case, the average values obtained by Tayyebi and Sun [6] correspond to 0.014α and 0.023α for the direct-formed regular- and high-strength SHS/RHS, respectively. Since there is no unified rule for the correlation of initial imperfections to FE models, the larger value of the two different approaches was attempted in this study (i.e., $0.12t$ and 0.023α). The comparison is discussed in Section 3.3.5.

3.3.5 Verification of FE modelling

Results of the numerical models were verified against the 24 stub column test results from Tayyebi and Sun [6]. Comparisons of numerical analyses and experimental tests were made using representative load-displacement relationships and failure modes in Figs. 3.5 and 3.6. Tables 3.4 and 3.5 include the comparisons of ultimate loads from the stub column tests and FE analyses for the direct-formed regular- and high-strength SHS/RHS, respectively. In all cases, good agreements were observed. Therefore, credence was given to the accuracy of the FE modelling. As shown in Tables 3.4 and 3.5, the application of the two geometric imperfection modelling approaches (i.e., $0.12t$ and 0.023α) resulted in negligible differences. For the subsequent parametric study, a maximum local geometric imperfection of 0.12t was applied.

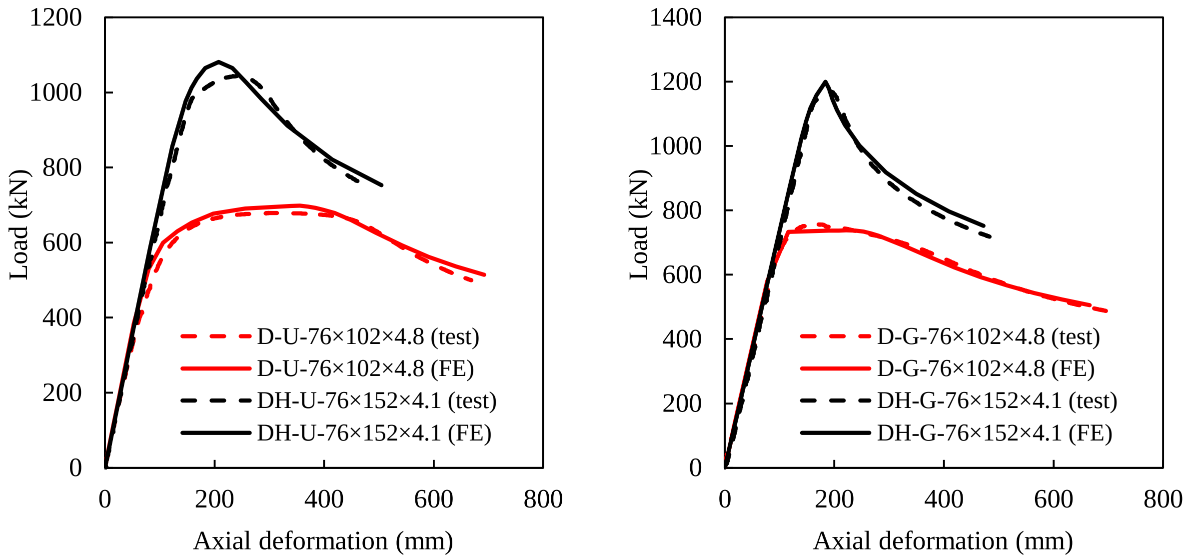

(a) Untreated RHS

(b) Galvanized RHS

Figure 3.5 Comparison of load-displacement relationships

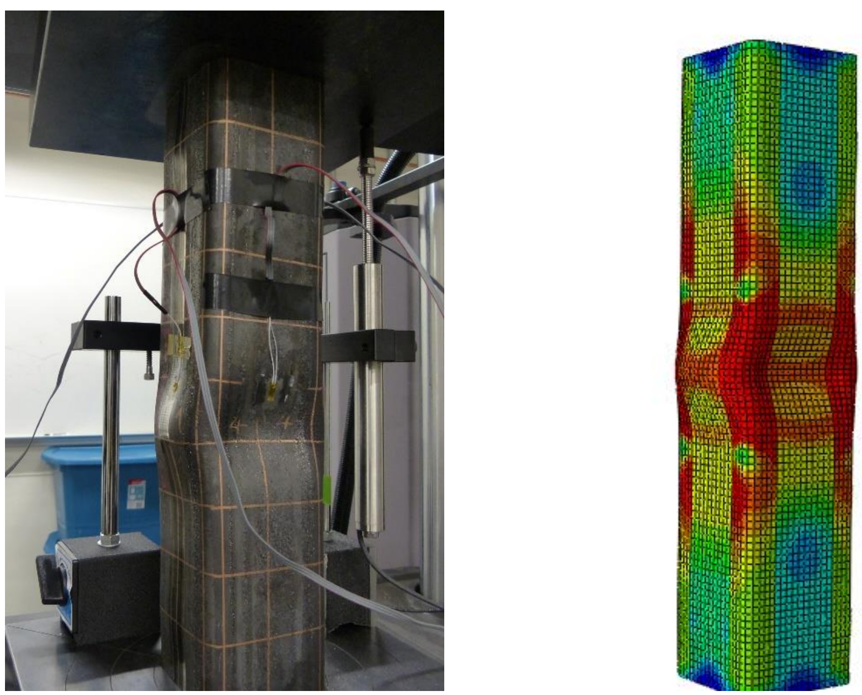

Figure 3.6 Comparison of failure modes

Table 3.4 Comparison of ultimate loads for direct-formed regular-strength SHS/RHS

Specimen ID		Maximum local geometric imperfection	
		$0.12t$	0.023α
	P_{test} (kN)	P_{FE}/P_{test}	P_{FE}/P_{test}
D-U-76×102×3.2	459	0.89	0.88
D-G-76×102×3.2	507	0.95	0.94
D-U-76×102×4.8	679	0.99	1.01
D-G-76×102×4.8	757	0.96	0.97
D-U-102×102×3.2	478	0.93	0.92
D-G-102×102×3.2	539	0.97	0.96
D-U-102×102×4.8	839	0.93	0.96
D-G-102×102×4.8	913	0.93	0.94
D-U-127×127×4.8	969	0.89	0.91
D-G-127×127×4.8	1091	0.92	0.94
Mean		0.94	0.94
COV		0.033	0.035

Table 3.5 Comparison of ultimate loads for direct-formed high-strength SHS/RHS

Specimen ID		Maximum local geometric imperfection	
		$0.12t$	0.023α
	P_{test} (kN)	P_{FE}/P_{test}	P_{FE}/P_{test}
DH-U-76×76×4.8	1116	0.96	0.97
DH-G-76×76×4.8	1100	0.97	0.97
DH-U-76×102×3.2	666	0.97	0.91
DH-U-76×102×3.2*	678	0.95	0.90
DH-G-76×102×3.2	773	0.92	0.86
DH-G-76×102×3.2*	784	0.91	0.85
DH-U-76×102×4.1	1052	0.96	0.92
DH-G-76×102×4.1	1109	0.95	0.91
DH-U-76×102×4.8	1276	0.98	0.98
DH-G-76×102×4.8	1241	1.02	1.02
DH-U-76×152×4.1	1043	1.02	0.99
DH-U-76×152×4.1*	1052	1.01	0.98
DH-G-76×152×4.1	1169	0.99	0.95
DH-G-76×152×4.1*	1189	0.97	0.94
Mean		0.97	0.94
COV		0.033	0.051

* indicates a repeated test

3.3.6 Parametric studies

The FE modelling approach verified in Section 3.3.5 was subsequently used to perform a parametric study, including a total of 624 stub column models (156 untreated SHS, 156 galvanized SHS, 156 untreated RHS, and 156 galvanized RHS). The 624 stub column models included 314 high-strength sections and 310 regular-strength sections. The material and residual stress properties in Sections 3.3.2 and 3.3.3 were used in the analyses. The width (and depth) of the sections ranged from 75 to 310 mm. The wall thickness varied from 2.5 to 13 mm. The cross-sectional width-to-depth ratio of the RHS ranged from 0.5 to 0.75. The selected dimensions cover the practical ranges of commonly available SHS/RHS products. The width-to-thickness (and depth-to-thickness) ratio ranged from 7 to 97. A length of three times the larger external dimension of the cross section was set as the stub column length, following the recommendations by the Structural Stability Research Council (SSRC) [31].

3.4 Stub column behaviours of SHS with different production histories

In this section, the experimental and FE data for the direct-formed SHS are compared to the indirect-formed SHS from [23,41,42,60], and to the hot-finished SHS from [23,42,61], to study the effects of different production techniques. The comparison was made among sections with similar nominal yield strengths and cross-sectional dimensions. The effect of hot-dip galvanizing on the stub column behaviour of regular- and high-strength SHS was also studied.

The experimentally and numerically obtained ultimate loads (P_u) are normalized to the cross-sectional squash loads (P_y) in Figs. 3.7-3.10. The squash loads were calculated using the experimentally measured yield stress of the flat face material, which is consistent with the approach used in previous research (e.g., [20,42]). This is also consistent with the rationale for cross-section classification in existing design standards (e.g., [12,29,52]), where the strength difference between the flat face and corner region is not considered.

Since the experimental data for indirect-formed and hot-finished SHS from [23,41,42,60,61] was only available for a certain range of plate slenderness, Figs. 3.7 and 3.8 only included the experimental and FE data for direct-formed SHS within the same range of plate slenderness for direct comparison. Since different design standards have different formulae for calculation of slenderness, following the approach adopted by [20,42], in this study a normalized plate slenderness ($\bar{\lambda}$) was calculated using Eq. 3.8. This also standardizes the evaluation of the slenderness limits in various design specifications, which will be further discussed in Section 3.5.

$$\bar{\lambda} = \frac{b\sqrt{f_y/E}}{t} \tag{3.8}$$

where b = internal width of SHS/RHS excluding corner portions, and E = Young's modulus.

In comparison to the untreated direct-formed SHS data in Fig. 3.7, the results of the indirect-formed SHS in Fig. 3.7 exhibit a relatively larger scatter. As shown in Fig. 3.7, the indirect-formed SHS in many cases have lower P_u/P_y -ratios due to the existence of high residual stresses, which subsequently lead to loss of stiffness and load-carrying capacities. To differentiate nonslender and slender cross sections, previous studies (e.g., [20,42]) often involve linear regression of the available data. For the best fit line, the normalized plate slenderness ratio ($\bar{\lambda}$) corresponding to a P_u/P_y -ratio of one is often considered as the slenderness limit. For the indirect-formed SHS in Fig. 3.7, instead of a linear regression of the scatter, it is logical and conservative to consider the lower bound of the data. Nevertheless, based on the available data in Fig. 3.7, the slenderness limit suitable for the direct-formed SHS can be larger than that of the indirect-formed SHS, due to the inherently low level of residual stress as a result of the direct forming approach. The untreated direct-formed SHS and the hot-finished SHS are compared in Fig. 3.8. It should be noted that the hot-finished SHS are typically heated to a normalizing temperature of approximately 900 ºC for a fine and homogeneous grain structure. This process improves material toughness and relieves residual stress. However, heat treatment at such temperature removes the strength enhancement from cold forming. Clear trade-offs between material strength and residual stress have been found in previous research [6,55] by comparing cold-formed hollow section materials heat-treated to 595 ºC to their untreated counterparts. For a similar reason, the hot-finished SHS in many cases have lower P_u/P_y -ratios than the untreated direct-formed SHS in Fig. 3.8. In all, the direct-formed SHS exhibited superior stub column capacities over a wide range of cross-section slenderness.

Based on the experimental data from a limited number of hollow section specimens in the complimentary research [6,55], it was concluded that the application of hot-dip galvanizing in many cases increased stub column capacity and delayed local buckling, and in some cases, converted slender cross sections to nonslender cross sections. By performing a comprehensive parametric study in this research, such observation is confirmed by the comparisons in Figs. 3.9 and 3.10. As shown, the application of hot-dip galvanizing increased the P_u/P_y -ratios over a wide range of cross-section slenderness. Also shown in many cases in the figures are the conversions from slender to nonslender behaviour after galvanizing, as galvanizing reduces residual stress and delay local buckling.

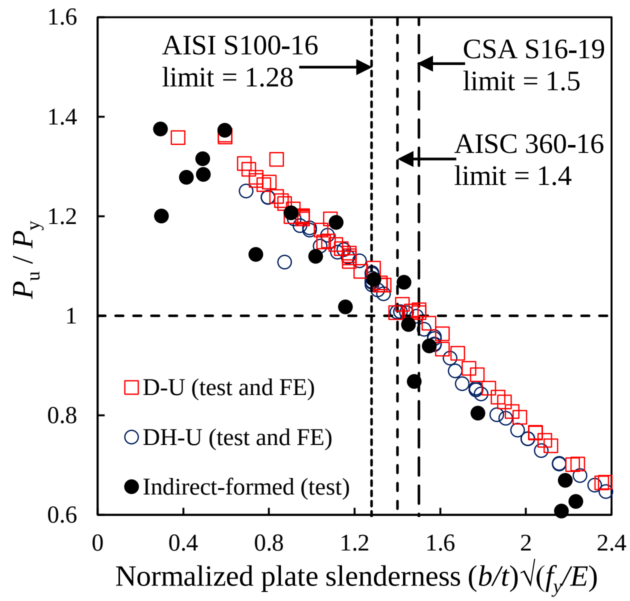

Figure 3.7 Comparison of direct-formed SHS and indirect-formed SHS from [3,4,29,30]

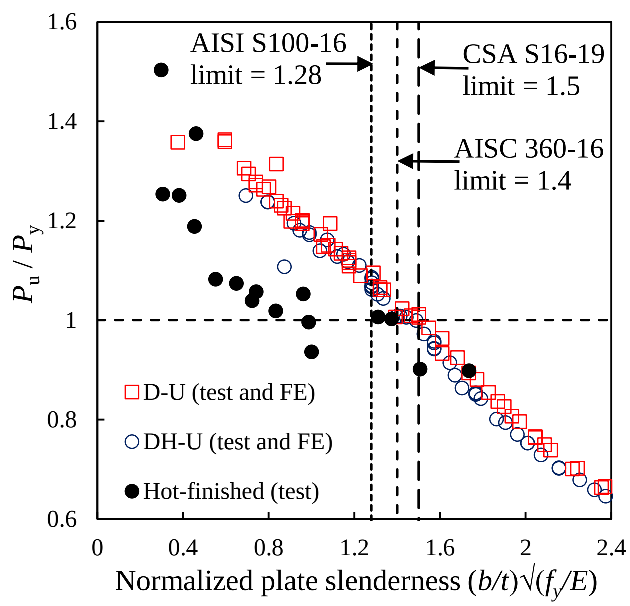

Figure 3.8 Comparison of direct-formed SHS and hot-finished SHS from [4,29,31]

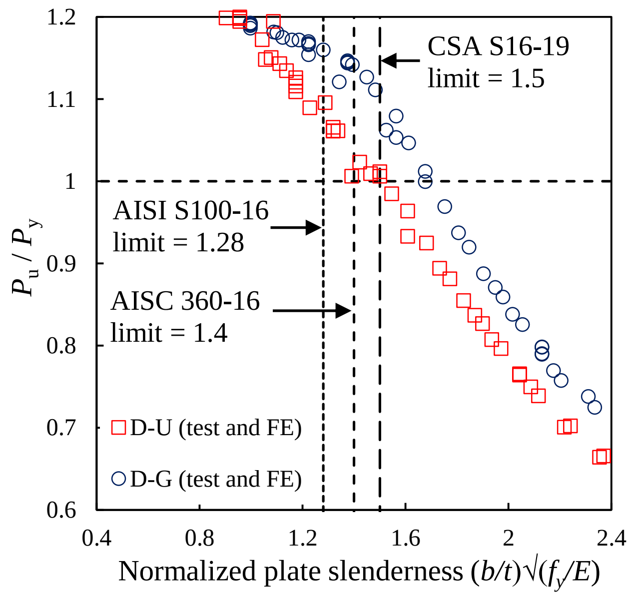

Figure 3.9 Comparison of untreated and galvanized regular-strength direct-formed SHS

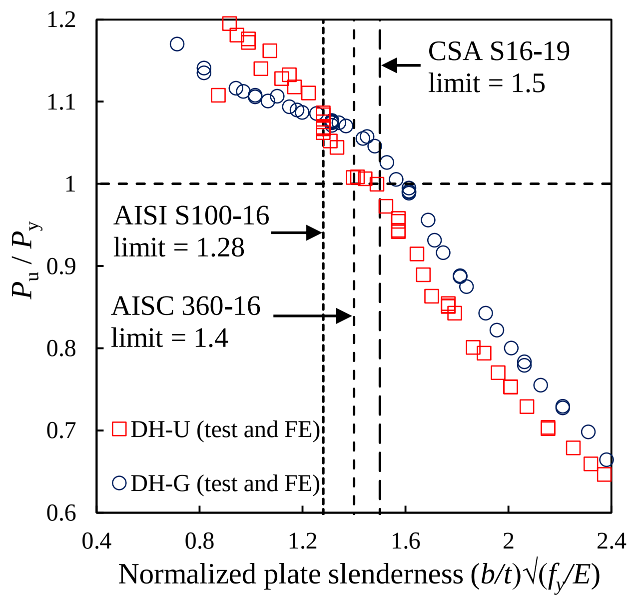

Figure 3.10 Comparison of the untreated and galvanized high-strength direct-formed SHS

3.5 Evaluation of effective width method in AISC 360 and CSA S16

For the design of SHS/RHS members under axial compression using AISC 360-16 [29] and CSA S16-19 [12], cross-section classification is a critical procedure, where the width-to-thickness ratio of each plate element is evaluated against the slenderness limit individually. For SHS/RHS members with slender elements, AISC 360-16 [29] and CSA S16-19 [12] use the effective width method, which calculates the effective area of each plate element individually. In other words, this approach does not consider the entire cross-section directly, and the same methodology is applied to SHS and RHS. In this section, all 624 stub column models (312 SHS and 312 RHS) are used to evaluate the effective width method in AISC 360-16 [29] and CSA S16-19 [12]. However, for clarity, only the SHS data is used in the figures in this section for graphical examination of the slenderness limits. This is consistent with the approach adopted by [20,42].

3.5.1 Cross-section classification

For the design of SHS/RHS under axial compression, members can be classified as cross sections without slender elements (i.e. nonslender) or cross sections with slender elements (i.e. slender). Slender sections under axial compression will experience local buckling before reaching the squash load. The yield slenderness limits in AISC 360-16 [29], CSA S16-19 [12] and AISI S100-16 [52] (based on the effective width method) are developed based on the elastic critical local buckling stress of a plate element under compression. A detailed discussion of this topic can be found in [6]. It should be noted that the existing cross-section classification and column design rules in various steel design standards do not differentiate SHS/RHS produced by different cold-forming methods. On the other hand, the experimental and numerical research evidence in the previous sections showed that: (1) the application of post-cold-forming hot-dip galvanizing can effectively reduce residual stress and, in return, improve stub column behaviour; and (2) direct-formed SHS/RHS in many cases exhibit better stub column behaviours than their indirect-formed and hot-finished counterparts. Therefore, the applicability of the existing cross-section classification rules to untreated and galvanized direct-formed SHS/RHS (regular- and high-strengths) needs to be evaluated individually.

To ensure that the comparisons are made based on the same criteria, the limiting width-to-thickness ratios for SHS/RHS plate elements from the three design standards are converted to the normalized yield slenderness limits ($\bar{\lambda}_{lim}$) in Table 3.6, using Eq. 3.8. A clear disparity among the selected design standards can be observed, as the $\bar{\lambda}_{lim}$-values range from 1.28 to 1.50. The normalized yield slenderness limits are shown in Figs. 3.7-3.10 and are evaluated against the experimental and numerical data for direct-formed SHS/RHS from this study. It should be noted that the yield slenderness limit in EN 1993-1-1 [27] corresponds to a $\bar{\lambda}_{lim}$-value of 1.405, which is similar to AISC 360-16 [29]. Therefore, EN 1993-1-1 [27] and the other design standards with similar limits are not included in the comparisons in Table 3.6 and Figs. 3.7-3.10. The slenderness limit from AISI S100-16 [52] (based on the effective width method) has been proven very conservative for cold-formed SHS/RHS in previous studies [6,20,42]. Therefore, only the slenderness limits in AISC 360-16 [29] and CSA S16-19 [12] will be further evaluated in this section.

Table 3.6 Yield slenderness limits for SHS/RHS plate elements in existing standards

Design standard	Normalized yield slenderness limit
CSA S16-19 [12]	$\bar{\lambda}_{lim} = 1.50$
ANSI/AISC 360-16 [29]	$\bar{\lambda}_{lim} = 1.40$
AISI S100-16 [52] based on the effective width method	$\bar{\lambda}_{lim} = 1.28$

As discussed earlier, to differentiate non-slender and slender cross-sections, previous research (e.g., [6,20,42]) often consider the normalized plate slenderness ratio ($\bar{\lambda}$) corresponding to a P_u/P_y -ratio of one as the slenderness limit ($\bar{\lambda}_{lim}$). Following the same approach, based on the data in Figs. 3.9 and 3.10, the CSA S16-19 slenderness limit ($\bar{\lambda}_{lim}$ = 1.50) is appropriate for the untreated direct-formed SHS (regular- and high-strength), while the AISC 360-16 limit ($\bar{\lambda}_{lim}$ = 1.40) is conservative. On the other hand, slenderness limits of $\bar{\lambda}_{lim}$ = 1.70 and 1.60 were observed from Figs. 3.9 and 3.10 for galvanized regular-strength SHS and galvanized high-strength SHS, respectively. Therefore, a $\bar{\lambda}_{lim}$-value of 1.60 can be conservatively assigned to galvanized SHS (regular- and high-strength). For a more accurate evaluation of proposed yield slenderness limits, reliability analyses are performed in Section 3.6.

3.5.2 Cross-sectional capacity

In AISC 360-16 [29] and CSA S16-19 [12], the squash load is used as the nominal stub column strength for members without slender plate elements. For members with slender plate elements, the effective area is determined by deducting from the gross area, the ineffective area calculated as (b – b_e)/t, where b_e is the effective width of the plate element. The nominal stub column strength, in this case, is the product of the effective area and yield stress.

For all SHS/RHS specimens and FE models, following the design rules in AISC 360-16 and CSA S16-19, the nominal compressive strengths (P_n) (i.e., resistance factor = 1.0) are calculated. The nominal compressive strengths are then normalized by the cross-sectional squash loads (P_y). Using the normalized nominal strengths, the AISC and CSA design curves for the SHS specimens and FE models are plotted in Figs. 3.11 and 3.12, respectively. The normalized ultimate loads (P_u /P_y) from experimental testing and FE analysis are also shown in Figs. 3.11 and 3.12 for comparison. The key statistics are listed in Table 3.7. The following observations can be made:

(1) As shown in Fig. 3.11, for SHS without slenderness elements, the AISC 360-16 approach provides very conservative predictions, since the strength enhancement due to cold forming is not considered.

(2) As shown in Fig. 3.11, for untreated direct-formed SHS with slender elements, the AISC 360-16 approach provides accurate predictions. On the other hand, this approach is conservative for galvanized direct-formed SHS with intermediate slenderness since the existing slenderness limit ($\bar{\lambda}_{lim}$ = 1.40) is conservative. As a result, the effective width method based on the existing slenderness limits caused strength underestimation due to unnecessary penalties on the effective cross-sectional area.

(3) It should be noted that Fig. 3.11 shows only the SHS data (i.e. the plate slenderness is the same for all four sides). For RHS with slender elements, very often the two shorter sides are "nonslender". In other words, the two shorter sides usually have $P_u/P_y > 1.0$, while the squash load is used as the nominal design strength for them. Also different from SHS, for RHS the shorter sides provide relatively stronger resistance to the longer sides against local buckling. Therefore, comparing to SHS, the AISC 360-16 approach is more conservative for RHS.

(4) For all SHS and RHS, the test and FE results are compared to the nominal design strengths calculated using the AISC 360-16 approach (calculated using the measured geometric and material properties). The key statistics are shown in Table 3.7. As shown, the AISC 360-16 approach is conservative when considering all SHS and RHS. However, the statistics do not reflect explicitly the different levels of conservativeness over the full range of normalized plate slenderness, especially for RHS (i.e. the four sides have different plate slenderness-values). Therefore, in Section 3.6, reliability analysis is performed for nonslender and slender sections individually.

(5) As shown in Table 3.7, the CSA S16-19 approach is in general more conservative than the AISC 360-16 approach. As shown in Fig. 3.12, the CSA S16-19 approach is more accurate for sections with intermediate slenderness since it has a higher slenderness limit ($\bar{\lambda}_{lim}$ = 1.50). However, this approach becomes inaccurate when the plate slenderness increases. Again, comparing to SHS, the effective width method in CSA S16-19 becomes even more conservative for RHS.

(6) Overall, the AISC 360-16 approach in general gives better predictions. Therefore, only the AISC 360-16 approach will be further studied and modified in Section 3.6.

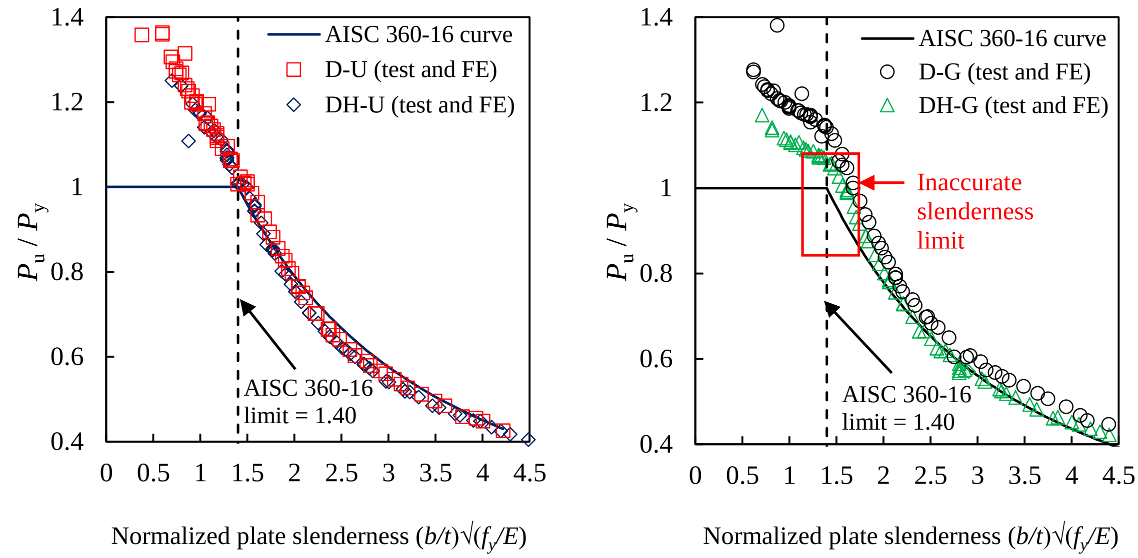

(a) Untreated SHS

(b) Galvanized SHS

Figure 3.11 Comparisons of SHS results with nominal strengths calculated using AISC 360-16

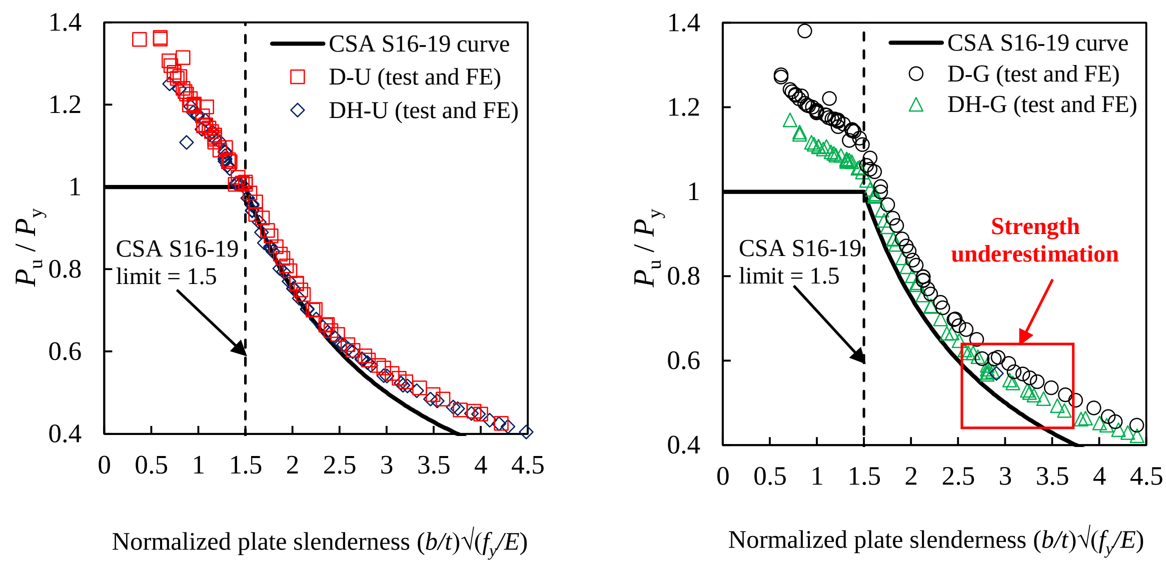

(a) Untreated SHS

(b) Galvanized SHS

Figure 3.12 Comparisons of SHS results with nominal strengths calculated using CSA S16-19

Table 3.7 Comparison of SHS/RHS test and FE results with design standard predictions

Design standard	Untreated $(P_u/P_n)_{mean}$	Untreated $(P_u/P_n)_{COV}$	Galvanized $(P_u/P_n)_{mean}$	Galvanized $(P_u/P_n)_{COV}$
CSA S16-19 [12]	1.10	0.084	1.14	0.054
AISC 360-16 [29]	1.07	0.107	1.10	0.074

3.6 Design recommendations based on the effective width method

3.6.1 Modified approach based on AISC 360

As discussed earlier, comparing to CSA S16-19, the existing formula in AISC 360-16 gives better predictions of the experimental and FE results over a wide range of normalized plate slenderness. Therefore, the existing design rules in AISC 360-16 are used in this section to develop the modified effective width method (MEWM) for the stub column design of untreated and galvanized direct-formed SHS/RHS.

In AISC 360-16, for the design of SHS/RHS members under compression, the limit states include flexural buckling and local buckling. For SHS/RHS members without slender element, the nominal compressive strength (P_n) (based on the limit state of flexural buckling) is the product of the gross cross-sectional area and the critical stress. On the other hand, for SHS/RHS members with slender elements, the nominal compressive strength (P_n) (based on the limit state of flexural buckling and local buckling) is the product of the effective cross-sectional area and the critical stress. For stub columns (with or without slender element), the critical stress approximately equals the yield stress.

For SHS/RHS members with slender elements, the total effective cross-sectional area is the sum of corner areas and the effective flat face areas. The corner areas are calculated, assuming an outer corner radius of two times the wall thickness. The effective flat face areas are calculated by multiplying the wall thickness by the effective plate element widths (b_e). The current approach in AISC 360-16 for calculation of the effective width of plate elements in SHS/RHS stub columns (i.e., critical stress = yield stress) is reproduced herein as Eq. 3.9.

$$\frac{b_e}{b} = \begin{cases} 1 & \bar{\lambda} \le \bar{\lambda}_{lim} \\ \left[1 - c_1\left(\frac{c_2\bar{\lambda}_{lim}}{\bar{\lambda}}\right)\right] . \left(\frac{c_2\bar{\lambda}_{lim}}{\bar{\lambda}}\right) & \bar{\lambda} > \bar{\lambda}_{lim} \end{cases} \tag{3.9}$$

where $\bar{\lambda} = (b/t)\sqrt{f_y/E}$ (i.e. Eq. 3.8); c_1 and c_2 are effective width imperfection adjustment factors.

For SHS/RHS members, the values of c_1 = 0.2 and c_2 = 1.38 are proposed in AISC 360-16. As shown in Table 3.6, for plate elements in SHS/RHS members under axial compression, a $\bar{\lambda}_{lim}$-value of 1.40 is currently used in AISC 360-16.

Based on the evidence in Sections 3.4 and 3.5, this research proposes a modified effective width method (MEWM) which uses of a $\bar{\lambda}_{lim}$-value of 1.50 for untreated direct-formed SHS/RHS, and a $\bar{\lambda}_{lim}$-value of 1.60 for galvanized direct-formed SHS/RHS. To be consistent with the existing plate element classification formula in Table B4.1a of AISC 360-16, the new formulae corresponding to the proposed $\bar{\lambda}_{lim}$-values are listed in Table 3.8. The proposed slenderness limits apply to direct-formed SHS/RHS with nominal yield stresses of 350 and 690 MPa. Using the proposed slenderness limits together with the existing AISC 360-16 design rules, the nominal compressive strengths (P_n) (i.e., resistance factor = 1.0) are calculated. The nominal compressive strengths are compared to all SHS/RHS test and FE results. For untreated direct-formed SHS/RHS, the mean of the P_u / P_n -ratio is 1.05, with a COV of 0.127. For galvanized direct-formed SHS (D-G and DH-G in Fig. 3.12b), the mean of the P_u / P_n -ratio is 1.05, with a COV of 0.111.

Table 3.8 Proposed yield slenderness limits for direct-formed SHS/RHS plate elements

Design standard	Proposed normalized yield slenderness limit	Corresponding formula
ANSI/AISC 360-16 [29]	Untreated: $\lambda_{lim} = 1.50$	$b/t \leq 1.50\sqrt{E/f_y}$
	Galvanized: $\lambda_{lim} = 1.60$	$b/t \leq 1.60\sqrt{E/f_y}$

3.6.2 Reliability analysis of the modified approach based on AISC 360

To evaluate whether the modifications proposed in Section 3.6.1 (to the existing AISC 360-16 design rules) provide adequate or excessive safety margins over different ranges of plate slenderness, reliability analyses were conducted considering a target reliability index of 2.6 recommended by AISC 360-16. The load combination used in the reliability analysis follows [29] (i.e., a load combination of 1.2DL + 1.6LL and a LL-over-DL-ratio of three, where LL = live load and DL = dead load). For the design of members under axial compression, AISC 360-16 [29] uses a resistance factor (ϕ) of 0.9.

The AISI S100-16 [52] formula (reproduced as Eq. 3.10 herein) was used to calculate the reliability index (β). It should be noted that Eq. 3.10 is the same as the reliability index formula in Commentary Chapter B of AISC 360-16. The later can be derived using the specified load combination and LL-over-DL ratio. The definitions of the parameters in Eq. 3.10 are included in "Nomenclatures." The parameters were calculated using the experimental and FE data in this study and are listed in Table 3.9.

$$\beta = \frac{\ln\left(\frac{C_\phi . M_m . F_m . P_m}{\phi}\right)}{\sqrt{V_M^2 + V_F^2 + V_P^2 + V_Q^2}} \tag{3.10}$$

Table 3.9 Parameters for calculation of reliability indices for modified effective width method (MEWM)

	Untreated			Galvanized		
	Nonslender Sections	Slender Sections	Nonslender + Slender Sections	Nonslender Sections	Slender Sections	Nonslender + Slender Sections
C_ϕ	1.49	1.49	1.49	1.49	1.49	1.49
M_m	1.07	1.07	1.07	1.14	1.14	1.14
F_m	1.03	1.03	1.03	1.03	1.03	1.03
P_m	1.18	0.95	1.05	1.16	0.97	1.05
V_M	0.087	0.087	0.087	0.089	0.089	0.089
V_F	0.030	0.030	0.030	0.030	0.030	0.030
V_P	0.077	0.057	0.127	0.054	0.080	0.111
V_Q	0.187	0.187	0.187	0.187	0.187	0.187

Using the parameters listed in Table 3.9, reliability analyses were performed on the proposed modified effective width method (MEWM) for stub column design of untreated direct-formed SHS/RHS ($\bar{\lambda}_{lim}$ = 1.50) and galvanized direct-formed SHS/RHS ($\bar{\lambda}_{lim}$ = 1.60). The calculated β-values are listed in Table 3.10. The following observations can be made:

(1) When considering, from the experimental and FE data pool, only the SHS/RHS with slender elements, for a resistance factor of 0.90, the reliability indices for untreated sections and galvanized sections are 2.60 and 2.84, respectively. Both reliability indices are no less than the target value of 2.6 recommended by AISC 360-16. Therefore, adequate safety margins are inherent in the proposed modified effective width method (MEWM) for sections with slender elements.

(2) When considering only the SHS/RHS without slender elements, for a resistance factor of 0.90, the reliability indices for untreated sections and galvanized sections are 3.48 and 3.77, respectively. The values are much larger than 2.6. This indicates an excessive safety margins since, as discussed earlier, the effective width method uses the squash load as the nominal stub column strength of sections without slender elements (i.e. does not account for the strength enhancement due to cold forming).

(3) Based on the experimental and FE data from all SHS/RHS (i.e. sections with and without slender elements), for a resistance factor of 0.90, the reliability indices for untreated sections and galvanized sections are 2.69 and 3.02, respectively. Both reliability indices are larger than the target value of 2.6 recommended by AISC 360-16. Therefore, the proposed modified effective width method (MEWM) is overall reliable.

Table 3.10 Reliability indices calculated based on modified effective width method (MEWM)

Material Type	Nonslender ϕ	Nonslender β	Slender ϕ	Slender β	Nonslender + Slender ϕ	Nonslender + Slender β
Untreated (D-U + DH-U)	0.9	3.48	0.9	2.60	0.9	2.69
Galvanized (D-G + DH-G)	0.9	3.77	0.9	2.84	0.9	3.02

3.7 Design recommendations based on the direct strength method

3.7.1 Modified approach based on AISI S100

As discussed in Section 3.6, for cross sections without slender elements, the effective width method in AISC 360-16 and CSA S16-19 use the squash load (P_y) as the nominal stub column strength. Therefore, for cross sections with small slenderness ratios, the nominal stub column strengths are significantly lower than the actual ultimate loading capacities (P_u from experimental testing and FE analysis), since the strength enhancement due to cold forming is ignored. This is consistent with the findings in [20,41]. In order to fully appreciate the advantage of untreated and galvanized direct-formed RHS (i.e. low overall level of residual stress and strength enhancement due to cold forming), a modified direct strength method (MDSM) based on AISI S100-16 is proposed in this section, using the experimental and FE results of all SHS and RHS.

As discussed previously, the effective width method calculates the member strength based on the evaluation of individual plate elements. On the other hand, the direct strength method (DSM) in AISI S100-16 is based on the behaviour of the entire cross section, where inter-element compatibility and equilibrium are considered [62,63]. For sections with slender elements under compression and flexure, the direct strength method (DSM) in AISI S100-16 does not involve calculation of effective area and effective section modulus. Therefore, it is particularly efficient for thin-walled cold-formed steel structural members. The existing DSM formula from AISI S100-16 for calculation of nominal compressive strength involving local buckling is reproduced here in as Eq. 3.11.

$$\frac{p_{nl}}{p_{ne}} = \begin{cases} 1 & \lambda_l \leq 0.776 \\ \left[1 - 0.15\left(\frac{1}{\lambda_l}\right)^{0.8}\right].\left(\frac{1}{\lambda_l}\right)^{0.8} & \lambda_l > 0.776 \end{cases} \tag{3.11}$$

where P_{nl} = nominal compressive strength for local buckling; P_{ne} = global column strength; $\lambda_l = \sqrt{P_{ne}/P_{crl}}$ = slenderness factor; and P_{crl} = critical elastic local column buckling load.

For all direct-formed SHS/RHS stub column specimens and FE models, P_{ne} is determined by multiplying the gross section area by f_y. Following the recommendation in AISI S100-16, P_{crl} is obtained by conducting a finite strip analysis using the CUFSM software [63]. Following this approach, the DSM design curves are obtained, and are shown in Figs. 3.13a and 3.13b for untreated and galvanized sections, respectively.

The experimental and numerical ultimate strengths of the stub columns are normalized by the cross-sectional squash loads (P_y). The normalized values are plotted against $\sqrt{P_{ne}/P_{crl}}$ in Fig. 3.13 for comparison. The following observations can be made:

(1) Similar to the effective width method, the existing DSM is very conservative for sections with slenderness factor (λ_l) below the threshold (0.776).

(2) Comparing to untreated SHS/RHS, DSM is more conservative for galvanized SHS/RHS.

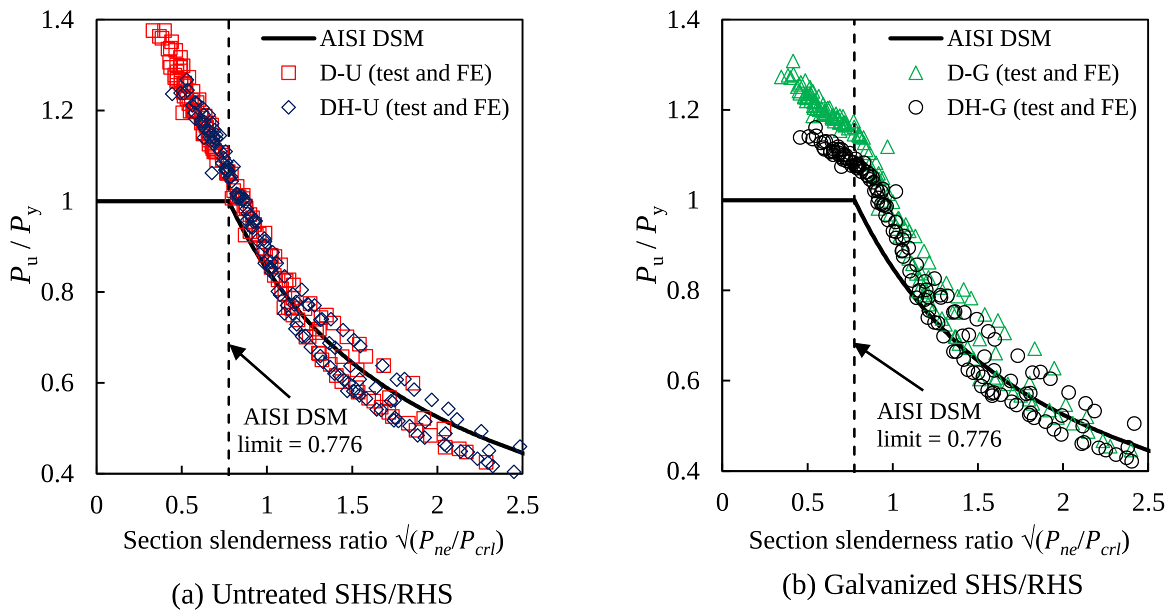

Figure 3.13 Comparisons of SHS/RHS results with nominal strengths calculated using direct strength method in AISI S100-16

To consider the cold-forming-induced strength enhancement and the effect of hot-dip galvanizing, based on nonlinear least squares regressions, Eqs. 3.12 and 3.13 are proposed in this study for untreated and galvanized direct-formed SHS/RHS. The formulae can be used to determine the local-to-global buckling strength ratio (P_{nl}/P_{ne}).

For untreated direct-formed SHS/RHS with regular- and high-strength:

$$\frac{p_{nl}}{p_{ne}} = \begin{cases} -\left[1 - 0.13\left(\frac{1}{\lambda}\right)^{0.9}\right]\left(\frac{1}{\lambda}\right)^{0.9} + 2 & (\lambda = -\lambda_l + 1.66\ when\ \lambda_l \leq 0.83) \\ \left[1 - 0.13\left(\frac{1}{\lambda}\right)^{0.9}\right]\left(\frac{1}{\lambda}\right)^{0.9} & (\lambda = \lambda_l\ when\ \lambda_l > 0.83) \end{cases} \quad (3.12)$$

For galvanized direct-formed SHS/RHS with regular- and high-strength:

$$\frac{p_{nl}}{p_{ne}} = \begin{cases} -\left[1 - 0.034\left(\frac{1}{\lambda}\right)^{0.5}\right]\left(\frac{1}{\lambda}\right)^{0.5} + 2 & (\lambda = -\lambda_l + 1.86\ when\ \lambda_l \leq 0.93) \\ \left[1 - 0.059\left(\frac{1}{\lambda}\right)^{0.9}\right]\left(\frac{1}{\lambda}\right)^{0.9} & (\lambda = \lambda_l\ when\ \lambda_l > 0.93) \end{cases} \quad (3.13)$$

where λ = new slenderness factor based on λ_l in Eq. 3.11 from the direct strength method (DSM) in AISI S100-16.

The nominal strength calculated using Eqs. 3.12 and 3.13 are compared to the experimental and FE data in Figs. 3.14a and 3.14b for untreated and galvanized direct-formed SHS/RHS, respectively. As shown, the proposed modified direct strength method (MDSM) formulae provide accurate predictions in both cases. To evaluate whether the proposed modifications provide adequate or excessive safety margins, a reliability analysis is performed in Section 3.7.2.

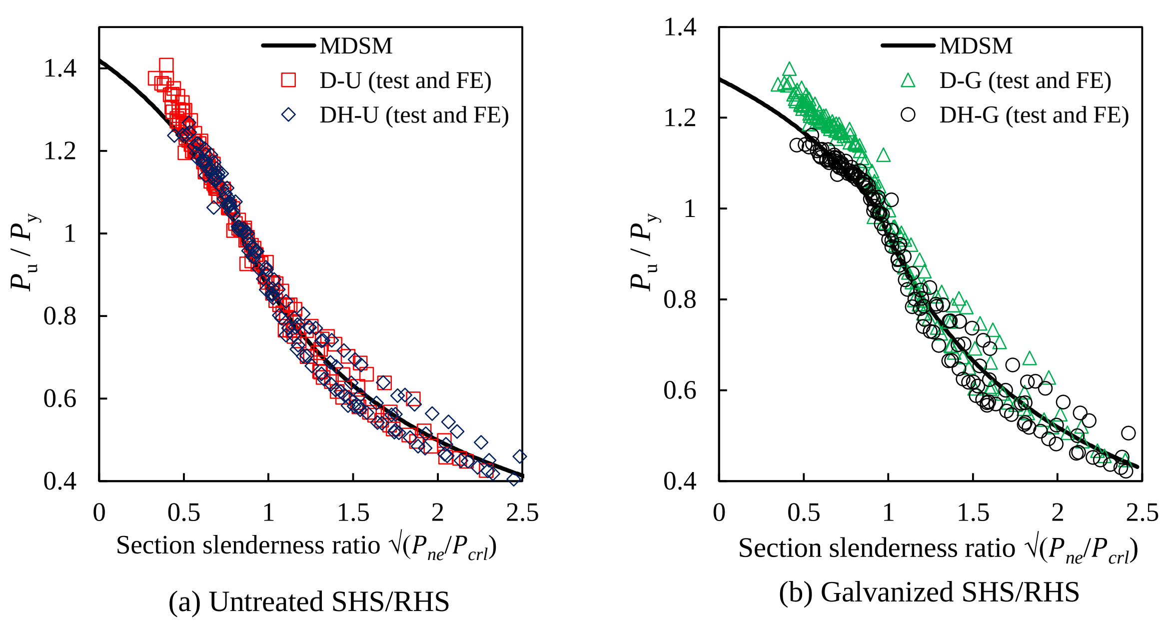

Figure 3.14 Comparisons of SHS/RHS results with nominal strengths calculated using modified direct strength method (MDSM)

3.7.2 Reliability analysis of the modified approach based on AISI S100

Unlike the effective width method (e.g. Figs. 3.11 and 3.12), as shown in Fig. 3.14 the proposed MDSM generate a relatively uniform margin of safety for all SHS/RHS over the entire range of slenderness ratios. Therefore, in this section the reliability analyses for the untreated and galvanized SHS/RHS are performed using all experimental and FE data in each category. For design of members in compression, AISI S100-16 adopts a resistance factor of 0.85. For reliability analysis, AISI S100-16 uses a LL/DL-ratio of five, and a target reliability index of 2.5. Based on the approach discussed in Section 3.6.2, using the experimental and FE data, the parameters for use in Eq. 3.10 are calculated and listed in Table 3.11. The calculated reliability indices are listed in Table 3.12. As shown, for both untreated and galvanized sections, the values are larger than the target reliability index of 2.5. Therefore, adequate safety margins are inherent in the proposed MDSM.

Table 3.11 Parameters for calculation of reliability indices for modified direct strength method (MDSM)

	Untreated	Galvanized
	Nonslender + Slender Sections	Nonslender + Slender Sections
C_ϕ	1.52	1.52
M_m	1.07	1.14
F_m	1.03	1.03
P_m	1.01	1.02
V_M	0.087	0.089
V_F	0.030	0.030
V_P	0.046	0.055
V_Q	0.21	0.21

Table 3.12 Reliability indices calculated based on modified direct strength method (MDSM)

	Nonslender + Slender	
Material Type	ϕ	β
Untreated (D-U + DH-U)	0.85	2.97
Galvanized (D-G + DH-G)	0.85	3.23

3.8 Conclusions

This paper presents a comprehensive research on the effects of direct-forming and post-production hot-dip galvanizing on the stub column behaviour of cold-formed SHS/RHS. A total of 624 FE models were developed using the previously measured residual stresses, strength properties and geometric imperfections in direct-formed SHS/RHS. The FE modelling approach was validated against previous experimental data from 24 stub column tests. Both the stub column specimens and FE models cover wide ranges of geometric and material strength properties. By comparing to the stub column test results from previous studies for indirect-formed and hot-finished SHS/RHS, it was found that: (1) direct-formed SHS/RHS have superior stub column behaviour; and (2) the application of post-production galvanizing can effectively improve the stub column behaviour by relieving the residual stress. Based on the research evidence, the effective width method in AISC 360-16 [29] and CSA S16-19 [12], and the direct strength method in AISI S100-16 [52] were found to be conservative for both untreated and galvanized direct-formed SHS/RHS. Modified effective width method (MEWM) and modified direct strength method (MDSM) are proposed. The proposed modifications were proven accurate based on reliability analyses.

Nomenclatures

B	Measured external width of RHS
b	Flat width of plate element
b_e	Effective width of plate element
c_1 , c_2	Material coefficient
C_ϕ	Calibration coefficient for reliability analysis
E	Young's modulus
$E_{0.2}$	Tangent modulus of steel material at 0.2% proof stress
E_{sh}	Initial slope of strain hardening
F_m	Mean value of fabrication factor for reliability analysis
f_u	Ultimate stress
f_y	Yield stress
H	Measured external depth of RHS
m	Second strain hardening exponent
M_m	Mean value of material factor for reliability analysis
n	First strain hardening exponent
P_{crl}	Elastic local buckling load in AISI S100-16
P_{FE}	Stub column strength from finite element analysis
P_m	Mean value of test/FEA-to-predicted load ratios for reliability analysis
P_n	Nominal compressive strength of stub column
P_{ne}	Nominal axial strength for overall buckling in AISI S100-16
P_{nl}	Nominal axial strength for local buckling in AISI S100-16
P_{test}	Experimental stub column strength
P_u	Stub column strength from test or FE analysis
P_y	Cross-section yield load of stub column
t	Wall thickness of SHS/RHS
V_F	Coefficient of variation of the fabrication factor for reliability analysis
V_M	Coefficient of variation of material factor for reliability analysis
V_P	Coefficient of variation of test/FE-to-predicted load ratios for reliability analysis
V_Q	Coefficient of variation of load effect for reliability analysis
α	Flat width-to-thickness ratio for the initial geometric imperfection model
β	Reliability index

δ	Measured magnitude of initial geometric imperfection
$\varepsilon_{0.2}$	Strain at 0.2% proof stress
ε_{sh}	Strain at the onset of strain hardening
ε_{u}	Strain at ultimate stress
ε_{y}	Strain at yield stress
λ	Slenderness factor in modified direct strength method
λ_{l}	Slenderness factor in AISI S100-16
$\bar{\lambda}$	Normalized plate slenderness
$\bar{\lambda}_{lim}$	Normalized yield slenderness limit
$\sigma_{0.05}$	0.05% proof stress of material
σ_{b}	Magnitude of longitudinal bending residual stress
σ_{in}	Total through-thickness residual stress at the inside surface of SHS/RHS
σ_{m}	Longitudinal membrane residual stress
σ_{out}	Total through-thickness residual stress at the outside surface of SHS/RHS
ϕ	Resistance factor

Chapter 4: Experimental investigation of direct-formed square and rectangular hollow section beams

Kamran Tayyebi, Min Sun, Kian Karimi, Ray Daxon, Brandon Rossi, *Experimental investigation of direct-formed square and rectangular hollow section beams*, J. Constr. Steel Res. (2021) (under review).

4.1 Abstract

In North America, cold-formed square and rectangular hollow sections (collectively referred to as RHS herein) are conventionally manufactured using the indirect-forming approach. The design provisions in the current North American steel design standards were developed based on research on indirect-formed RHS. New-generation regular- and high-strength RHS produced using a different cold-forming approach (direct-forming) are now available in North America. According to a complementary study, such new products, although cold-formed, have inherently low levels of residual stresses around cross sections as only the corner regions are cold-worked during production. In this paper, by testing a total of 22 beam specimens, the flexural behaviours of direct-formed RHS (nominal yield stresses of 350 and 690 MPa) are studied and compared to indirect-formed and hot-finished RHS from previous research. The effects of post-production hot-dip galvanizing on residual stresses and flexural behaviours are also studied. The applicability of slenderness limits and flexural design formulae in the current North American steel design standards are examined using the experimental data.

4.2 Introduction

In practice, cold-formed square and rectangular hollow sections (collectively referred to as RHS herein) with commonly specified cross-sectional dimensions are produced in North America using either the indirect-forming or the direct-forming approach (Fig. 1.3). The indirect-forming approach, as the conventional approach of the two, gradually roll-forms steel coil into a circular hollow section (CHS) before further shaping it into the desired rectangular shape. The direct-forming approach, as the new approach of the two, roll-forms steel coil directly into the final rectangular shape. The design provisions for RHS members in the existing North American steel design standards (AISC 360-16 [29] and CSA S16-19 [12]) are in general developed based on research on indirect-formed RHS, and currently do not differentiate RHS cold-formed by different methods [6,44,55].

Recent research involving measurement of residual stresses in 26 RHS specimens with different production histories [3] showed that, comparing to indirect-formed RHS, direct-formed RHS in general have lower levels of residual stresses since the cold-working is mainly concentrated at the four corner regions during production. A complementary experimental investigation involving testing of 36 stub columns [6] showed that direct-formed RHS often have superior stub column behaviours than their indirect-formed counterparts. By comparing the failure modes and load carrying capacities of the stub column specimens to the predictions by the existing North American steel design standards [12,29], the current slenderness limits for compression elements in RHS subject to axial compression are shown to be excessively conservative for direct-formed RHS due to the inherently low levels of residual stresses. In many cases, the existing slenderness limits in [12,29] misjudged nonslender direct-formed sections as slender sections, resulting in unnecessary penalty to effective cross-sectional area. The existing design formulae in [12,29] for members under axial compression are found to be very conservative since they are derived heavily based on the existing slenderness limits. To address this practical design issue,[44] performed a subsequent finite element (FE) parametric investigation and proposed modified design recommendations for direct-formed RHS stub columns against cross-sectional yielding and local buckling. One of the primary objectives of this research is to extend the above work to study the structural behaviours of direct-formed RHS under flexural loading.

Other than direct-formed regular-strength RHS (nominal yield strength = 350 MPa), direct-formed high-strength RHS (nominal yield strength = 690 MPa) produced to ASTM A1112 [25] are now available in the North American market. Such high-strength RHS have already been extensively used in the North American transportation and agricultural industries. However, their application in the building industry is limited. Previous research on high-strength RHS for building applications in general focuses on indirect-formed products (e.g., [6,13,15,16,24,39,44,55]). On the other hand, research on direct-formed high-strength RHS is limited. Detailed literature review and discussions can be found in [6,44,55]. As the newest ASTM standard for cold-formed high-strength hollow structural sections, ASTM A1112 [25] currently does not appear as approved materials in [12,29] due to the lack of research. As the second objective of this research, the applicability of the existing flexural member design rules in [12,29] on direct-formed high-strength RHS is examined for the first time.

From power generation to transmission and distribution, the application of galvanized tubular steel structures covers nearly all fields of the energy infrastructure. To facilitate the application of galvanized high-strength hollow sections in durable energy infrastructure standing up to harsh environment and test of time, recent experimental research investigated the effect of post-production hot-dip galvanizing on residual stresses in cold-formed CHS [5] and RHS [3,55]. It was found that similar to the application of the heat treatment per ASTM A1085 Supplement S1 [7], or the Class H finish per CSA G40.20/G40.21 [8] (both at 450 °C), post-production hot-dip galvanizing can also effectively reduce the cold-forming-induced residual stresses. It should be noted that for hot-dip galvanizing, the molten zinc bath is typically maintained at 450 °C [2]. For batch galvanizing of hollow structural sections of commonly specified sizes, nearly the same steps are followed in all facilities. The immersion time for individual member is strictly controlled (approximately ten minutes) to produce the best coating quality [2]. It is therefore speculated that the application of post-production galvanizing will influence cold-formed RHS member behaviours under flexural loading. The third objective of this research is to substantiate this speculation.

In all, this paper presents an experimental investigation involving a total of 22 full-scale beam specimens to address the above research questions. The applicability of the existing slenderness limits for compression elements in RHS subject to flexure and the corresponding flexural design formulae in [12,29] on direct-formed regular- and high-strength RHS (untreated and galvanized) are examined using the experimental data.

4.3 Experimental Investigation

4.3.1 Preparation of beam specimens

In this research, five regular-strength and five high-strength parent RHS are used to fabricate the beam specimens. For each parent RHS, half of the material is hot-dip galvanized and the other half remains untreated. The material properties of the untreated and galvanized RHS are obtained via tensile testing of coupons machined from flat faces and corners of the sections. The procedures and detailed discussions on the tensile testing can be found in [6]. The key tensile test results are listed in Table 4.1, where the RHS are given IDs with multiple components to differentiate material type, post-cold-forming process, and cross-sectional sizes. For the first component, D = direct-formed RHS (nominal yield stress = 350 MPa), and DH = direct-formed high-strength RHS (nominal yield stress = 690 MPa). For the second component, U = untreated, and G = galvanized. The third component gives the nominal width, depth, and thickness of the cross section (in mm). As shown in Table 4.1, post-production hot-dip galvanizing has minor effects on the material strength properties.

Table 4.1 Key tensile coupon test results

Specimen	Flat coupons				Corner Coupons			
	E (GPa)	f_y (MPa)	f_u (MPa)	ε_{rup} (%)	E (GPa)	f_y (MPa)	f_u (MPa)	ε_{rup} (%)
D-U-76×102×3.2	203	367	492	34	200	601	672	14
D-G-76×102×3.2	211	400	509	32	208	599	664	16
D-U-76×102×4.8	200	409	470	39	217	568	605	18
D-G-76×102×4.8	204	424	463	36	225	574	595	20
D-U-102×102×3.2	203	344	469	32	220	567	623	15
D-G-102×102×3.2	198	380	497	32	223	536	638	15
D-U-102×102×4.8	205	399	487	38	206	574	618	18
D-G-102×102×4.8	219	470	515	30	218	596	620	20
D-U-127×127×4.8	202	395	457	40	213	553	588	16
D-G-127×127×4.8	200	427	468	37	223	574	603	22
DH-U-76×76×4.8	199	638	767	27	190	789	863	19
DH-G-76×76×4.8	203	743	786	28	229	878	893	22
DH-U-76×102×3.2	217	730	802	27	206	862	945	12
DH-G-76×102×3.2	217	742	803	20	207	876	904	14
DH-U-76×102×4.1	202	692	776	26	211	879	960	12
DH-G-76×102×4.1	202	711	792	26	227	901	909	17
DH-U-76×102×4.8	194	651	761	29	206	849	928	16
DH-G-76×102×4.8	191	720	777	26	225	816	876	20
DH-U-76×152×4.1	198	713	815	30	204	930	1054	14
DH-G-76×152×4.1	208	744	819	28	222	918	949	16

In a complimentary study [55], the residual stresses in 14 of the 20 RHS in Table 1 are measured using the sectioning method, where the measured values are resolved into membrane and bending components (σ_m and σ_b, respectively). For ease of discussions in the following sections of this paper, the key results are normalized by the measured yield stress (f_y) in Table 4.2, where the tensile membrane residual stresses are reported as positive values, and the compressive membrane residual stresses are reported as negative values. The tabulated bending residual stresses are the tensile residual stresses from the external surfaces of the RHS specimens. The bending residual stresses on the internal surfaces have the same magnitudes but opposite senses. As shown in Table 4.2, the application of post-production galvanizing can effectively lower the residual stress levels.

Table 4.2 Summary of longitudinal residual stress measurements in direct-formed RHS

Specimen	Flat		Corner		Overall	
	σ_b/f_y (%)	σ_m/f_y (%)	σ_b/f_y (%)	σ_m/f_y (%)	σ_b/f_y (%)	σ_m/f_y (%)
D-U-76×102×3.2	64	-35	45	16	62	-27
D-G-76×102×3.2	40	-8	27	2	38	-6
D-U-76×102×4.8	62	-6	29	11	56	-3
D-G-76×102×4.8	37	-10	12	3	33	-8
D-U-102×102×4.8	88	-9	40	8	81	-7
DH-U-76×76×4.8	77	-5	35	11	69	-2
DH-G-76×76×4.8	41	-12	18	0	37	-10
DH-U-76×102×3.2	48	-17	33	19	46	-12
DH-G-76×102×3.2	25	-2	13	-2	24	-2
DH-U-76×102×4.1	54	-4	24	12	49	-2
DH-U-76×102×4.8	76	0	24	2	67	0
DH-G-76×102×4.8	37	-2	18	-3	34	-2
DH-U-76×152×4.1	52	-9	25	7	49	-7
DH-G-76×152×4.1	30	-10	10	6	27	-8

As shown in Table 4.3, the 20 RHS in Table 1 are used to produce a total of 22 beam specimens (including two additional specimens for repeated tests). Table 4.3 lists the measured cross-sectional dimensions including the average values of the measured flange external widths (B), web external depths (H), wall thicknesses (t) and internal corner radii (r). For measurement of internal corner radii, the RHS cross sections are scanned and input into AutoCAD where three-point arcs are drawn to fit the internal surfaces of all corners. The corner radii are obtained by measuring the radii of these arcs. The flange internal width-to-thickness ratios (b/t) and the web internal depth-to-thickness ratios (h/t) are also included in Table 4.3. It should be noted that all beam specimens are tested under bending about minor axes. Therefore, the flanges are the longer sides in all cases (Tables 4.1-4.3).

Table 4.3 Measured geometrical properties of RHS beam specimens

Beam specimen	B (mm)	H (mm)	t (mm)	b/t	h/t	r (mm)	S (×10^3 mm^3)	Z (×10^3 mm^3)
D-U-102×76×3.2 D-G-102×76×3.2	101.9	76.5	3.03	29.6	21.2	2.4	25.5	29.3
D-U-102×76×4.8 D-G-102×76×4.8	101.9	76.4	4.36	19.4	13.5	3.4	34.3	40.2
D-U-102×102×3.2 D-G-102×102×3.2	101.9	101.1	3.03	29.6	29.4	3.4	36.8	42.8
D-U-102×102×4.8 D-G-102×102×4.8	102.1	101.6	4.4	19.2	19.1	5.6	50.9	60.1
D-U-127×127×4.8 D-G-127×127×4.8	127.6	127	4.4	25.0	24.9	6.6	82.5	96.4
DH-U-76×76×4.8 DH-G-76×76×4.8 DH-G-76×76×4.8(1)	76.3	76.6	4.81	11.9	11.9	8.5	28.8	34.8
DH-U-102×76×3.2 DH-U-102×76×3.2(1) DH-G-102×76×3.2	102.6	76.9	3.02	30.0	21.5	2.6	25.8	29.6
DH-U-102×76×4.1 DH-G-102×76×4.1	101.8	76.3	4.06	21.1	14.8	4.8	32.4	37.7
DH-U-102×76×4.8 DH-G-102×76×4.8	102	76.6	4.82	17.2	11.9	8.9	37.2	43.9
DH-U-152×76×4.1 DH-G-152×76×4.1	153.1	77.2	4.04	33.9	15.1	5.1	47.1	53.3

(1) Repeated test

In AISC 360-16 [29], for flexural design of RHS, sections are designated as compact, noncompact or slender based on the width-to-thickness ratios of section elements under compression. Compact sections are capable of developing plastic moment $M_P = Zf_y$ (where Z = plastic section modulus) and rotation capacity (R) of 3. In other words, compact sections exhibit sufficient rotational ductility before onset of local buckling which makes them suitable for seismic applications. The definition and calculation of rotation capacity will be explained in Section 2.3. Compact sections in AISC 360-16 [29] are equivalent to Class 1 sections in CSA S16-19 [12]. In AISC 360-16 [29], noncompact sections are defined as those capable of exceeding yield moment $M_y = Sf_y$ (where S = elastic section modulus). Based on the cross-sectional dimensions, AISC 360-16 [29] calculates the nominal flexural strengths of noncompact sections using a linear transition from plastic to yield moment. Noncompact sections are equivalent to Class 2 and Class 3 sections in CSA S16-19 [12], where Class 2 sections can develop plastic moment (but do not possess a rotation capacity of 3) and Class 3 sections can develop yield moments. Sections not capable of developing yield moments (i.e., having elastic local buckling of elements in compression as the limit state) are designated as slender section (or section with slender elements) in AISC 360-16 [29] and Class 4 sections in CSA S16-19 [12]. For ease of evaluation of the existing slenderness limits in [12,29] in Section 4.1, the elastic and plastic section moduli based on the entire cross-sectional area are calculated using the measured dimensions and are listed in Table 4.3. In Section 4.5.2, for calculation of nominal flexural strengths of slender (Class 4) sections, using the effective width method in [12,29], the effective section moduli (S_e) are calculated considering the shift of neutral axes.

4.3.2 Beam Tests

Using the setup illustrated in Fig. 4.1, four-point bending tests are performed on the 22 direct-formed RHS beam specimens to study their flexural behaviours as well as the effects of post-production galvanizing and different strength grades. The beam specimens are simply supported at the two ends. Using a Tinius Olsen hydraulic testing machine with a capacity of 1000 kN and a spreader beam, a pair of concentrated forces are applied on each beam specimen at the two load application points to generate constant moment on the moment span. The moments are calculated using the recorded force data and the length of the shear span (L_s). String pots (with an accuracy of 0.01 mm) are installed at the locations of interest to record displacements, which are subsequently used to calculate curvature and rotation capacity of beam specimens. The beam specimens are loaded at a displacement rate of 2 mm/min. The loads and displacements are logged at one second intervals by the data acquisition system. All regular-strength RHS beam specimens have the same total length of 2 m and the same moment span length (L_m) of 0.6 m. All high-strength RHS beam specimens have the same total length of 1.4 m and the same moment span length of 0.4 m. In both cases, sufficient shear span lengths are provided to ensure that the sections fail by reaching their ultimate moment capacities before shear failures. To achieve the intended failure within the moment span, reinforcement (steel stiffeners and wood blocks in Fig. 4.2) is applied at load application points and supports to prevent unintended premature failure under concentrated forces. With the test setup and the application of proper reinforcement, all 22 beam specimens reach their ultimate capacities by exhibiting failures between the two load application points (i.e., on moment span). Typical failures are shown in Fig. 4.3. Therefore, credence can be given to the test results.

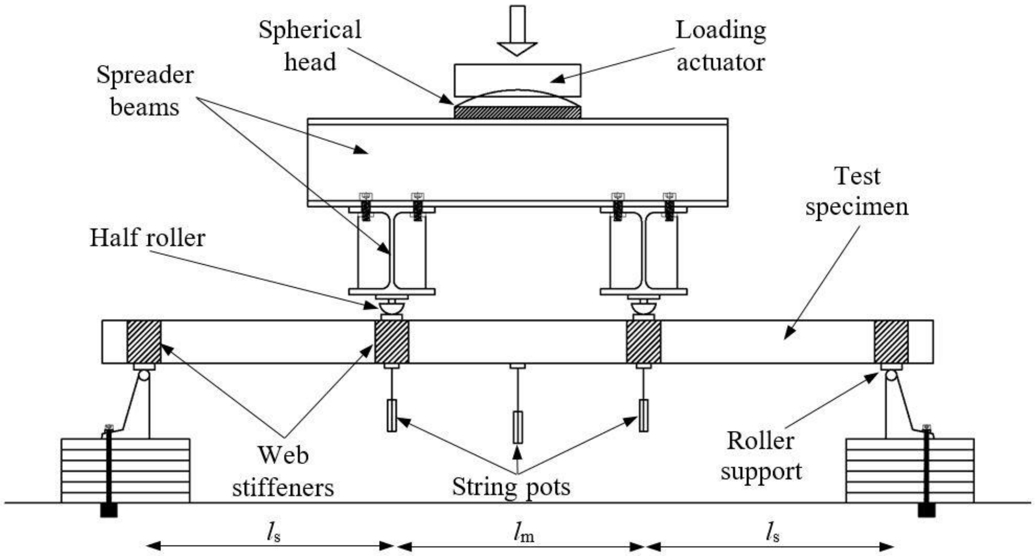

Figure 4.1 Four-point bending test setup

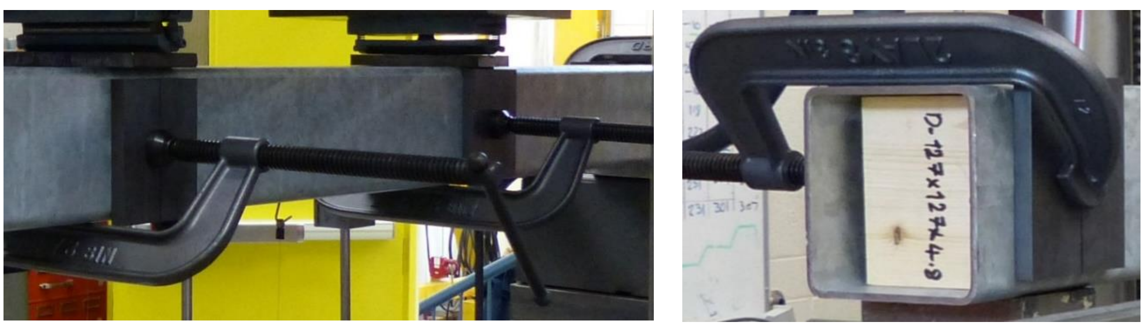

Figure 4.2 Reinforcement at load application points and supports

(a) D-U-76×102×4.8

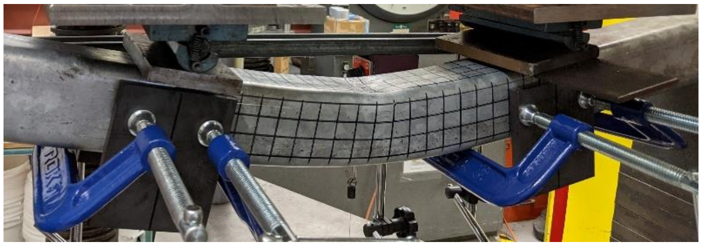

(b) DH-G-76×76×4.8

Figure 4.3 Typical failures of beam specimens

4.3.3 Test results

The bending moments from the four-point bending tests (M) are normalized by the plastic moments ($M_p = Zf_y$) and plotted against normalized curvatures (κ/κ_p) in Fig. 4.4 for the regular- and high-strength RHS, where $\kappa_p = M_p/EI$ is the elastic curvature corresponding to M_p. The actual curvature of moment span (κ) is calculated using Eq. (4.1), where D_m is the deflection at the middle of moment span, and D_l is the average of the deflections at the two load application points [17]. The rotation capacities of the moment spans beam specimens are calculated using Eq. (4.2), where κ_u is curvature at plastic moment during unloading (Fig. 4.5). Such calculation approach is consistent with [12,29]. The calculated rotation capacities of all beam specimens are listed in Table 4.4 and will be used to evaluate: (i) the compact slenderness limit in AISC 360-16 [29] and (ii) the Class 1 slenderness limit from CSA S16-19 [12]. As discussed in Section 4.3.1, the other slenderness limits in [12,29] are based on section ultimate moment capacity (M_u). Therefore, the experimentally obtained M_u are normalized by the calculated M_y and M_p in Table 4.4. M_y and M_p are calculated using: (i) the measured yield strength of tensile coupons machined from flat faces of the RHS specimens, and (ii) the elastic and plastic section moduli in Table 4.3 based on the entire cross-sectional area of the RHS specimens. The key test results are listed in Table 4.4.

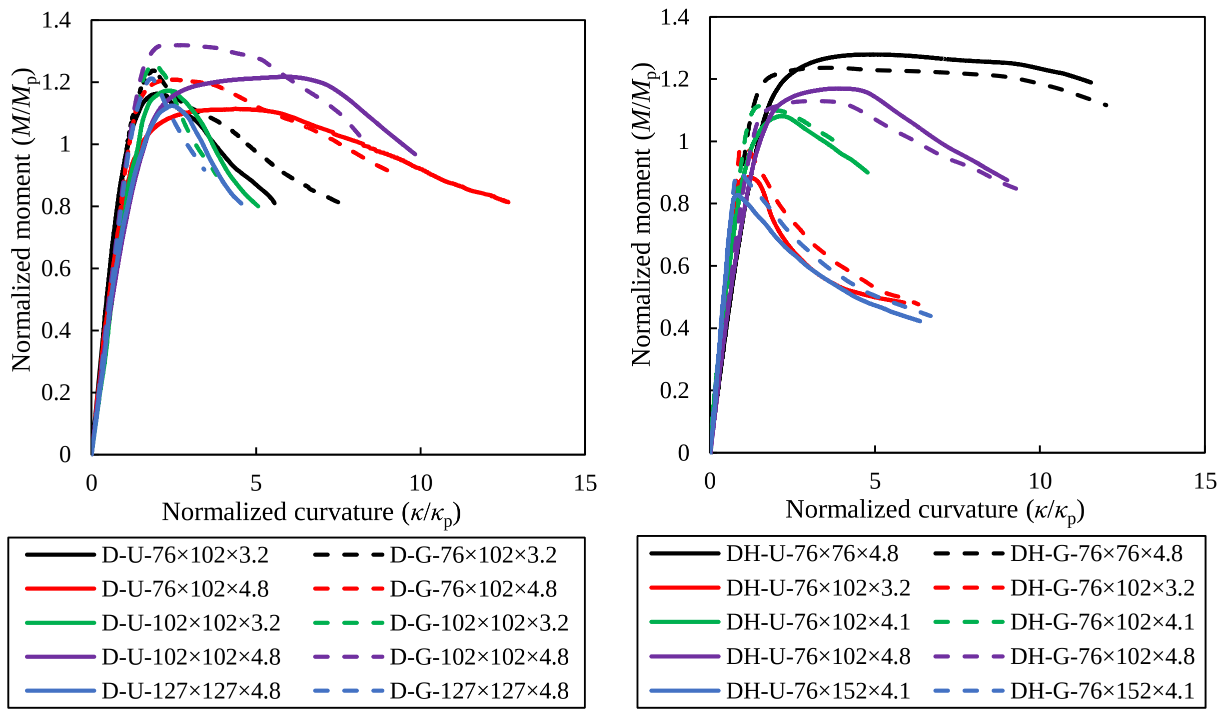

(a) Regular-strength RHS (b) High-strength RHS

Figure 4.4 Normalized moment-curvature relationships of direct-formed RHS beam specimens

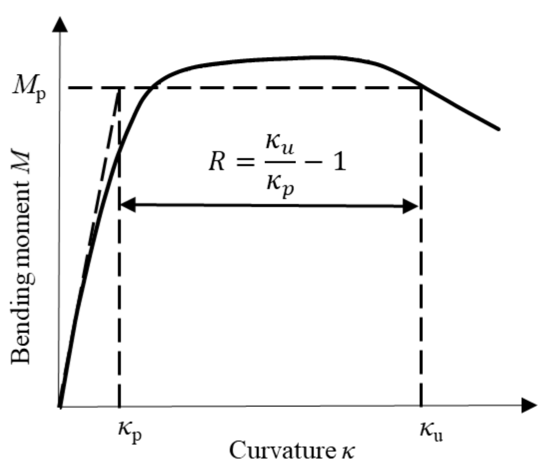

Figure 4.5 Calculation of rotation capacity

$$\kappa = \frac{8(D_m - D_l)}{4(D_m - D_l)^2 + {L_m}^2} \tag{4.1}$$

$$R = \frac{\kappa_u}{\kappa_p} - 1 \tag{4.2}$$

Table 4.4 Four-point bending test results

Beam specimen	M_u (kNm)	M_y (kNm)	M_p (kNm)	M_u/M_y	M_u/M_p	R
D-U-102×76×3.2	12.5	9.4	10.8	1.34	1.17	3.1
D-G-102×76×3.2	13.3	9.4	10.8	1.42	1.24	4.2
D-U-102×76×4.8	18.3	14.0	16.4	1.30	1.11	6.6
D-G-102×76×4.8	19.8	14.0	16.4	1.41	1.21	6.0
D-U-102×102×3.2	17.1	12.7	14.7	1.35	1.16	1.6
D-G-102×102×3.2	18.4	12.7	14.7	1.45	1.25	2.8
D-U-102×102×4.8	29.0	20.3	24.0	1.43	1.21	7.1
D-G-102×102×4.8	29.9	20.3	24.0	1.47	1.25	5.8
D-U-127×127×4.8	42.1	32.6	38.1	1.29	1.11	1.5
D-G-127×127×4.8	45.5	32.6	38.1	1.40	1.20	1.5
DH-U-76×76×4.8	28.4	18.4	22.2	1.55	1.28	>9.6(2)
DH-G-76×76×4.8	27.5	18.4	22.2	1.50	1.24	>10.7(2)
DH-G-76×76×4.8(1)	27.5	18.4	22.2	1.50	1.24	>9.9(2)
DH-U-102×76×3.2	19.1	18.8	21.6	1.02	0.89	0.0(3)
DH-U-102×76×3.2(1)	19.2	18.8	21.6	1.02	0.89	0.0(3)
DH-G-102×76×3.2	21.3	18.8	21.6	1.13	0.99	0.0(3)
DH-U-102×76×4.1	28.3	22.4	26.1	1.26	1.08	2.0
DH-G-102×76×4.1	29.1	22.4	26.1	1.30	1.12	2.7
DH-U-102×76×4.8	33.4	24.2	28.6	1.38	1.17	4.2
DH-G-102×76×4.8	32.3	24.2	28.6	1.33	1.13	4.0
DH-U-152×76×4.1	31.5	33.6	38.0	0.94	0.83	0.0(3)
DH-G-152×76×4.1	34.3	33.6	38.0	1.02	0.90	0.0(3)

(1) Repeated test
(2) Test stopped before moment reduced to M_p during unloading
(3) Beam specimen did not reach M_p during loading

4.4 Flexural behaviours of sections with different production histories

This section presents a direct comparison of the flexural behaviours of RHS with similar cross-sectional dimensions and strength grades but different production histories (indirect-cold-formed versus direct-cold formed; cold-formed versus hot-finished; and untreated versus hot-dip galvanized). The evaluation of applicability of the existing slenderness limits and flexural design formulae in the current North American steel design standards [12,29] is performed in Section 4.5. The ultimate moment capacities of the indirect-cold-formed RHS (untreated) from [17,23,64,65] and the hot-finished RHS from [61,66] are shown in Fig. 4.6 for comparison to the direct-cold-formed RHS (untreated) from this research. For meaningful comparison, only the RHS from [17,23,61,64–66] with nominal yield stresses ranging from 350 to 700 MPa are selected. The ultimate moment capacities (M_u) are normalized by the corresponding plastic moments (M_p) calculated using the measured material and geometric properties using the approach discussed in Section 4.3. The normalized moment capacities are plotted against the normalized flange slenderness values $b/t\sqrt{f_y/E}$ (where b = internal flange width excluding corner portions; and E = Young's modulus). The moment capacities are not plotted against the normalized web slenderness values in this section since the flange slenderness values govern the cross-section classifications of all RHS specimens in this research. This is usually the case for flexural design of RHS with commonly specified (available) cross-sectional sizes based on the commentaries in [12,29]. Further discussions on the cross-section classification rules and flexural design formulae relevant to both flanges and webs of RHS and built-up box sections (with very small flange-width-to-web-depth ratios) are included in Section 4.5.

Associated with cold working is the development of high levels of residual stresses. The existence of high compressive residual stress (in RHS longitudinal direction) in general accelerates failure of compression flange in RHS under flexural loading. As illustrated in Fig. 1.3, the indirect-forming process roll-forms coil material into a CHS before further shaping it to an RHS. Therefore, the entire cross section has experience high degrees of cold working. Recent research involving measurement of residual stresses in 26 RHS specimens with different production histories [55] showed that, comparing to indirect-formed RHS, direct-formed RHS in general have lower levels of residual stresses since the cold-working is mainly concentrated at the four corner regions during production (Fig. 1.3). Therefore, it can be speculated that the compression flange in a direct-formed RHS can resist higher stress under flexural loading since the flat portion of the compression flange is not heavily cold-worked during production. Such speculation is substantiated by the comparison in Fig. 4.6a. As shown, in many cases the direct-formed RHS specimens have superior flexural strengths comparing to the indirect-formed RHS counterparts due to the delay of compression flange failure. This is consistent with the findings in [6,44] for stub column behaviours where the onsets of local buckling in direct-formed RHS are delayed considerably due to the inherently low levels of residual stresses.

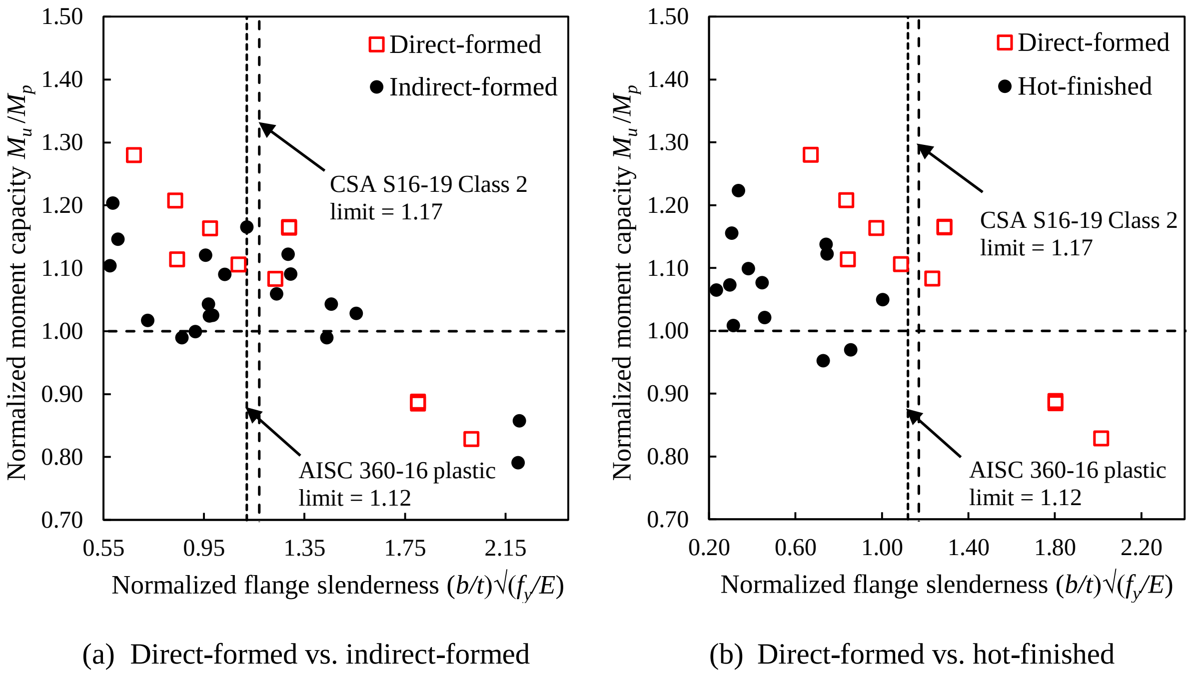

Figure 4.6 Comparisons of direct-formed RHS (untreated) to indirect-formed RHS from [17,23,64,65] and hot-finished RHS from [61,66]

As shown in Fig. 4.6b, over the range of flange slenderness values where previous experimental data [61,66] is available, the direct-cold-formed RHS specimens have superior flexural strengths comparing to the hot-finished RHS counterparts. It should be noted that the hot-finished RHS in [61,66] are produced by cold-forming coil material into CHS before hot-shaping it into RHS. The hot-shaping process (also know as hot-finishing) is performed at a normalizing temperature of approximately 900 ºC. Such finishing intends to alter microstructure of steel, resulting in reduced hardness and increased ductility. Therefore, hot-finished products are excellent choices for applications such as dynamically loaded elements in welded structures, etc., where low-temperature notch-toughness properties may be important. It is also expected that all cold-forming-induced residual stresses are completely relieved at the normalized temperature. However, as a trade-off the cold-forming-induced strength enhancement is also removed, which explains the flexural strengths difference between the direct-cold-formed RHS specimens and the hot-finished RHS specimens in Fig. 4.6b.

Also shown in Figs. 4.6a and 4.6b are the existing flange slenderness limits for compact section from AISC 360-16 [29] and Class 2 section from CSA S16-19 [12]. In both cases, the sections are expected to reach the plastic moments (M_p). As shown, such flange slenderness limits are in general applicable for indirect-cold-formed and hot-finished RHS but conservative for direct-cold-formed RHS (untreated).

The comparisons of ultimate moment capacities of untreated and galvanized direct-formed RHS are shown in Figs. 4.7a and 4.7b for the regular- and high-strength materials, respectively. The following observations can be made:

i. For regular-strength RHS, consistent increases of flexural strengths after hot-dip galvanizing are observed. This is consistent with the findings in the previous research on the effect of galvanizing on residual stresses in CHS [5] and RHS [55], where post-production galvanizing has been experimentally proven effective in partially relieving the cold-forming-induced residual stresses. The level of reduction is similar to the intended levels through the applications of post-production heat treatment per ASTM A1085 Supplement S1 [7], or the Class H finish per CSA G40.20/G40.21 [8] (both at 450 °C). Similar to such heat treatment, the molten zinc bath is typically maintained at 450 °C [5,55]. Such temperature does not alter grain structure and hence have minor effects on the material strengths. It can be seen in Fig. 11a that the existing flange slenderness limits for compact section from AISC 360-16 [29] and Class 2 section from CSA S16-19 [12] become even more conservative for galvanized direct-formed regular-strength RHS.

ii. For high-strength RHS, increases of flexural strengths after hot-dip galvanizing are observed for sections with large slenderness values. On the other hand, no evident increase is observed for sections with small slenderness values based on the available experimental data in this study. It should be noted that all RHS specimens in this study are hot dipped in the same molten zinc bath at the same time for the same immersion duration. Therefore, there is no variation of thermal input among all RHS specimens. The RHS specimens with smaller slenderness values (corresponding to larger wall thicknesses in this research) have larger thermal masses. Therefore, for the same thermal input, the changes of residual stresses in them are smaller. In theory, the onset of local buckling is primarily affected by the residual stress-over-yield stress ratio. Therefore, it can be speculated that the galvanizing-induced improvement of flexural strengths would be smaller for high-strength RHS with large wall thicknesses, considering the smaller change of residual stress and high yield stress.

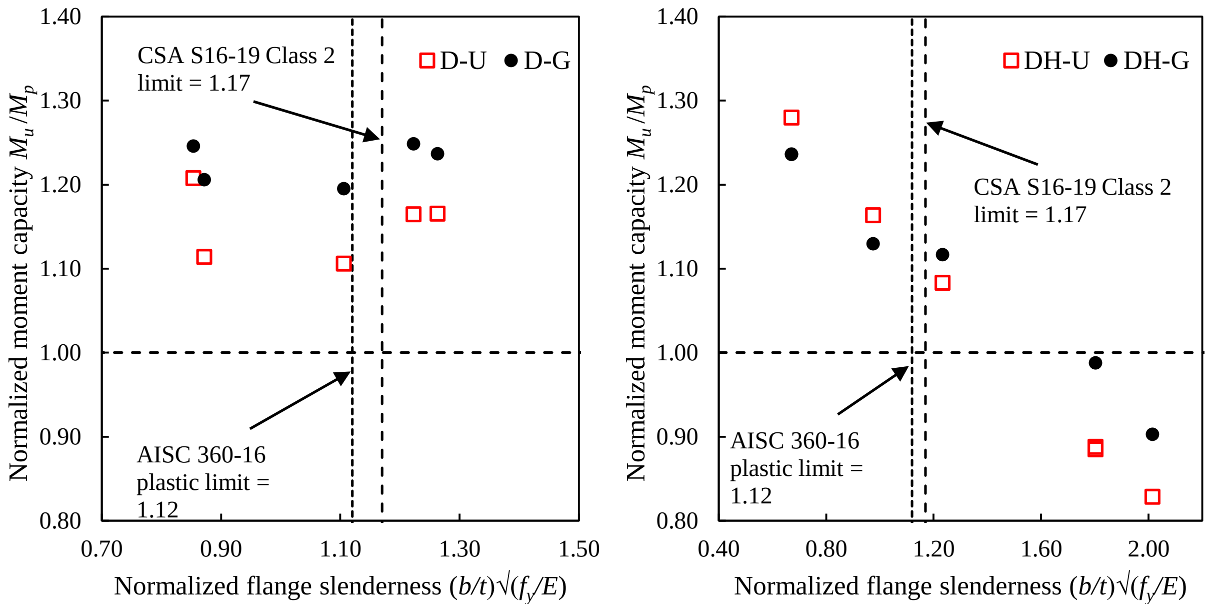

(a) Regular strength (b) High strength

Figure 4.7 Comparisons of untreated and galvanized direct-formed RHS

4.5 Evaluation of current North American flexural design rules

4.5.1 Cross-section slenderness limits

For flexural design, in AISC 360-16 [29] Table B4.1b, depending on the width-to-thickness ratios of the compression elements in members subject to flexure, steel sections are classified as compact, noncompact or slender. The slenderness limits for RHS and built-up box sections from [29] are reproduced here in Table 4.5, where the plastic slenderness limit (λ_p) differentiates compact and noncompact elements, and the yield slenderness limit (λ_r) differentiates noncompact and slender elements. After cross-section classification, the member nominal flexural strength can be calculated as the lowest values obtained according to the limit states of yielding (plastic moment), flange local buckling and web local buckling using the design formulae in Section F7 of AISC 360-16 [29]. Similarly, in CSA S16-19 [12] Table 1, depending on the width-to-thickness ratios of the compression elements in members subject to flexure, steel sections are classified as Class 1, 2, 3 or 4. The slenderness limits for RHS from [12] are reproduced here in Table 4.6, where λ_{c1}, λ_{c2} and λ_{c3} are the maximum slenderness values for Classes 1, 2 and 3. After cross-section classification, the member nominal flexural strength can be calculated using the design formulae in Section 13.5 of CSA S16-19 [12]. For design of sections with slender elements, both AISC 360-16 [29] and CSA S16-19 [12] apply the effective width method, where the effective section moduli are calculated considering the effective element widths and the shift of neutral axes. In this paper, Section 4.5.1 examines the applicability of the cross-section classification rules from AISC 360-16 [29] and CSA S16-19 [12] on direct-formed regular- and high-strength RHS (untreated and galvanized). Section 4.5.2 examines the applicability of existing flexural design formulae in [12,29].

Table 4.5 Slenderness limits for compression elements subject to flexure based on ANSI/AISC 360-16 [29]

Element description	Normalized slenderness	Normalized slenderness limits λ_p	Normalized slenderness limits λ_r
Flanges of RHS	$(b/t)\sqrt{f_y/E}$	1.12	1.40
Webs of RHS and built-up box sections	$(h/t)\sqrt{f_y/E}$	2.42	5.70

Table 4.6 Slenderness limits for compression elements subject to flexure based on CSA S16-19 [12]

Element description	Normalized slenderness	Normalized slenderness limits λ_{c1}	λ_{c2}	λ_{c3}
Flanges of RHS	$(b/t)\sqrt{f_y/E}$	0.94	1.17	1.50
Webs of RHS	$(h/t)\sqrt{f_y/E}$	2.46	3.80	4.25

The following observations can be made by comparing the slenderness limits in Tables 4.5 and 4.6:

i. The plastic slenderness limits for compact sections from AISC 360-16 [29] (λ_p = 1.12 and 2.24 for flanges and webs in Table 4.5) and those for Class 1 sections from CSA S16-19 [12] (λ_{c1} = 0.94 and 2.46 for flanges and webs in Table 4.6) are slightly different. In design practice, actual corner radii are in general not available. Therefore, AISC 360-16 [29] calculates the internal width as external width minus 3t, while CSA S16-19 [12] calculates internal width as external width minus 4t. On the other hand, all section moduli in this research are calculated using the measured cross-sectional dimensions.

ii. The flange slenderness limits for noncompact sections from AISC 360-16 [29] (λ_r = 1.40 in Table 4.5) and that for Class 3 sections from CSA S16-19 [12] (λ_{c3} = 1.50 in Table 4.6) are similar. However, the web slenderness limits for noncompact sections from AISC 360-16 [29] (λ_r = 5.70 in Table 4.5) is a lot more conservative than that for Class 3 sections from CSA S16-19 [12] (λ_{c3} = 4.25 in Table 4.6). As noted in Table 4.5, such web slenderness limit in general caters to built-up box sections with very small flange-width-to-web-depth ratios. Therefore, it is often not applicable for cold-formed RHS with commonly specified (available) cross-sectional dimensions.

In AISC 360-16 [29] and CSA S16-19 [12], compact (Class 1) sections refer to those capable of developing plastic moments (M_P) and rotation capacity (R) of 3. Therefore, the rotational capacities of all RHS beam specimens (untreated and galvanized) are plotted against the normalized flange slenderness values in Fig 4.8. The existing compact (Class 1) section slenderness limits for flanges (λ_p in Table 4.5 and λ_{c1} in Table 4.6) are also shown for direct comparison. Based on the best fit lines of the data points, both the AISC 360-16 [29] plastic limit and the CSA S16-19 [12] Class 1 limit are applicable. The applicability of the existing web slenderness limits cannot be evaluated (irrelevant) since the flange slenderness values govern the cross-section classifications of all RHS specimens in this research, which is often the case for flexural design of RHS with commonly specified (available) cross-sectional sizes. The same applies to the noncompact (Class 2 and Class 3) and noncompact (Class 4) RHS sections discussed herein.

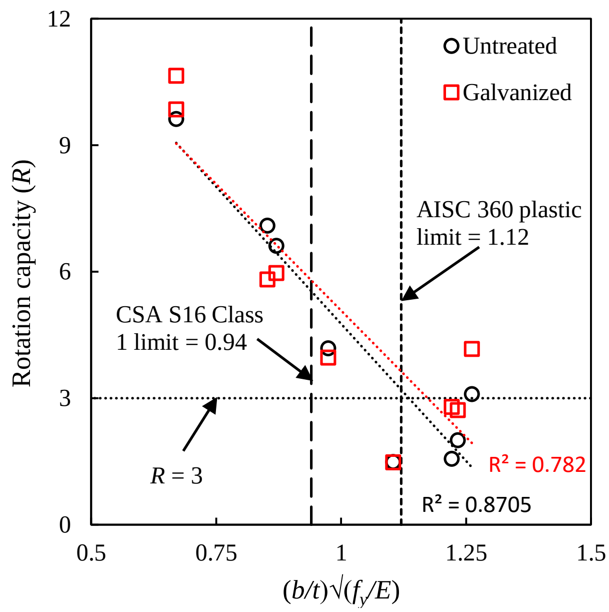

Figure 4.8 Evaluation of Class 1 (plastic) flange slenderness limits in [12,29]

In CSA S16-19 [12], Class 2 sections refer to those capable of developing plastic moments (M_P) but need not allow for subsequent moment redistribution. Therefore, for all RHS beam specimens (untreated and galvanized), the ultimate moment capacities (M_u) are normalized by the calculated plastic moments (M_P) and plotted against the normalized flange slenderness values in Fig. 4.9. The existing Class 2 section slenderness limits (λ_{c2} in Table 4.6) are also shown for direct comparison. The following observations can be made:

i. Based on the best fit line for untreated direct-formed RHS in Fig. 4.9, the Class 2 flange slenderness limit from CSA S16-19 [12] is very conservative. A λ_{c2}-value of 1.50 may be more appropriate in this case. However, to propose accurate slenderness limit, a comprehensive FE parametric study is needed to produce more data points covering extended range of cross-sectional dimensions. As discussed in Section 1, comparing to the indirect-forming approach, the direct-forming approach is relatively new. The existing cross-section classification rules for RHS in the North American steel design standards [12,29] were in general developed based on research on indirect-formed RHS. Since direct-formed RHS have inherently lower residual stress levels, it is intuitive that the existing flange slenderness limits can be conservative for them.

ii. Based on the best fit line for galvanized direct-formed RHS in Fig. 4.9, the Class 2 flange slenderness limit from CSA S16-19 [12] becomes even more conservative. As discussed earlier, similar to the application of the heat treatment per ASTM A1085 Supplement S1 [7], or the Class H finish per CSA G40.20/G40.21 [8], the application of post-production galvanizing can effectively lower cold-forming-induced residual stresses (without removing the cold-forming-induced strength enhancement) and this in turn improves the member flexural behaviours. As shown, a λ_{c2}-value of 1.70 may be more appropriate for the flanges of the galvanized direct-formed RHS specimens.

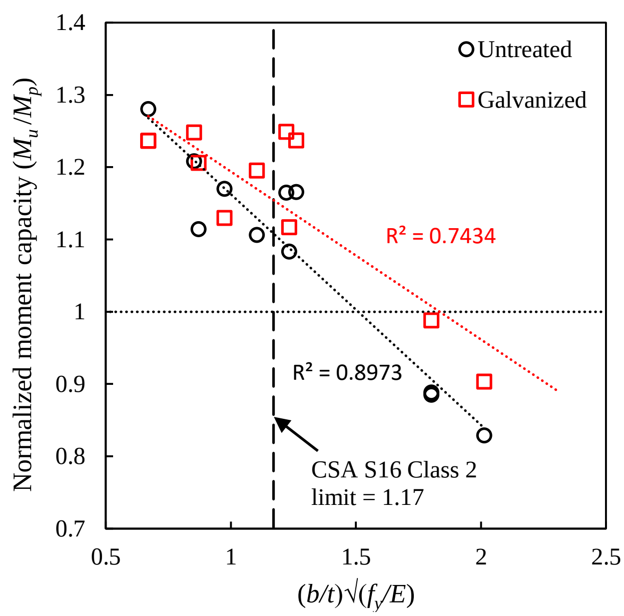

Figure 4.9 Evaluation of Class 2 flange slenderness limits in [12]

In AISC 360-16 [29] and CSA S16-19 [12], noncompact (Class 3) sections refer to those capable of developing yield moments (M_y). Therefore, for all RHS beam specimens (untreated and galvanized), the ultimate moment capacities (M_u) are normalized by the calculated yield moments (M_y) and plotted against the normalized flange slenderness values in Fig 4.10. The existing yield slenderness limit for noncompact (Class 3) sections (λ_r in Table 4.5 and λ_{c3} in Table 4.6) are also shown for direct comparison. The following observations can be made:

i. Based on the best fit line for untreated direct-formed RHS in Fig. 4.10, both the AISC 360-16 [29] and CSA S16-19 [12] flange slenderness limits are very conservative. The existing yield (Class 3) slenderness limits (λ_r in Table 4.5 and λ_{c3} in Table 4.6) tend to misjudge nonslender sections as slender sections, since the inherently low levels of residual stresses in direct-formed RHS are not considered. This will result in unnecessary penalty and member strength underestimation when using the effective width method for flexural strength calculation. Based on the best fit line for untreated direct-formed RHS in Fig. 4.10, a λ_r (or λ_{c3})-value of 1.95 may be more appropriate for the flanges of the untreated direct-formed RHS specimens.

ii. Similar to the comparisons between untreated and galvanized RHS specimens in Fig. 4.9, the codified yield (Class 3) slenderness limits become more conservative for the flanges of the galvanized direct-formed RHS specimens. A λ_r (or λ_{c3})-value of 2.25 may be more appropriate in this case.

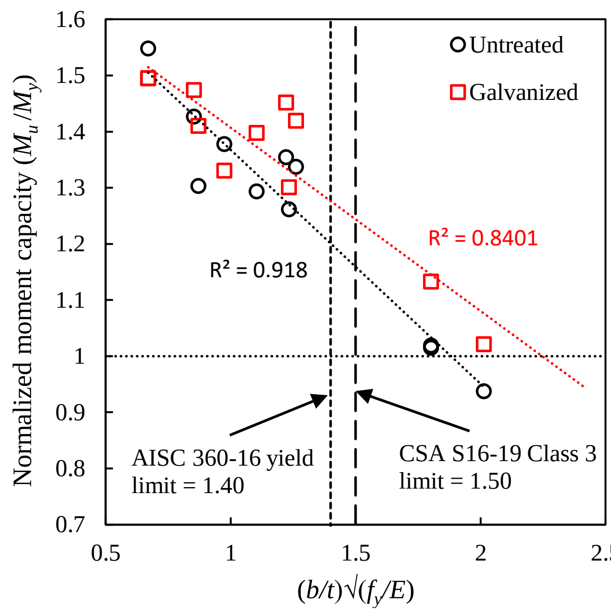

Figure 4.10 Evaluation of Class 3 (yield) flange slenderness limits in [12,29]

As discussed in Section 3, for flexural design of cold-formed RHS of commonly specified (available) cross-sectional dimensions, the flange slenderness values usually govern the cross-section classifications, which is consistent with the RHS specimens in this experimental research and the commentaries in [12,29]. Therefore, the predicted cross-sectional behaviours based on the measured dimensions and the existing flange slenderness limits in Tables 4.5 and 4.6 from [12,29] are compared to the experimentally observed behaviours in Table 4.7. As shown, the existing slenderness limits from AISC 360-16 [29] and CSA S16-19 [12] are in many cases too conservative for direct-formed RHS (untreated and galvanized). Therefore, based on the available experimental data, this section has suggested some slenderness limits more suitable for direct-formed RHS (untreated and galvanized). However, a comprehensive FE parametric study is needed to cover extended ranges of cross-sectional dimensions to substantiate the suggested limits. It can also be seen in Table 4.7 (DH-U-76×152×4.1 versus DH-G-76×152×4.1) that the application of post-production galvanizing converted a slender section into a nonslender section in this study.

Table 4.7 Predicted and experimentally observed cross-sectional behaviours of beam specimens

Beam specimen	$(b/t)\sqrt{f_y/E}$	Predicted behaviour based on [12,29]	Experimentally observed behaviour
D-U-102×76×3.2	1.26	Class 3 (noncompact)	Class 1 (compact)
D-G-102×76×3.2		Class 3 (noncompact)	Class 1 (compact)
D-U-102×76×4.8	0.87	Class 1 (compact)	Class 1 (compact)
D-G-102×76×4.8		Class 1 (compact)	Class 1 (compact)
D-U-102×102×3.2	1.22	Class 3 (noncompact)	Class 2 (noncompact)
D-G-102×102×3.2		Class 3 (noncompact)	Class 2 (noncompact)
D-U-102×102×4.8	0.85	Class 1 (compact)	Class 1 (compact)
D-G-102×102×4.8		Class 1 (compact)	Class 1 (compact)
D-U-127×127×4.8	1.11	Class 2 (compact)	Class 2 (noncompact)
D-G-127×127×4.8		Class 2 (compact)	Class 2 (noncompact)
DH-U-76×76×4.8	0.67	Class 1 (compact)	Class 1 (compact)
DH-G-76×76×4.8		Class 1 (compact)	Class 1 (compact)
DH-G-76×76×4.8 (1)		Class 1 (compact)	Class 1 (compact)
DH-U-102×76×3.2	1.80	Class 4 (slender) with FLB (2)	Class 3 (noncompact)
DH-U-102×76×3.2 (1)		Class 4 (slender) with FLB (2)	Class 3 (noncompact)
DH-G-102×76×3.2		Class 4 (slender) with FLB (2)	Class 3 (noncompact)
DH-U-102×76×4.1	1.23	Class 3 (noncompact)	Class 2 (noncompact)
DH-G-102×76×4.1		Class 3 (noncompact)	Class 2 (noncompact)
DH-U-102×76×4.8	0.97	Class 2 (compact)	Class 1 (compact)
DH-G-102×76×4.8		Class 2 (compact)	Class 1 (compact)
DH-U-152×76×4.1	2.01	Class 4 (slender) with FLB (2)	Class 4 (slender) with FLB (2)
DH-G-152×76×4.1		Class 4 (slender) with FLB (2)	Class 3 (noncompact)

(1) Repeated test
(2) FLB = flange local buckling

4.5.2 Flexural strengths

In this section, the experimentally obtained flexural strengths (i.e., ultimate moment capacities) are compared to the calculated nominal values (i.e., resistance factor = 1.00) to examine the flexural design formulae from AISC 360-16 [29] and CSA S16-19 [12].

In AISC 360-16 [29], for compact sections, the nominal flexural strengths equal the plastic moments. For sections with noncompact flanges and/or webs, two design formulae considering the limit states of flange local buckling and web local buckling are available. Both formulae provide linear transition from M_p to M_y, and M_n is determined as the lesser of the two. For design of sections with slender flange elements, AISC 360-16 [29] adopts the effective width approach, where effective section moduli (S_e) are calculated using effective flange widths (b_e) based on the λ_r-values in Table 4.7, considering the shift of neutral axis. AISC 360-16 Section F7.3 [29] contains formulae for calculation of nominal flexural strengths for sections with slender webs. However, this is an extremely rare case for cold-formed RHS with commonly specified cross-sectional dimensions. Such formulae in general cater to built-up box sections with very small flange-width-to-web-depth ratios. Therefore, such limit state and the corresponding design formulae are not evaluated in this section. In summary, for flexural design of RHS, the nominal strength shall be calculated as the lowest value obtained from Eqs. (4.3), (4.4), (4.6), and (4.8) herein. As shown by Eqs. (4.5), (4.7) and (4.10), the flexural design formulae are heavily based on the existing slenderness limits in Table 4.5. As shown in Section 5.5.1, such limits are in many cases very conservative for direct-formed regular- and high-strength RHS (untreated and galvanized). Therefore, it can be expected that the predicted nominal flexural strengths will be conservative as well.

Limit state: yielding of entire cross section

$$M_n = M_p = f_y Z \tag{4.3}$$

Limit state: flange local buckling for sections with noncompact flanges

$$M_n = M_p - (M_p - M_y).\left[3.57(b/t)\sqrt{f_y/E} - 4.0\right] \leq M_p \tag{4.4}$$

Eq. (4.4) is derived using the following general formula (Eq. (4.5)):

$$M_n = M_p - (M_p - M_y).\left[\frac{(b/t)\sqrt{f_y/E} - \lambda_p}{\lambda_r - \lambda_p}\right] \leq M_p \tag{4.5}$$

where λ_p = 1.12 and λ_r = 1.40 from Table 4.5.

Limit state: web local buckling for sections with noncompact webs

$$M_n = M_p - (M_p - M_y).\left[0.305(h/t)\sqrt{f_y/E} - 0.738\right] \leq M_p \tag{4.6}$$

Eq. (4.6) is derived using the following general formula (Eq. (4.7)):

$$M_n = M_p - (M_p - M_y).\left[\frac{(h/t)\sqrt{f_y/E} - \lambda_p}{\lambda_r - \lambda_p}\right] \leq M_p \tag{4.7}$$

where λ_p = 2.42 and λ_r = 5.70 from Table 4.5.

Limit state: flange local buckling for sections with slender flanges

$$M_n = f_y S_e \tag{4.8}$$

where S_e = effective section modulus determined with the effective width, b_e, of the compression flange taken as:

$$b_e = \begin{cases} b & \text{when } (b/t)\sqrt{f_y/E} \leq 1.40 \\ 1.92t\sqrt{E/f_y}\left(1 - \dfrac{0.38\sqrt{E/f_y}}{b/t}\right) & \text{when } (b/t)\sqrt{f_y/E} > 1.40 \end{cases} \tag{4.9}$$

Eq. (4.9) is derived using the following general formula (Eq. (4.10)):

$$b_e = \begin{cases} b & \text{when } (b/t)\sqrt{f_y/E} \leq \lambda_r \\ \left[\dfrac{c_2\lambda_r}{(b/t)\sqrt{f_y/E}} - c_1\left(\dfrac{c_2\lambda_r}{(b/t)\sqrt{f_y/E}}\right)^2\right].b & \text{when } (b/t)\sqrt{f_y/E} > \lambda_r \end{cases} \tag{4.10}$$

where c_1 = 0.2 and c_2 = 1.38 are the effective width imperfection adjustment factors from Table E7.1 in AISC 360-16 [29]. λ_r = 1.40 is from Table 4.5.

In CSA S16-19 [12], for Class 1 and Class 2 RHS sections, $M_n = M_p = f_y Z$. For Class 3 RHS sections $M_n = M_y = f_y S$. For Class 4 RHS sections with slender webs, similar to the approach in AISC 360-16 [29], effective section moduli (S_e) are determined using an effective flange width of $670t/\sqrt{f_y}$ (based on the Class 3 slenderness limit in Table 4.6), considering the shift of neutral axes, and $M_n = M_y = f_y S_e$. Calculation rule is available for sections with flanges meeting the requirements of Class 3 but the web slenderness exceeding the limit for Class 3. However, such calculation rule in general cater to built-up box sections with very small flange-width-to-web-depth ratios and is thus not applicable to cold-formed RHS with commonly specified (available) cross-sectional dimensions.

The experimentally obtained ultimate moment capacities (M_u) of the RHS beam specimens are compared to the design curves based on the formulae in [12,29] in Figs. 4.11 and 4.12. The key statistics of the comparisons between M_u and the nominal flexural strengths calculated based on [12,29] ($M_{u,AISC}$ and $M_{u,CSA}$, respectively) are listed in Table 4.8. The following observations can be made:

i. As shown in Figs. 4.11 and 4.12, in all cases the predictions by AISC 360-16 [29] and CSA S16-19 [12] are conservative for direct-formed regular- and high-strength RHS (untreated and galvanized). CSA S16-19 [12] is slightly more conservative based on the average M_u/M_n-ratios in Tables 4.8 and 4.9.

ii. For the RHS specimens classified as compact (Class 1) sections based on the existing slenderness limits, both AISC 360-16 [29] and CSA S16-19 [12] provides conservative predictions for flexural strengths (Figs. 4.11 and 4.12) since the cold-forming-induced strength enhancements above f_y are not considered in calculation.

iii. For the RHS specimens classified as noncompact (Class 2 and Class 3) sections based on the existing slenderness limits, both AISC 360-16 [29] and CSA S16-19 [12] provides conservative predictions (Figs. 4.11 and 4.12) since the inherently low levels of residual stresses in direct-formed RHS are not considered. AISC 360-16 [29] provides better predictions since a linear transition from M_p to M_y is considered for noncompact sections.

iv. For the RHS specimens classified as slender (Class 4) sections based on the existing slenderness limits, both AISC 360-16 [29] and CSA S16-19 [12] provides conservative predictions. As shown in Figs. 4.11 and 4.12, the existing design curves have the tendency to misjudge nonslender direct-formed sections as slender sections, resulting in unnecessary penalty to effective cross-sectional area and underestimation of flexural strengths.

v. Based on available data and the average M_u/M_n-ratios in Tables 4.8 and 4.9, it can be seen that: (a) the existing design provisions are more conservative for galvanized RHS than untreated RHS; and (b) the existing design provisions are more conservative for regular-strength RHS than high-strength RHS.

vi. Based on the above, it will be desirable to use the experimental results from the 22 full-scale beam tests to validate FE models for a comprehensive parametric study to produce more data points covering extended range of cross-sectional dimensions. A reliability analysis can then be performed to accurately assess the applicability of existing design rules and propose modified design rule as necessary.

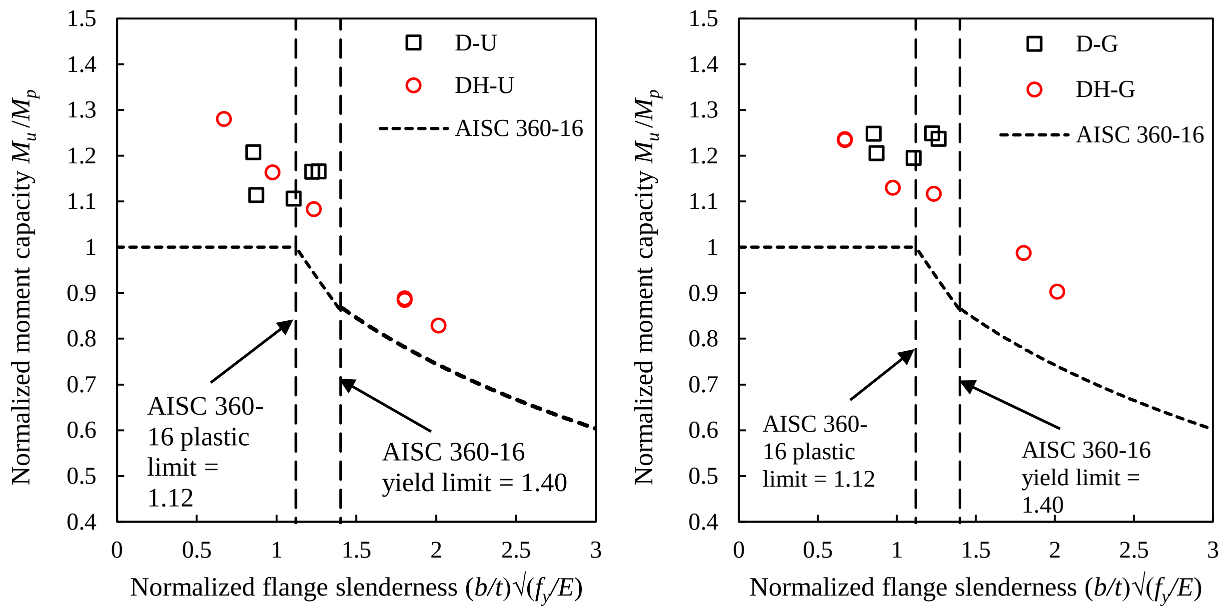

(a) Untreated RHS (b) Galvanized RHS

Figure 4.11 Comparisons of experimental results with nominal flexural strengths calculated using AISC 360-16 [29]

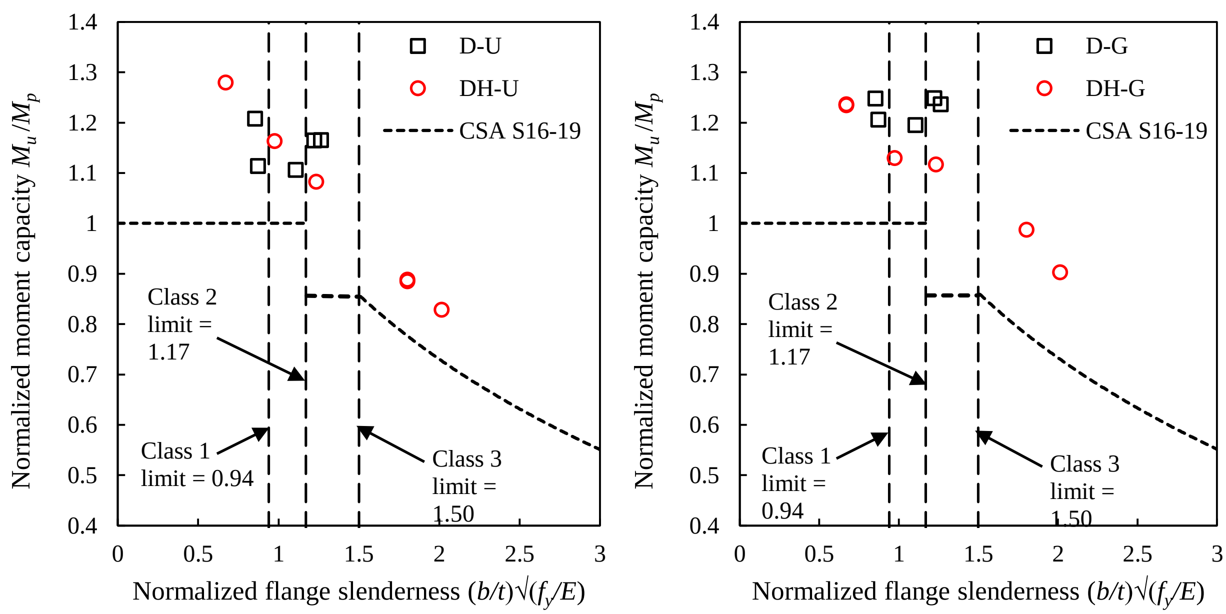

(a) Untreated RHS (b) Galvanized RHS

Figure 4.12 Comparisons of experimental results with nominal flexural strengths calculated using CSA S16-19 [12]

Table 4.8 Key comparison results for untreated direct-formed RHS beam specimens

Beam specimen	M_u (kN.m)	M_u / $M_{n,\mathrm{AISC}}$	M_u / $M_{n,\mathrm{CSA}}$
D-U-102×76×3.2	12.5	1.21	1.29
D-U-102×76×4.8	18.3	1.19	1.19
D-U-102×102×3.2	17.1	1.15	1.22
D-U-102×102×4.8	29.0	1.26	1.26
D-U-127×127×4.8	42.1	1.14	1.14
DH-U-76×76×4.8	28.4	1.19	1.19
DH-U-102×76×3.2	19.1	1.19	1.19
DH-U-102×76×3.2(1)	19.2	1.19	1.20
DH-U-102×76×4.1	28.3	1.16	1.27
DH-U-102×76×4.8	33.2	1.11	1.11
DH-U-152×76×4.1	31.5	1.15	1.18
Mean (D-U)		1.19	1.22
COV (D-U)		0.041	0.048
Mean (DH-U)		1.17	1.19
COV (DH-U)		0.028	0.043
Mean (D-U+DH-U)		1.18	1.20
COV (D-U+DH-U)		0.034	0.043

(1) Repeated test

Table 4.9 Key comparison results for galvanized direct-formed RHS beam specimens

Beam specimen	M_u (kN.m)	M_u / $M_{n,\mathrm{AISC}}$	M_u / $M_{n,\mathrm{CSA}}$
D-G-102×76×3.2	12.5	1.29	1.36
D-G-102×76×4.8	18.3	1.29	1.29
D-G-102×102×3.2	17.1	1.23	1.31
D-G-102×102×4.8	29.0	1.30	1.30
D-G-127×127×4.8	42.1	1.24	1.24
DH-G-76×76×4.8	28.4	1.15	1.15
DH-G-76×76×4.8$^{(1)}$	19.1	1.15	1.15
DH-G-102×76×3.2	19.2	1.32	1.33
DH-G-102×76×4.1	28.3	1.19	1.31
DH-G-102×76×4.8	33.2	1.07	1.07
DH-G-152×76×4.1	31.5	1.25	1.29
Mean (D-G)		1.27	1.30
COV (D-G)		0.026	0.033
Mean (DH-G)		1.19	1.22
COV (DH-G)		0.073	0.088
Mean (D-G+DH-G)		1.23	
COV (D-G+DH-G)		0.060	

(1) Repeated test

4.6 Conclusions

In this paper, the flexural behaviours of new-generation direct-formed RHS (nominal yield stresses of 350 and 690 MPa) are examined for the first time via a comprehensive testing program including a total of 22 full-scale beam specimens. The direct-formed RHS specimens are shown to have superior flexural behaviours by comparison to the indirect-cold-formed and hot-finished RHS specimens from previous studies. The application of post-production hot-dip galvanizing is proven effective in partially relieving cold-forming-induced residual stresses and improving the flexural behaviours of the direct-formed RHS specimens. The applicability of the flexural design rules in the current North American steel design standards on direct-formed regular- and high-strength RHS (untreated and galvanized) is evaluated using the experimental data. The existing slenderness limits and flexural design formulae are shown very conservative in many cases.

Nomenclatures

B	External width
b	Flat width
D_{l}	Average of deflections at two loading points
D_{m}	Deflection at mid-span
E	Young’s modulus
f_{u}	Ultimate stress
f_{y}	Yield stress
H	External depth
κ_{p}	Elastic curvature corresponding to plastic moment
κ_{u}	Curvature at plastic moment during unloading
L_{m}	Length of moment span
L_{s}	Length of shear span
$M_{n,\mathrm{AISC}}$	Nominal flexural strength based on ANSI/AISC 360-16
$M_{n,\mathrm{CSA}}$	Nominal flexural strength based on CSA S16-19
M_{p}	Plastic moment
M_{u}	Ultimate moment
M_{y}	Yield moment
r	Internal corner radius
t	Wall thickness
S	Elastic section modulus
Z	Plastic section modulus
$\varepsilon_{\mathrm{rup}}$	Rupture strain from tensile coupon test
σ_{b}	Bending residual stress
σ_{m}	Membrane residual stress

Chapter 5: Design of Direct-Formed Square and Rectangular Hollow Section Beams

Kamran Tayyebi, Min Sun, Kian Karimi, Ray Daxon, Brandon Rossi, *Design of direct-formed square and rectangular hollow section beams*, Eng. Struct. (2021) (under review).

5.1 Abstract

A complementary experimental study showed that the flexural member design rules in the North American steel design standards (AISC 360-16 and CSA S16-19) can be excessively conservative for direct-formed regular- and high-strength steel square and rectangular hollow sections (hereinafter collectively referred to as RHS). It was also found that post-production hot-dip galvanizing can further improve member flexural behaviours through effective reduction of cold-forming-induced residual stresses. In this study, the experimental results of 22 full-scale beam tests from the complementary experimental study are used to validate non-linear finite element (FE) models. The FE models are developed using previously measured stress-strain relationships, residual stresses, and geometric imperfections. A subsequent parametric study including 708 beam models is performed to cover extended ranges of cross-sectional dimensions. The applicability of the existing slenderness limits and flexural design formulae are examined using the experimental and numerical data. The results justify the use of less stringent slenderness limits and higher design curves for direct-formed regular- and high-strength RHS beams (non-galvanized and galvanized). Modifications to the existing design rules are proposed. Based on reliability analyses, the modified approaches are proven accurate and provide adequate safety margins.

5.2 Introduction

In North America, cold-formed square and rectangular hollow sections (hereinafter collectively referred to as RHS) of commonly specified cross-sectional dimensions are produced using either the indirect-forming approach or the direct-forming approach. The indirect-forming approach (Fig. 1.3d) consists of three steps: (1) roll-forming the coil material progressively into a circular hollow section; (2) closing the section using electric resistance welding (ERW); and (3) reshaping the circular section into the final square or rectangular shape. On the other hand, the direct-forming approach (Fig. 1.3b) roll-forms the coil material directly into the final square or rectangular shape.

RHS with similar cross-sectional dimensions but different production histories (i.e., different cold-forming approaches and post-production treatments) can have significantly different material and residual stress properties (e.g., [6,16,23,24,44,55,68]). Comparing to indirect-formed RHS, direct-formed RHS in general contain lower levels of residual stresses over cross sections, since the flat faces are not severely cold worked during production [16,24,55]. As a result, direct-formed RHS are proven experimentally by [6,68] to have superior stub column and beam behaviours, comparing to their indirect-formed counterparts. Provisions in the current North American steel design standards (AISC 360-16 [29] and CSA S16-19 [12]) do not differentiate RHS members cold-formed by different approaches. In particular, the experimental investigations by [12,29], covering a wide range of cross-section dimensions and two strength grades (nominal yield stresses of 350 and 690 MPa) showed that the slenderness limits in the existing North American steel design standards tend to misjudge nonslender direct-formed sections as slender sections, resulting in unnecessary penalty and member strength underestimation. In response to this, a subsequent numerical investigation by [44] proposed modified stub column design recommendations for direct-formed regular- and high-strength RHS stub columns against cross-sectional yielding or local buckling. The numerical research presented in this paper will extend the above research to propose design recommendations for regular- and high-strength direct-formed RHS members under flexural loading.

From power generation to transmission and distribution, many of the energy infrastructure are built with galvanized tubular steel structures. For transportation infrastructure, the application of galvanized tubular steel structures covers nearly all fields. Such infrastructure projects are long-term and costly investments. Design and fabrication of robust and durable energy infrastructure standing up to not only the static and fatigue loadings but also the harsh environment and test of time continues to be one of the largest challenges in the engineering community. For hot-dip galvanizing, the molten zinc bath is typically maintained at 450 °C [2,3]. For batch galvanizing of hollow structural sections of commonly specified sizes, nearly the same steps are followed in all facilities. The immersion time for individual member is strictly controlled (approximately ten minutes) to produce the best coating quality [2,3]. In practice, application of the heat treatment (also at 450 °C) per ASTM A1085 Supplement S1 [7], or the Class H finish per CSA G40.20/G40.21 [8] improves the column behaviour of cold-formed hollow structural sections. This justifies the use of a high column design curve in CSA S16-19 [12]. To facilitate the application of galvanized regular- and high-strength hollow structural sections in the above infrastructure projects, recent experimental research studied the effect of galvanizing on residual stresses in cold-formed RHS [3,55] and circular hollow sections (CHS) [5]. As shown, similar to the ASTM A1085 and CSA G40.20/G40.21 heat treatment, the galvanizing process can effectively lower residual stress levels in cold-formed RHS and CHS. In response to this, recent experimental research by [68] involving full-scale testing of 22 non-galvanized and galvanized regular- and high-strength RHS beams showed that the latter has improved flexural behaviour due to residual stress reductions from galvanizing. The existing flexural member design rules in the North American steel design standards [12,29] were shown to be excessively conservative in many cases for galvanized RHS members, as they are considered as untreated cold-formed members.

This paper presents a comprehensive finite element (FE) parametric study to address the above research questions. The applicability of the existing slenderness limits and flexural design formulae on direct-formed regular- and high-strength RHS (non-galvanized and galvanized) are examined using the combined experimental and numerical data. Modified flexural member design rules are proposed and assessed via reliability analyses.

5.3 Numerical investigation

In this study, the nonlinear FE analysis is performed using ABAQUS [56]. The experimental results of 22 full-scale beam tests from [68] are used to validate non-linear FE models. The FE models are developed using previously measured stress-strain relationships, residual stresses, and geometric imperfections from [6,55]. A subsequent parametric study including 708 beam models is performed to study the effects of direct-forming and galvanizing over two strength grades as well as extended ranges of cross-sectional dimensions and plate slenderness values. Same as the experimental investigation in [68], the numerical investigation in this paper covers regular-strength direct-formed RHS produced to CSA G40.20/G40.21 Gr. 350W Class C (nominal yield stress of 350 MPa) [12], and high-strength direct-formed RHS produced to ASTM A1112 Class 100 (nominal yield stress of 690 MPa) [25].

5.3.1 Modelling details and validation

Four-noded shell elements with reduced integration (S4R in ABAQUS element library [56]) are adopted to model RHS beams. Such elements have been successfully used in previous FE investigations on tubular beams [19,69]. Similar to [19,69], based on a mesh sensitivity analysis, for modelling of flat faces, a mesh size of $(H+B)/25$ mm is adopted, where H and B are respectively the external depth and width of RHS. For modelling of corner regions (Fig. 5.1), a finer mesh pattern, consisting of four shell elements, is adopted. All FE beam models have internal and external corner radii of t and $2t$, respectively, where t is the RHS wall thickness.

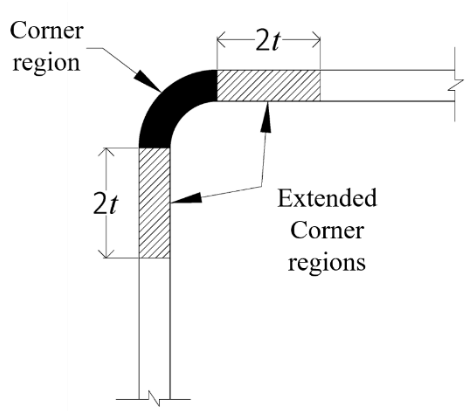

Figure 5.1 Extension of corner material properties to adjacent flat faces

In this research, as shown in Figs. 5.2-5.4, the RHS are given IDs with multiple components to differentiate material type, post-cold-forming process, and cross-sectional sizes. For the first component, D = direct-formed RHS (nominal yield stress = 350 MPa), and DH = direct-formed high-strength RHS (nominal yield stress = 690 MPa). For the second component, U = untreated, and G = galvanized. The third component gives the nominal width, depth, and thickness of the cross-section (in mm).

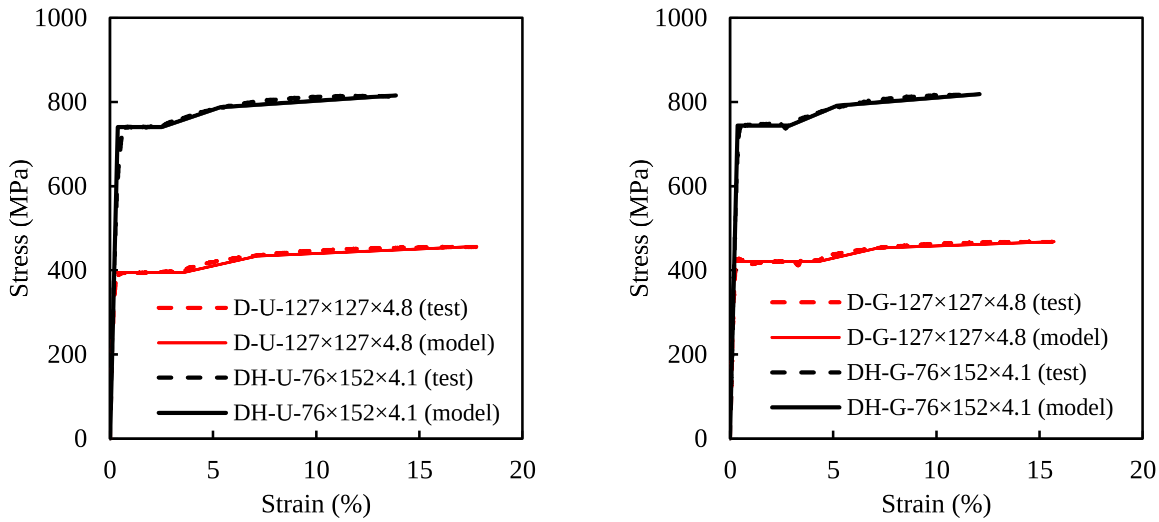

(a) Untreated RHS

(b) Galvanized RHS

Figure 5.2 Typical engineering stress-strain curves of flat faces of untreated and galvanized RHS

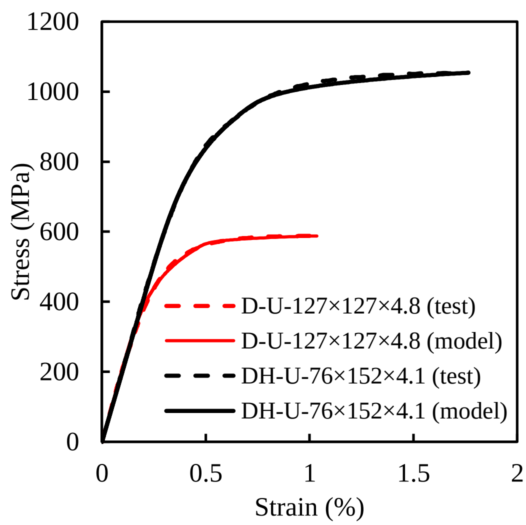

Figure 5.3 Typical engineering stress-strain curves of corner regions of untreated RHS

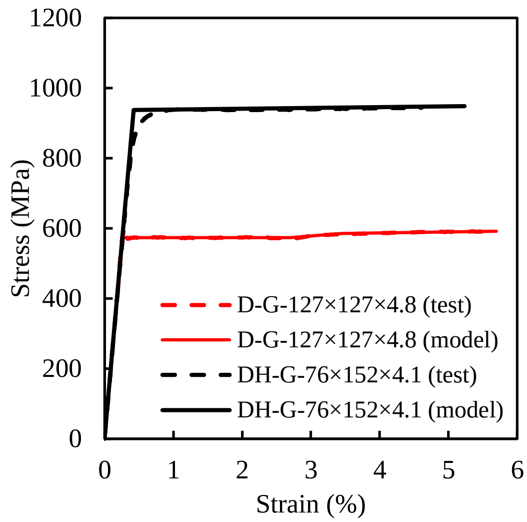

Figure 5.4 Typical engineering stress-strain curves of corner regions of galvanized RHS

For FE analyses in this study, the experimentally obtained engineering stress-strain relationships from [6] are simulated using material models proposed by Yun and Gardner [19] for hot-rolled steels (reproduced as Eqs. 3.1-3.3) and Gardner and Yun [20] for cold-formed steels (reproduced as Eqs. 3.4-3.7). The modelled engineering stress-strain relationships are subsequently converted to true stress-strain relationships for use in FE analysis. The rationale and details for selection and implementation of Eqs. 3.1-3.7 are discussed in [44]. The residual stresses in most cases are considered separately, which will be discussed later.

Specifically, Eqs. 3.1-3.3 are used to model the engineering stress-strain relationships of flat faces of untreated and galvanized RHS (regular- and high-strength), where yield plateaus are observed (Fig. 5.2) in the tensile coupon tests in [6], since the flat faces of the direct-formed RHS are not severely cold worked during production. On the other hand, Eqs. 3.4-3.7 are used to model the engineering stress-strain relationships of corner and extended regions (Fig. 5.1) of untreated RHS (regular- and high-strength). As shown in Fig. 5.3, the application of Eqs. 3.4-3.7 captures the strength enhancement due to heavy cold working at the corner regions. As discussed in detail in [44], the early yielding (rounded stress-strain curve) at the corner regions due to the bending residual stresses is also captured using Eqs. 3.4-3.7. Representative engineering stress-strain relationships of corner and extended regions (Fig. 5.1) of galvanized RHS (regular- and high-strength) are shown in Fig. 5.4. By comparing Figs. 5.3 and 5.4, it is evident that the application of post-production hot-dip galvanizing can effectively reduce residual stress levels, as the proportional limits increase significantly, and the engineering stress-strain curves become a lot less rounded. Therefore, Eqs. 3.1-3.3 are used to model the engineering stress-strain relationships of corner and extended regions of galvanized RHS.

A comprehensive tensile coupon test program is discussed in [6]. For each material type, the average values of the key material characteristics are listed in Tables 3.1 and 3.2, for use in Eqs. Eqs. 3.1-3.7. Typical comparisons of the experimentally obtained and modelled engineering stress-strain relationships are shown in Figs. 5.2-5.4. As shown, good agreements are achieved and hence credence can be given to the simulation.

The initial geometric imperfections measured in the complementary study by [6] on direct-formed RHS are considered in the FE models in this study. For incorporation of geometric imperfections in FE beam analysis, [19,49,66] suggest that the lowest eigenmode shape can be used as the local geometric imperfection profile, and the maximum magnitude over the entire profile can be obtained from experimental measurements. In [6], the local geometric imperfections were measured on four representative direct-formed RHS over the entire cross sections in the longitudinal directions. The averages of the maximum imperfections along the length were 0.387 mm and 0.366 mm for regular- and high-strength RHS, respectively. By normalizing the measured imperfections to the RHS wall thicknesses (t), these correspond to $0.12t$ and $0.08t$ for the direct-formed regular- and high-strength RHS, respectively. Same as [19,49,66], the normalized values are used throughout the FE study in this paper.

In the complimentary research, [55] measured the longitudinal residual stresses in 14 direct-formed regular- and high-strength RHS specimens (untreated and galvanized). The measured residual stresses are normalized to the measured yield strengths (f_y) from tensile coupon tests. The averages of the normalized membrane and bending residual stresses are listed in Table 3.3, where the tensile membrane residual stresses are reported as positive values, and the compressive membrane residual stresses are reported as negative values. The tabulated bending residual stresses are the tensile residual stresses from the external surfaces of the RHS specimens. The bending residual stresses on the internal surfaces have the same magnitudes but opposite signs. Similar to the comparison between Figs. 5.3 and 5.4, Table 3.3 also shows that the residual stress levels are reduced after hot-dip galvanizing.

In this FE study, using the same approach in [44], for each shell element five through-thickness integration points are used to accurately apply the measured residual stress distribution. The residual stress values at each integration point are added using the Subroutine SIGINI from ABAQUS [56]. Following the same rationale discussed in [44], for flat faces of untreated and galvanized RHS and corner regions of galvanized RHS, both the measured membrane and bending residual stresses are applied in the FE analysis in this study. On the other hand, for corner regions of untreated RHS, only the measured membrane residual stresses are applied in the FE models. This is because the tensile coupons obtained from corner regions of untreated RHS were curved and were clamped in the universal testing machine to the in-situ straight state before testing. In other words, incorporation of the rounded tensile-strain curves (Fig. 5.3) accounts for the effect of the bending residual stresses already. Further discussions can be found in [44].

The loading and boundary conditions applied to the FE models (Fig. 5.5) simulates the four-point bending test setup reported in [68], where the moment spans of the RHS beam specimens were subjected to uniform moment via the application of two vertical loads. In the FE models, the critical cross sections are rigidly attached to the reference points for which the relevant degrees of freedoms are restricted to simulate the pin and roller supports used in the test setup in [68]. In the FE models, two vertical displacements are applied to the two ends of moment span to generate bending moments.

For validation of modelling approach herein, the FE results are verified against the test data from the 22 full-scale four-point bending tests reported in [68]. The FE moment-curvature (M - κ) curves are determined using the same approach from [68]. Typical M - κ curves from the FE analysis are compared to the experimental results in Fig. 5.6. Comparison between the numerical and the experimental failure modes is made in Fig. 5.7. Finally, the ultimate bending moment capacities from the 22 FE beam analyses and the 22 beam tests are compared in Tables 5.1 and 5.2 for the untreated and galvanized RHS, respectively. For DH-G-76×76×4.8 and DH-U-76×102×3.2, repeated tests were performed in [68], and the average results are shown in Tables 5.1 and 5.2. As shown by Figs. 5.6 and 5.7, as well as the statistics in Tables 5.1 and 5.2, good agreements are achieved. Therefore, credence can be given to the accuracy of the FE modelling approach herein.

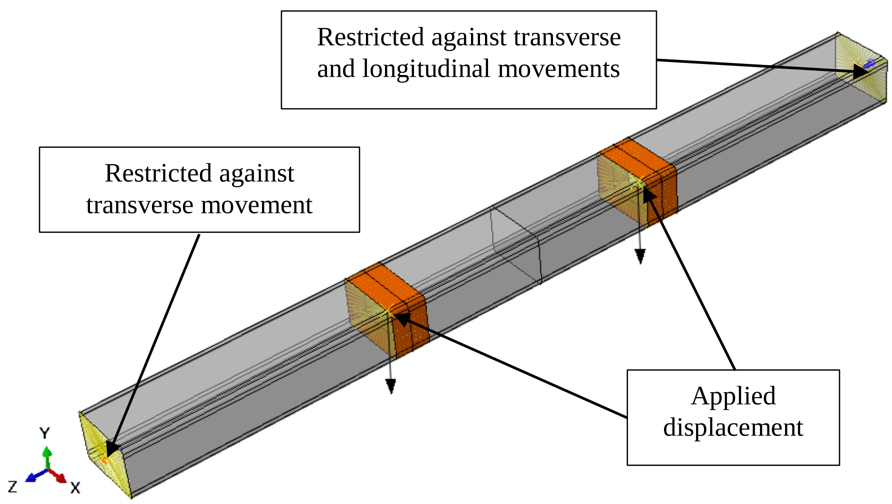

Figure 5.5 Loading and boundary conditions of the FE models

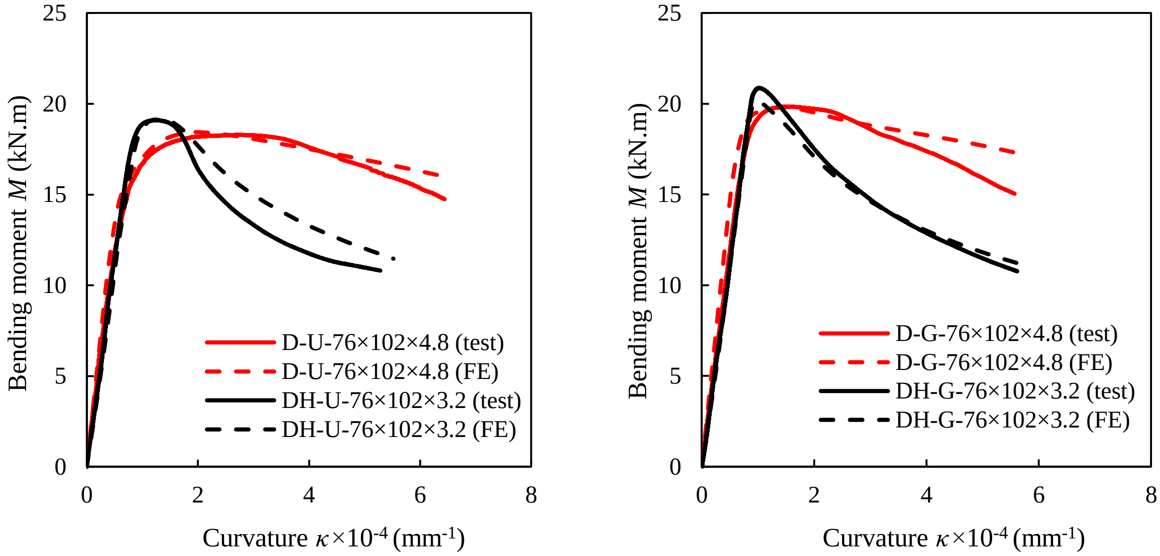

(a) Untreated

(b) Galvanized

Figure 5.6 Comparison of moment-curvature relationships

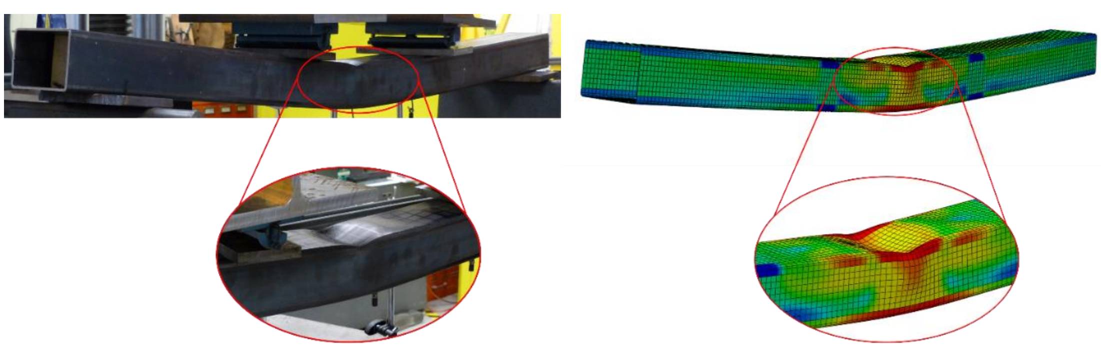

Figure 5.7 Comparison of experimental and FE failure modes for DH-U-76×102×3.2

Table 5.1 Comparison of ultimate moment capacities from tests and FE analyses for untreated RHS

Specimen ID	M_{test} (kN.m)	M_{FE} (kN.m)	M_{test}/M_{FE}
D-U-76×102×3.2	12.50	11.88	1.05
D-U-76×102×4.8	18.30	18.43	0.99
D-U-102×102×3.2	17.26	17.26	1.00
D-U-102×102×4.8	29.19	27.45	1.06
D-U-127×127×4.8	42.81	40.86	1.05
DH-U-76×76×4.8	28.43	28.99	0.98
DH-U-76×102×3.2	19.09	19.11	1.00
DH-U-76×102×4.1	28.21	27.98	1.01
DH-U-76×102×4.8	33.22	33.41	0.99
DH-U-76×152×4.1	31.42	32.64	0.96
Mean			1.01
COV			0.031

Table 5.2 Comparison of ultimate moment capacities from tests and FE analyses for galvanized RHS

Specimen ID	M_{test} (kN.m)	M_{FE} (kN.m)	M_{test}/M_{FE}
D-G-76×102×3.2	13.30	13.44	0.99
D-G-76×102×4.8	19.81	19.79	1.00
D-G-102×102×3.2	18.55	19.41	0.96
D-G-102×102×4.8	31.81	29.44	1.08
D-G-127×127×4.8	46.16	44.99	1.03
DH-G-76×76×4.8	27.46	28.48	0.96
DH-G-76×102×3.2	20.88	20.03	1.04
DH-G-76×102×4.1	28.41	27.74	1.02
DH-G-76×102×4.8	32.26	34.15	0.94
DH-G-76×152×4.1	34.33	34.30	1.00
Mean			1.00
COV			0.040

5.3.2 Parametric investigation

After validation of the FE modelling approach, a subsequent FE parametric analysis is carried out, including a total of 708 FE models. The parametric study includes equal numbers of regular-strength steel sections (nominal yield strength = 350 MPa) and high-strength steel sections (nominal yield strength = 690 MPa). Following the procedures described in Section 5.3.1, the material constitutive models, initial geometric imperfections and residual stresses are incorporated in the parametric FE models. The overall widths (or depths) of the sections range from 75 to 310 mm, and the wall thicknesses range from 2.5 to 13 mm. The width-to-thickness (or depth-to-thickness) ratios range from 7 to 100, which covers the full range of commonly available RHS products. Same as the test setup in [68], the FE models are subjected to four-point bending. The moment span (i.e., middle span) and the two exterior spans have the same length of three times member depth for all models.

5.4 Flexural behaviours of sections with different production histories

As discussed in Section 5.2, RHS with similar cross-sectional dimensions but different production histories (e.g., indirect-cold-formed versus direct-cold formed; cold-formed versus hot-finished; untreated versus hot-dip galvanized; etc.) can have significantly different material and residual stress properties (e.g., [6,16,23,24,44,55,68]). To investigate the effects of different production histories on flexural behaviours, this section compares the experimental and FE data for the direct-cold-formed RHS beams (untreated) to the experimental data for the indirect-cold-formed RHS beams from [17,23,64,65] in Fig. 5.8a, and to the experimental data for the hot-finished RHS beams from [61,66] in Fig. 5.8b. The comparisons are made among sections with similar nominal yield strengths and cross-sectional dimensions. Different from cold forming, which is carried out at ambient temperature, the hot-finishing process is carried out at a normalizing temperature of approximately 900 ºC [3]. This process nearly relieves all cold-forming-induced residual stresses and improves material toughness through introducing a finer and a more homogeneous grain structure. The hot-finishing process also removes the strength enhancement from cold forming. However, it should be noted that hot-finished hollow sections are not manufactured in North America and hence are rarely used in North American construction projects [3]. In this section, the effect of post-production hot-dip galvanizing on the flexural behaviours of RHS is also investigated and shown in Fig. 5.9.

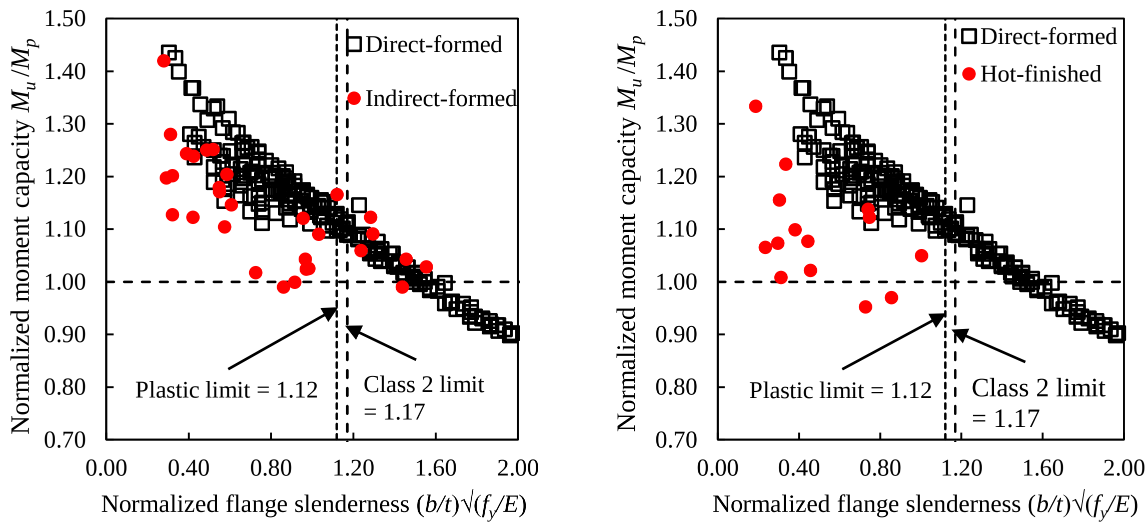

(a) Direct-formed vs. indirect-formed

(b) Direct-formed vs. hot-finished

Figure 5.8 Comparisons of direct-formed RHS (untreated) to indirect-formed RHS from [17,23,64,65] and hot-finished RHS from [61,66]

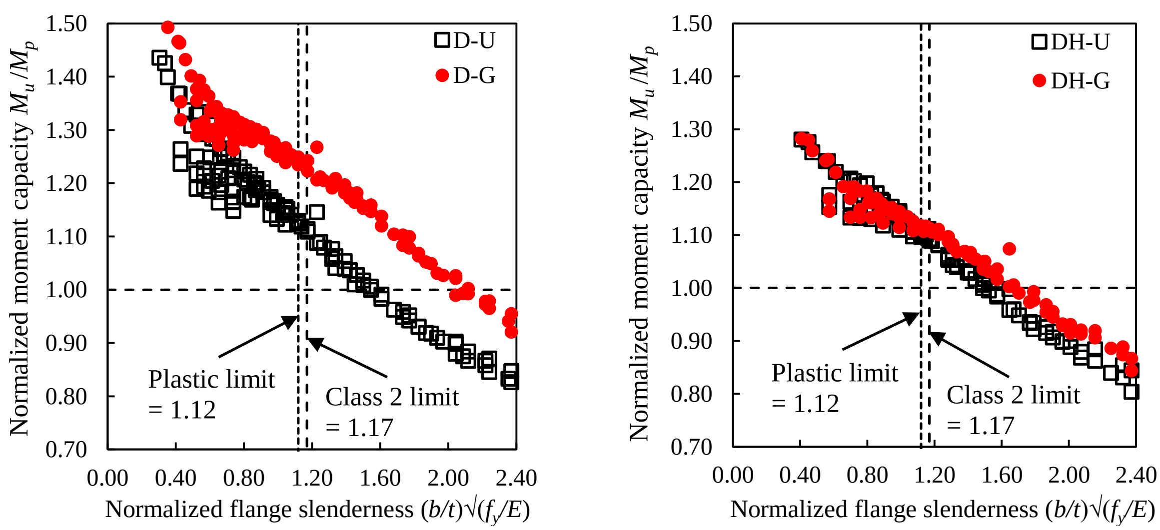

(a) Regular-strength RHS

(b) High-strength RHS

Figure 5.9 Comparisons of untreated and galvanized direct-formed RHS

The experimental and FE ultimate moments (M_u) in Figs. 5.8 and 5.9 are normalized by the plastic moments $M_P = Zf_y$ (where Z = plastic section modulus; and f_y = flat face tensile coupon yield stress) and are plotted against normalized flange slenderness values $b/t\sqrt{f_y/E}$ (where b = internal flange width excluding corner portions; and E = Young's modulus). Since AISC 360-16 [29] and CSA S16-19 [12] have different formulae for slenderness calculation, following the same approach in [44], the use of normalized slenderness values allows direct comparison and evaluation of cross-section classification rules from different design specifications, which will be further discussed in Section 5.5. The calculation of M_P in this study is consistent with the existing flexural design rules in North American steel design standards [12,29] where the cold-forming-induced strength enhancement from flat faces to corner regions is not accounted for. It should be noted that the direct-formed RHS investigated in this research has two strength grades (nominal yield stress = 350 and 690 MPa). Therefore, for meaningful comparisons, only the indirect-formed and hot-finished RHS from [17,23,61,64–66] with nominal yield stresses ranging from 350 to 700 MPa are included in Fig. 5.8.

In CSA S16-19 [12], for RHS, depending on the width-to-thickness ratios of the compression elements in members subject to flexure, the sections are designated as Class 1, 2, 3, or 4. Class 1 sections permit attainment of the plastic moment and subsequent redistribution of the bending moment. Class 1 sections possess a rotation capacity of approximately 3 before the onset of local buckling. Calculation of rotation capacity will be discussed in Section 5.5. Class 2 sections permit attainment of the plastic moment but need not allow for subsequent moment redistribution. Class 3 sections permit attainment of the yield moment $M_y = Sf_y$ (where S = elastic section modulus). Class 4 sections generally have elastic local buckling of elements in compression as the limit state of structural resistance. Class 1 sections per CSA S16-19 [12] are equivalent to compact sections defined in AISC 360-16 [29]. Class 2 plus 3 sections are equivalent to noncompact sections defined in AISC 360-16 [29]. In AISC 360-16 [29], for calculation of nominal flexural strengths of noncompact sections, formulae are available for linear transition from plastic moment to yield moment. Class 4 section per CSA S16-19 [12] are equivalent to slender-element sections defined in AISC 360-16 [29].

In research relevant to cross-section classification, the normalized moment capacities (M_u/M_p) are usually plotted against the normalized slenderness values of plate elements [19,44,66]. For example, to differentiate Class 2 and Class 3 sections, previous research [19,66] often involve linear regression of the experimental and/or FE results. Specifically, for determination of flange slenderness limit, based on the best fit line, the normalized flange slenderness value ($b/t\sqrt{f_y/E}$) corresponding to a normalized moment capacity (M_u/M_p) of unity is usually considered as the threshold. The same approach can be applied to determine the web slenderness limit. For better appreciation of flexural behaviours of sections with different production histories, the Class 2 flange slenderness limit from CSA S16-19 [12] and the compact (plastic) flange slenderness limit from AISC 360-16 [29] are shown in Figs. 5.8 and 5.9.

Based on the comparisons in Fig. 5.8a for both regular- and high-strength materials, direct-formed RHS (untreated) have superior flexural strengths comparing to their indirect-formed counterparts. By monitoring the load-deformation behaviours at various locations of the FE beam models, it is shown that direct-formed RHS generally attain higher flexural strengths due to the inherently low levels of residual stresses as a result of the direct-forming process. The onset of local buckling is delayed considerably due to the inherently low levels of residual stresses. This is consistent with the findings in [44] for stub column behaviours. It should be noted that comparing to the indirect-forming approach, the direct-forming approach is relatively new. As a result, the existing cross-section classification rules for RHS in the North American steel design standards [12,29] were in general developed based on research on indirect-formed RHS. It can be seen in Fig. 9a that the Class 2 flange slenderness limit from CSA S16-19 and the compact flange slenderness limit from AISC 360-16 are applicable for the indirect-formed RHS from [17,23,64,65]. However, such flange slenderness limits are excessively conservative for direct-formed RHS. Therefore, modified cross-section classification rules catering to direct-formed RHS will be developed based on further studies in Sections 5.5 and 5.6.

Similarly, according to the comparison in Fig. 5.8b, the direct-formed RHS (untreated) have higher flexural strengths than their hot-finished counterparts. As discussed previously, although the hot-finishing process nearly relieve all residual stresses, the cold-forming-induced strength enhancements are also removed. The flexural strength differences between direct-formed and hot-finished RHS are mainly due to such trade-offs. This is consistent with the findings in [44] for stub column behaviours.

As shown in Fig. 5.9a for regular-strength RHS, the application of post-production hot-dip galvanizing increased the flexural strengths. As discussed in Sections 5.2 and 5.3, according to recent experimental research on effect of galvanizing on residual stresses in cold-formed RHS [3,55] and circular hollow sections (CHS) [5], the hot dipping (at approximately 450 °C) can effectively lower residual stress levels in cold-formed RHS and CHS to a similar level from the heat treatment specified in ASTM A1085 Supplement S1 [7], or the Class H finish in CSA G40.20/G40.21 [8] (both also at 450 °C). It should be noted that the ASTM A1085 and CSA G40.20/G40.21 heat treatments are not intended to alter grain structure and hence have minor effects on the material strengths. Similarly, the application of post-production hot-dip galvanizing can reduce cold-forming-induced residual stresses without trading off the cold-forming-induced strength enhancement. It can be seen in Fig. 5.9a that the Class 2 flange slenderness limit from CSA S16-19 and the compact flange slenderness limit from AISC 360-16 become even more conservative for galvanized direct-formed regular-strength RHS.

On the other hand, as shown in Fig. 5.9b for high-strength RHS, the improvement of flexural strengths is smaller. As shown in the complementary study [55], the absolute cold-forming-induced residual stress values in regular- and high-strength RHS are similar. The absolute changes of residual stresses in regular- and high-strength RHS after galvanizing are also similar. In theory, the onset of local buckling is primarily affected by the residual stress-over-yield stress ratio. As a result, previous research [6,44] showed that the application of post-production galvanizing has smaller effects on stub column behaviours of high-strength RHS, comparing to regular-strength RHS. Similarly, galvanizing has relatively smaller effects on flexural behaviours of high-strength RHS according to Fig. 5.9b.

5.5 Evaluation of existing flexural design rules

As discussed in Section 5.4, in CSA S16-19, for RHS, depending on the width-to-thickness ratios of the compression elements in members subject to flexure, the cross sections are designated as

Class 1, 2, 3, or 4. CSA S16-19 Section 13.5 contains different sets of design formulae for determination of nominal flexural strengths for different cross-section classes. Similarly, in AISC 360-16 Section F7, for RHS, depending on the slenderness categories of flange and web elements (i.e., compact, noncompact and slender), the nominal flexural strengths are calculated as the lowest values obtained according to the limit states of yielding (plastic moment), flange local buckling and web local buckling. The lateral-torsional buckling design formulae in Section F7.4 caters only to built-up box sections with very high depth-to-width ratios. Such limit state is in practice not applicable for cold-formed RHS, and thus is not further discussed. For design of sections with slender elements, both AISC 360-16 and CSA S16-19 apply the effective width method. In this paper, Section 5.5.1 examines the applicability of the cross-section classification rules from AISC 360-16 and CSA S16-19 on direct-formed regular- and high-strength RHS (untreated and galvanized). Section 5.5.2 examines the applicability of existing flexural design formulae in [12,29]. Modified flexural design rules are proposed in Section 5.6.

5.5.1 Cross-section slenderness limits

Both AISC 360-16 and CSA S16-19 use internal flange width (*b*), internal web depth (*h*) and thickness (*t*) for cross-section classification of RHS. As discussed in Section 5.4, for direct comparison, the slenderness limits from AISC 360-16 and CSA S16-19 are normalized in Tables 5.3 and 5.4. In Table 5.3, λ_{c1}, λ_{c2} and λ_{c3} are the maximum slenderness values for Classes 1, 2 and 3 from CSA S16-19. Sections with flange and/or web elements exceeding the λ_{c3} limits in Table 5.3 are designated as Class 4. The definitions of Classes 1, 2, 3 and 4 have been discussed in Section 5.4. Table 5.4 lists from AISC 360-16 the plastic slenderness limit (λ_p) for differentiation of compact and noncompact elements, and the yield slenderness limit (λ_r) for differentiation of noncompact and slender elements.

Table 5.3 Slenderness limits for compression elements subject to flexure based on CSA S16-19

Element description	Normalized slenderness	Normalized slenderness limits		
		λ_{c1}	λ_{c2}	λ_{c3}
Flanges of RHS	$(b/t)\sqrt{f_y/E}$	0.94	1.17	1.50
Webs of RHS	$(h/t)\sqrt{f_y/E}$	2.46	3.80	4.25

Table 5.4 Slenderness limits for compression elements subject to flexure based on ANSI/AISC 360-16

Element description	Normalized slenderness	Normalized slenderness limits	
		λ_p	λ_r
Flanges of RHS	$(b/t)\sqrt{f_y/E}$	1.12	1.40
Webs of RHS and built-up box sections	$(h/t)\sqrt{f_y/E}$	2.42	5.70

Comparing Table 5.3 and 5.4, the following observations can be made:

(i) For Class 1 sections (equivalent to compact sections), the flange slenderness limit in CSA S16-19 is smaller than that in AISC 360-16 (λ_{c1} = 0.94 versus λ_p = 1.12). However, it should be noted that in the absence of measured corner radius (which is common in design practice), AISC 360-16 calculates the internal width as external width minus 3t, while CSA S16-19 calculates internal width as external width minus 4t. This makes the two limits from the two standards closer in design, considering the large wall thickness of typical Class 1 (compact) RHS. As discussed in Section 5.3.1, in this research all FE beam models are developed using exact internal and external corner radii of t and 2t, respectively. Therefore, internal width is precisely calculated as external width minus 4t for the following analysis. The comparison of Tables 5.3 and 5.4 also shows that the web slenderness limits for Class 1 sections from the two standards are similar (λ_{c1} = 2.46 versus λ_p = 2.42).

(ii) For designation of Class 4 (equivalent to slender sections), the yield slenderness limits from CSA S16-19 and AISC 360-16 for flanges are similar (λ_{c3} = 1.50 versus λ_r = 1.40). However, the yield slenderness limit for web from CSA S16-19 is much more stringent than that from AISC 360-16 (λ_{c3} = 4.25 versus λ_r = 5.70). As noted in Table 5.4, the web slenderness limits from AISC 360-16 are for both cold-formed RHS and built-up box sections. Specifically, λ_r = 5.70 caters to built-up box sections with very high depth-to-width ratios. In practice, the available cold-formed RHS cross-sectional sizes do not have such high web slenderness values. Therefore, λ_{c3} = 4.25 from CSA S16-19 in Table 5.3 is more relevant. This will be further elaborated in this section, since the parametric study herein covers full ranges of practical cross-sectional dimensions of cold-formed RHS.

As discussed in Section 5.4, Class 1 (compact) sections are defined as those exceeding plastic moments and possessing rotation capacities greater than 3 before the onset of local buckling by [12,29]. To examine slenderness limits for Class 1 (compact) sections (λ_{c1} in Table 5.3 and λ_p in Table 5.4), for all FE beam models, the rotational capacities are calculated using Eq. 5.1 from [29].

$$R = \frac{\kappa_l}{\kappa_p} - 1 \tag{5.1}$$

where R = measured rotation capacity on moment span; κ_l = curvature at plastic moment during unloading (i.e., onset of local buckling); and κ_p = elastic curvature corresponding to plastic moment. The definitions of all three symbols are illustrated in Fig. 5.10.

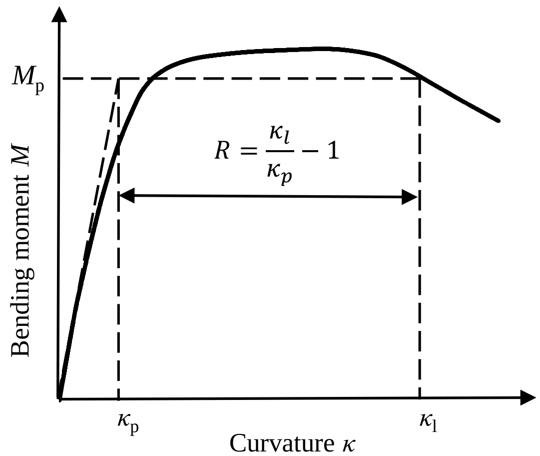

Figure 5.10 Measurement of rotation capacity based on [29]

For assessment of the codified Class 1 (plastic) slenderness limits from AISC 360-16 [29] and CSA S16-19 [12], the rotation capacities ($R \geq 3$ and $R < 3$) of all beam specimens and FE models are plotted against their normalized flange and web slenderness values in Fig. 5.11. The relevant slenderness limits (λ_{c1} in Table 5.3 and λ_p in Table 5.4) are also shown in the figure. The following observations can be made:

(i) Using the codified slenderness limits as reference lines, by comparing the red data points ($R \geq 3$) in Figs. 5.11a and 5.11b, the application of post-production hot-dip galvanizing improved the rotation capacities of the FE beam models.

(ii) Overall, the slenderness limits from AISC 360-16 and CSA S16-19 for Class 1 (compact) sections (λ_{c1} in Table 5.3 and λ_p in Table 5.4) are applicable for regular- and high-strength direct-formed RHS (untreated and galvanized).

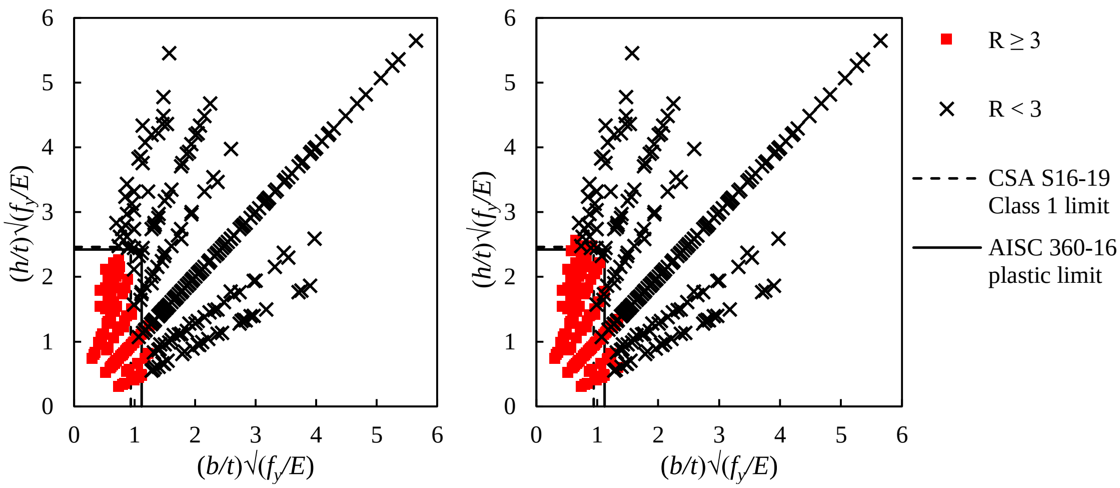

(a) Untreated RHS

(b) Galvanized RHS

Figure 5.11 Evaluation of Class 1 (plastic) slenderness limits in [12,29]

For assessment of the codified Class 2 slenderness limits from CSA S16-19, the flexural strengths (M_u) (i.e., ultimate moment capacities) of all beam specimens and FE models are compared to the calculated plastic moment capacities (M_p) and plotted against their normalized flange and web slenderness values in Fig. 5.12. The relevant slenderness limits (λ_{c2} in Table 5.3) are also shown in the figure. The following observations can be made:

For untreated direct-formed RHS in Fig. 5.12a, the Class 2 flange slenderness limit from CSA S16-19 is conservative. As discussed in Section 5.4, comparing to the indirect-forming approach, the direct-forming approach is relatively new. The existing cross-section classification rules for RHS in the North American steel design standards [12,29] were in general developed based on research on indirect-formed RHS. Since direct-formed RHS have inherently lower residual stress levels, it is intuitive that the existing flange slenderness limits can be conservative for them. On the other hand, as shown in Fig. 5.12a, the Class 2 web slenderness limit from CSA S16-19 is applicable. This is because for a section subject to flexure, the entire width of flange is highly stressed, while only a portion of web is highly stressed. Therefore, the residual-to-yield-stress ratio has a smaller effect on web.

For galvanized direct-formed RHS in Fig. 5.12b, both the Class 2 flange and web slenderness limits become more conservative. As discussed earlier, similar to the application of the heat treatment per ASTM A1085 Supplement S1 [7], or the Class H finish per CSA G40.20/G40.21 [8], the application of post-production galvanizing can effectively lower cold-forming-induced residual stresses (without removing the cold-forming-induced strength enhancement) and in turn improve member behaviours.

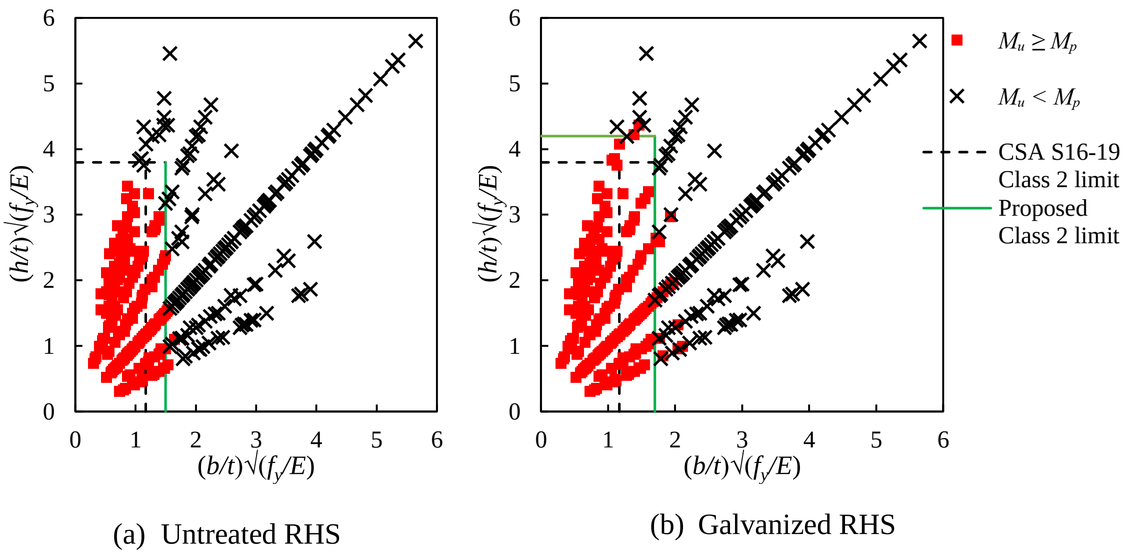

Figure 5.12 Evaluation of Class 2 slenderness limits in [12]

For assessment of the codified Class 3 (yield) slenderness limits from AISC 360-16 and CSA S16-19, the flexural strengths (M_u) of all beam specimens and FE models are compared to the calculated yield moment capacities (M_y) and plotted against their normalized flange and web slenderness values in Fig. 5.13. The relevant slenderness limits (λ_{c3} in Table 5.3 and λ_r in Table 5.4) are also shown in the figure. The following observations can be made:

(i) As shown in Fig. 5.13a, for untreated direct-formed RHS (regular- and high-strength), the yield slenderness limits from AISC 360-16 and CSA S16-19 tend to misjudge nonslender sections as slender sections, since the inherently low levels of residual stresses are not considered. This will result in unnecessary penalty and member strength underestimation when using the effective width method for flexural strength calculation.

(ii) As discussed earlier, the web yield slenderness limit from AISC 360-16 (λ_r = 5.70 in Table 5.4) for differentiation of noncompact and slender web elements caters to built-up box sections with very high depth-to-width ratios. As shown in Figs. 5.13a and 5.13b, such slenderness limit is in general irrelevant to cold-formed RHS (i.e., well above the data points of RHS covering the full practical ranges of cross-sectional dimensions). Therefore, λ_r = 5.70 in Table 5.4 will not be further discussed in this research. This research will propose slenderness limits for RHS only.

(iii) Similar to the comparisons in Figs. 5.12a and 5.12b, the codified Class 3 (yield) slenderness limits become more conservative for galvanized direct-formed RHS.

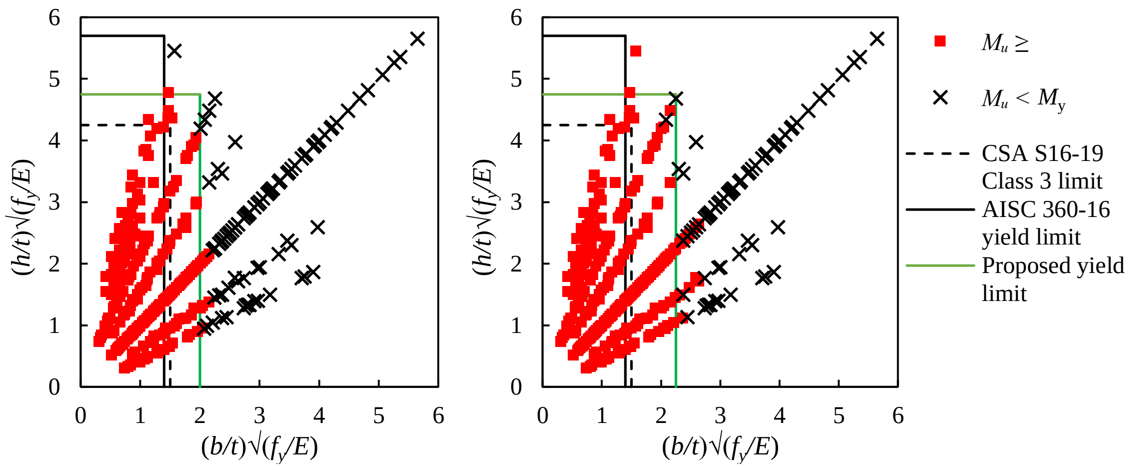

Figure 5.13 Evaluation of Class 3 (yield) slenderness limits in [12,29]

In all, the existing slenderness limits from AISC 360-16 and CSA S16-19 are in many cases too conservative for direct-formed RHS (untreated and galvanized). Therefore, modified slenderness limits will be proposed in Section 5 with subsequent reliability analyses to assess their accuracy.

5.5.2 Flexural strengths

In this section, the experimentally and numerically obtained flexural strengths (i.e., ultimate moment capacities) are compared to the calculated nominal values (i.e., resistance factor = 1.00) to examine the flexural design formulae from AISC 360-16 and CSA S16-19.

In CSA S16-19, for Class 1 and 2 sections, the nominal flexural strength (M_n) equals the plastic moment ($M_p = Zf_y$). For Class 3 sections, M_n equals the yield moment ($M_y = Sf_y$). For Class 4 sections with slender flange elements, $M_n = S_e f_y$ where is S_e is the effective section modulus determined with the effective width b_e. b_e is calculated using the λ_{c3} =1.50 limit in Table 5.3. When using the effective width method, the nominal flexural strength is determined from S_e referred to the compression flange using the distance from the shifted neutral axis. In design practice, a less accurate yet conservative estimate of the nominal flexural strength can be obtained by using the effective width for both the compression and tension flanges, thereby maintaining the symmetry of the cross section and simplifying the calculations. In this research, the former and more accurate approach is adopted. CSA S16-19 also contains flexural design provisions for conditions when Class 4 sections with slender web elements. However, as discussed in Section 5.5.1, this in general cater to sections with very high depth-to-width ratios, and hence does not apply to cold-formed RHS.

In AISC 360-16, for compact sections, $M_n = M_p$. For sections with noncompact flanges and/or webs, two design formulae considering the limit states of flange local buckling and web local buckling are available. Both formulae provide linear transition from M_p to M_y, and M_n is determined as the lesser of the two. For sections with slender flange elements, AISC 360-16 also adopts the effective width approach considering the shift of neutral axis. S_e is calculated using b_e based on λ_r

= 1.40 in Table 5.4 with a formula different from CSA S16-19. AISC 360-16 does not have specific formulae for calculation of effective web depth for sections with slender webs. Nevertheless, this is an extremely rare case for cold-formed RHS.

For all FE RHS beam models, the nominal flexural strengths (M_n) are calculated based on AISC 360-16 and CSA S16-19 and compared to the experimentally and numerically obtained ultimate moment capacities (M_u). The key statics of the comparison are shown in Table 5.5. The graphical comparisons are shown in Figs. 5.14 and 5.15, where M_u is normalized by M_p. The following observations can be made:

(i) For both untreated and galvanized RHS, AISC 360-16 produces very conservative predictions for compact sections since the strength enhancement due to cold forming is not considered.

(ii) It should be noted that existing flexural design formula in AISC 360-16 are derived heavily based on the existing slenderness limits in Table 5.4. As shown in Figs. 5.8, 5.9, 5.11-5.13, 5.14 and 5.15, such slenderness limits are excessively conservative for direct-formed RHS (untreated and galvanized). As a result, AISC 360-16 produces very conservative predictions for direct-formed RHS with noncompact and/or slender elements. Further details will be discussed in Section 5.6.

(iii) Similar conclusions can be obtained for CSA S16-19. Comparing Figs. 5.14 and 5.15, AISC 360-16 produces better predictions for sections with noncompact elements since it applies a linear transition from M_p to M_y. For sections with slender elements, AISC 360-16 in many cases also produces better predictions. Therefore, AISC 360-16 is selected as the basis to propose modified flexural design recommendations for direct-formed regular- and high-strength RHS (untreated and galvanized) in Section 5.6.

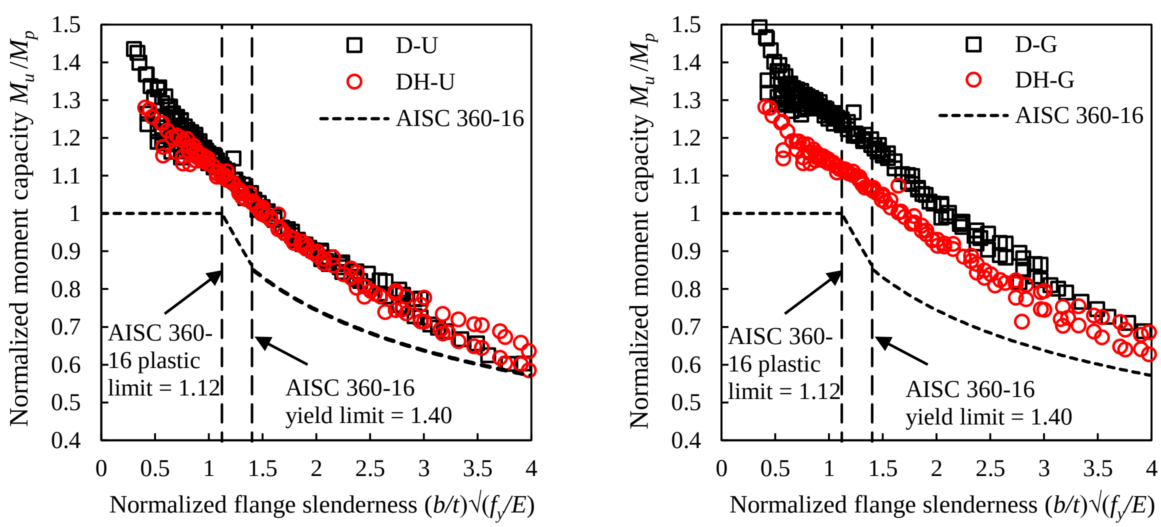

(a) Untreated RHS (b) Galvanized RHS

Figure 5.14 Comparisons of experimental and FE results with nominal flexural strengths calculated using AISC 360-16

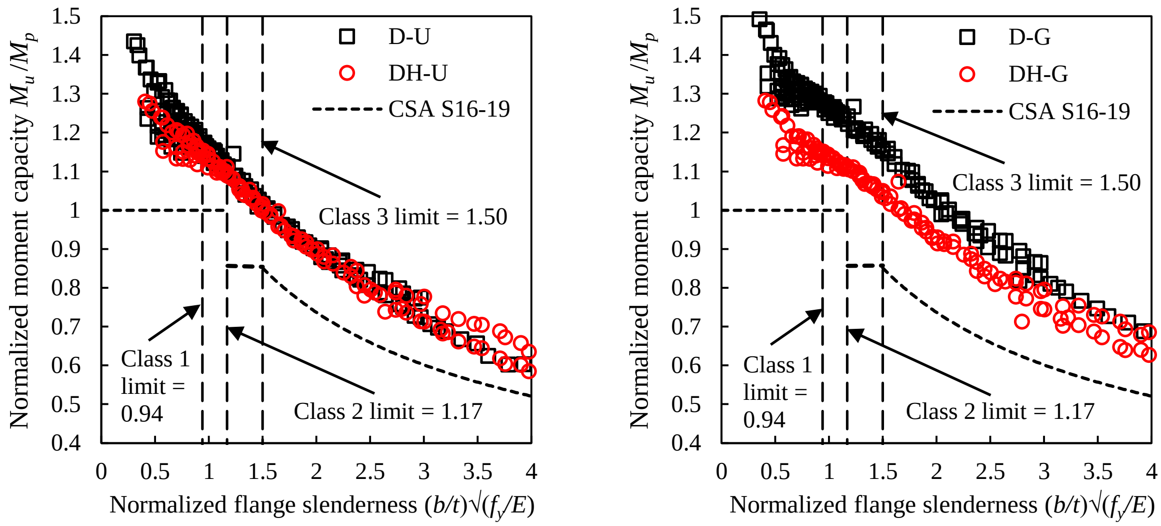

(a) Untreated RHS (b) Galvanized RHS

Figure 5.15 Comparisons of experimental and FE results with nominal flexural strengths calculated using CSA S16-19

Table 5.5 Comparison of FE results to nominal flexural strength calculated by [12,29]

	Untreated RHS		Galvanized RHS	
Specification	$(M_u/M_n)_{mean}$	$(M_u/M_n)_{cov}$	$(M_u/M_n)_{mean}$	$(M_u/M_n)_{cov}$
AISC 360-16 [29]	1.16	0.066	1.25	0.078
CSA S16-19 [12]	1.19	0.064	1.27	0.078

5.6 Modified design recommendations based on AISC 360-16

5.6.1 Slenderness limits and design formulae

As shown in Section 5.5, the AISC 360-16 approach provides better predictions over wide ranges of design parameters, comparing to CSA S16-19. Thus, the former is selected as the basis to propose modified flexural design recommendations for direct-formed regular- and high-strength RHS (untreated and galvanized).

For noncompact RHS, Eqs. F7-2 and F7-6 in AISC 360-16 [29] considers the limit states of flange and web local buckling, respectively. Both formulae provide linear transition from M_p to M_y, and M_n is determined as the lesser of the two. Eqs. F7-2 and F7-6 (reproduced as Eqs. 5.2 and 5.4 herein) are derived from the general formulae (shown as Eqs. 5.3 and 5.5 herein) using the existing slenderness limits in Table 5.4.

Flange local buckling for sections with noncompact flanges:

$$M_n = M_p - \left(M_p - M_y\right).\left[3.57(b/t)\sqrt{f_y/E} - 4.0\right] \leq M_p \tag{5.2}$$

Eq. 5.2 is derived using the following general formula (Eq. 5.3):

$$M_n = M_p - \left(M_p - M_y\right).\left[\frac{(b/t)\sqrt{f_y/E} - \lambda_p}{\lambda_r - \lambda_p}\right] \leq M_p \tag{5.3}$$

where $\lambda_p = 1.12$ and $\lambda_r = 1.40$ from Table 5.4.
Web local buckling for sections with noncompact webs:

$$M_n = M_p - \left(M_p - M_y\right).\left[0.305(h/t)\sqrt{f_y/E} - 0.738\right] \leq M_p \tag{5.4}$$

Eq. 5.4 is derived using the following general formula (Eq. 5.5):

$$M_n = M_p - \left(M_p - M_y\right).\left[\frac{(h/t)\sqrt{f_y/E} - \lambda_p}{\lambda_r - \lambda_p}\right] \leq M_p \tag{5.5}$$

where $\lambda_p = 2.42$ and $\lambda_r = 5.70$ from Table 5.4.
For RHS with slender flanges, the nominal flexural strengths are calculated using Eqs. F7-3 and F7-4 in AISC 360-16 (reproduced as Eqs. 5.6 and 5.7 herein).

$$M_n = f_y S_e \tag{5.6}$$

where S_e = effective section modulus determined with the effective width, b_e, of the compression flange taken as:

$$b_e = \begin{cases} b & \text{when } (b/t)\sqrt{f_y/E} \leq 1.40 \\ 1.92t\sqrt{E/f_y}\left(1 - \dfrac{0.38\sqrt{E/f_y}}{b/t}\right) & \text{when } (b/t)\sqrt{f_y/E} > 1.40 \end{cases} \tag{5.7}$$

Eq. 5.7 is derived using the following general formula (Eq. 5.8):

$$b_e = \begin{cases} b & \text{when } (b/t)\sqrt{f_y/E} \leq \lambda_r \\ \left[\dfrac{c_2\lambda_r}{(b/t)\sqrt{f_y/E}} - c_1\left(\dfrac{c_2\lambda_r}{(b/t)\sqrt{f_y/E}}\right)^2\right].b & \text{when } (b/t)\sqrt{f_y/E} > \lambda_r \end{cases} \tag{5.8}$$

where $c_1 = 0.2$ and $c_2 = 1.38$ are the effective width imperfection adjustment factors from Table

E7.1 in AISC 360-16. λ_r = 1.40 is from Table 5.4.

In all, the existing flexural design formula are derived heavily based on the slenderness limits in Table 5.4. As shown by the experimental and FE results in this study, the existing slenderness limits and flexural design rules in AISC 360-16 for compact sections are applicable for direct-formed RHS (untreated and galvanized). However, the existing slenderness limits and flexural design rules for noncompact sections and sections with slender elements are excessively conservative and hence not suitable. Therefore, this research proposes suitable slenderness limits in Table 5.6. By substituting the proposed slenderness limits (λ_r and λ_p in Table 5.6) into the general AISC 360-16 formulae (Eqs. 5.3, 5.5 and 5.8), this research proposes Eqs. 5.9-5.18 as the modified flexural design formulae for direct-formed RHS (untreated and galvanized).

Table 5.6 Proposed slenderness limits for compression elements subject to flexure

Element description	Normalized slenderness	Normalized slenderness limits		
		λ_p (or λ_{c1})	λ_{c2}	λ_r (or λ_{c3})
Flanges of RHS	$(b/t)\sqrt{f_y/E}$	1.12	Untreated: 1.50 Galvanized: 1.70	Untreated: 1.95 Galvanized: 2.25
Webs of RHS	$(h/t)\sqrt{f_y/E}$	2.42	Untreated: 3.80 Galvanized: 4.20	4.80

For <u>untreated</u> direct-formed regular- and high-strength RHS, the nominal flexural strength (M_n) shall be the lowest value calculated by Eqs. 5.9-5.11 and 5.13.

Limit state #1: Yielding (plastic moment)

$$M_n = M_p \tag{5.9}$$

Limit state #2: Flange local buckling

For RHS with noncompact flanges:

$$M_n = M_p - (M_p - M_y).\left[1.20(b/t)\sqrt{f_y/E} - 1.35\right] \leq M_p \tag{5.10}$$

For RHS with slender flanges:

$$M_n = f_y S_e \tag{5.11}$$

The effective section modulus can be determined with the effective width, b_e, of the compression flange taken as:

$$b_e = \begin{cases} b & \text{when } (b/t)\sqrt{f_y/E} \le 1.95 \\ 2.69t\sqrt{E/f_y}\left(1 - \dfrac{0.54\sqrt{E/f_y}}{b/t}\right) & \text{when } (b/t)\sqrt{f_y/E} > 1.95 \end{cases} \tag{5.12}$$

Limit state #3: Web local buckling

For RHS with noncompact webs:

$$M_n = M_p - (M_p - M_y).\left[0.42(h/t)\sqrt{f_y/E}\ - 1.017\right] \le M_p \tag{5.13}$$

For <u>galvanized</u> direct-formed regular- and high-strength RHS, the nominal flexural strength (M_n) shall be the lowest value calculated by Eqs. 5.14-5.16 and 5.18.

Limit state #1: Yielding (plastic moment)

$$M_n = M_p \tag{5.14}$$

Limit state #2: Flange local buckling

For RHS with noncompact flanges:

$$M_n = M_p - (M_p - M_y).\left[0.885(b/t)\sqrt{f_y/E}\ - 0.991\right] \le M_p \tag{5.15}$$

For RHS with slender flanges:

$$M_n = f_y S_e \tag{5.16}$$

The effective section modulus can be determined with the effective width, b_e, of the compression flange taken as:

$$b_e = \begin{cases} b & \text{when } (b/t)\sqrt{f_y/E} \le 2.25 \\ 3.11t\sqrt{E/f_y}\left(1 - \dfrac{0.62\sqrt{E/f_y}}{b/t}\right) & \text{when } (b/t)\sqrt{f_y/E} > 2.25 \end{cases} \tag{5.17}$$

Limit state #3: Web local buckling

For RHS with noncompact webs:

$$M_n = M_p - (M_p - M_y).\left[0.42(h/t)\sqrt{f_y/E}\ - 1.017\right] \le M_p \tag{5.18}$$

For direct-formed RHS (untreated and galvanized) over entire ranges of practical cross-sectional dimensions, the predicted nominal flexural strengths (M_n) calculated using Eqs. 5.9-5.18 are compared to the combined experimental and FE results in Figs. 5.16a and 5.16b. As shown, good agreement is achieved. Reliability analyses are performed in Section 5.6.2 to examine whether sufficient safety indices (or safety margins) are achieved.

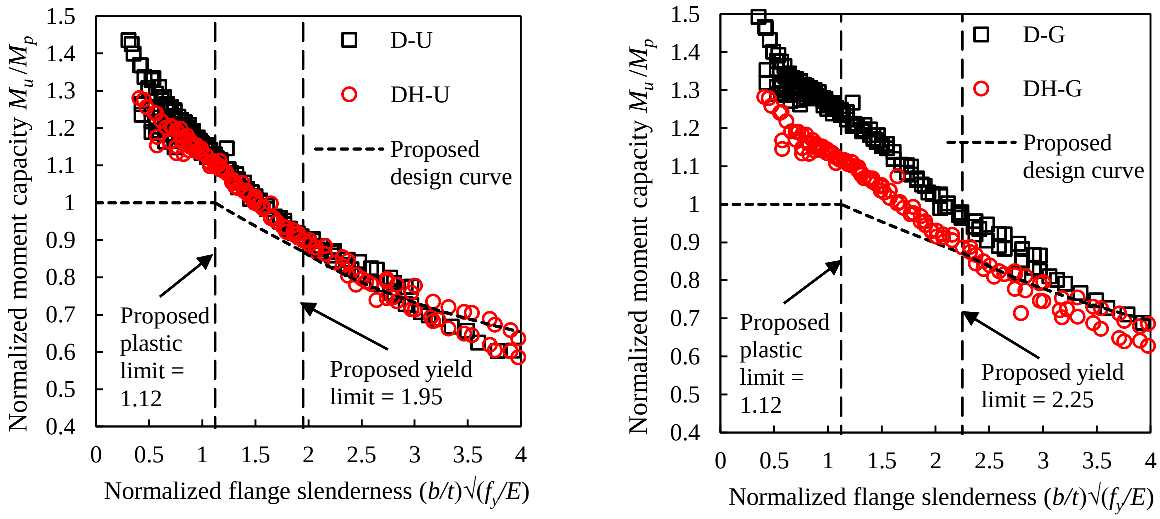

(a) Untreated RHS

(b) Galvanized RHS

Figure 5.16 Comparisons of experimental and FE results with nominal flexural strengths calculated using proposed formulae (Eqs. 5.19-5.18)

5.6.2 Reliability analysis

Reliability analyses are performed in this section to assess, for both untreated and galvanized direct-formed RHS, whether the proposed design recommendations (Table 5.6 and Eqs. 5.9-5.18) provide adequate or excessive safety margins. For flexural design, AISC 360-16 adopts a resistance factor (ϕ) of 0.9. The following reliability analyses use a target reliability index of 2.6 recommended by AISC 360-16, and a load combination of 1.2DL + 1.6LL and a LL-over-DL-ratio of three, where LL = live load and DL = dead load. The recommended formula in Commentary Chapter B of AISC 360-16 (reproduced as Eq. 3.10) is used to calculate the reliability index (β), using the parameters listed in Table 5.7. All parameters are calculated using the experimental and FE data following the AISC 360-16 recommendations [29].

Table 5.7 Reliability analysis of the modified design approaches based on ANSI/AISC 360-16

	Untreated RHS			Galvanized RHS		
Parameters	Noncompact	Slender	Compact + noncompact + slender	Noncompact	Slender	Compact + noncompact + slender
C_ϕ	1.49	1.49	1.49	1.49	1.49	1.49
M_m	1.07	1.07	1.07	1.07	1.07	1.07
F_m	1.03	1.03	1.03	1.03	1.03	1.03
P_m	1.07	0.99	1.09	1.13	1.00	1.14
V_M	0.087	0.087	0.087	0.087	0.087	0.087
V_F	0.030	0.030	0.030	0.030	0.030	0.030
V_P	0.047	0.056	0.094	0.072	0.063	0.111
V_Q	0.187	0.187	0.187	0.187	0.187	0.187
ϕ	0.9	0.9	0.9	0.9	0.9	0.9
β	3.15	2.77	3.03	3.29	2.77	3.14

As shown in Table 5.7, for $\phi = 0.9$, the reliability index calculations for untreated direct-formed RHS produce $\beta = 3.15$ and 2.77 for noncompact and slender compact sections, respectively. When considering all untreated RHS (i.e., compact + noncompact + slender), $\beta = 3.15$. All β-values are greater than the target reliability index of 2.6 recommended by AISC 360-16 [29]. Similarly, for galvanized direct-formed RHS, $\beta = 3.29$, 2.77 and 3.14 > 2.6 for the same three cases. Therefore, the proposed design recommendations (Table 5.6 and Eqs. 5.9-5.18) provide adequate safety margins for direct-formed regular- and high-strength RHS (untreated and galvanized).

5.7 Conclusions

The existing flexural design provisions in the current North American steel design standards (AISC 360-16 [29] and CSA S16-19 [12]) do not differentiate RHS members cold-formed by different approaches. The effect of post-production hot-dip galvanizing (similar to a post-production heat treatment) is not considered either. In this paper, the experimental results of 22 previous full-scale beam tests from [68] are used to validate the non-linear finite element (FE) modelling approach. A subsequent FE parametric study including 708 models is performed to study the effects of different cold-forming and post-production processes on member flexural behaviours. The existing flexural design provisions are proven excessively conservative for direct-formed regular- and high-strength RHS (untreated and galvanized) due to the inherently low levels of residual stresses. Therefore, modified slenderness limits and flexural design formulae are proposed using the combined experimental and FE data. The proposed design recommendations are proven to provide adequate safety margins based on reliability analyses.

Nomenclatures

B	External width
b	Internal flange width excluding corner portions
b_e	Effective internal flange width
c_1, c_2	Imperfection adjustment factors based on ANSI/AISC 360
C_1	Material coefficient
$C_{\square}$	Calibration coefficient for reliability analysis
E	Young's modulus
$E_{0.2}$	Tangent modulus of steel material at 0.2% proof stress
E_{sh}	Initial slope of strain hardening
F_m	Mean of fabrication factor for reliability analysis
f_u	Ultimate stress
f_y	Yield stress or 0.2% proof stress
H	External depth
h	Internal web depth excluding corner portions
M_{FE}	Flexural strength from finite element analysis
M_m	Mean value of material factor for reliability analysis
M_n	Nominal flexural strength
M_p	Plastic moment
M_{test}	Flexural strength from experimental testing
M_u	Flexural strength (ultimate moment)
M_y	Yield moment
m	Second strain hardening exponent
n	First strain hardening exponent
P_m	Mean of test/FE-to-nominal flexural strength ratios for reliability analysis
R	Rotation capacity
t	Wall thickness
V_F	Coefficient of variation of fabrication factor for reliability analysis
V_M	Coefficient of variation of material factor for reliability analysis
V_P	Coefficient of variation of test/FE-to-nominal flexural strength ratios for reliability analysis
V_Q	Coefficient of variation of load effect for reliability analysis
S	Elastic section modulus
Z	Plastic section modulus

β	Reliability index
$\varepsilon_{0.2}$	Strain at 0.2% proof stress
ε_{sh}	Strain at onset of strain hardening
ε_{u}	Strain at ultimate stress
ε_{y}	Strain at yield stress
κ	Curvature of moment span
κ_{l}	Curvature at plastic moment during unloading (i.e., onset of local buckling)
κ_{p}	Elastic curvature corresponding to plastic moment
λ_{C1}	Class 1 slenderness limit from CSA S16
λ_{C2}	Class 2 slenderness limit from CSA S16
λ_{C3}	Class 3 slenderness limit from CSA S16
λ_{p}	Compact/noncompact slenderness limit from ANSI/AISC 360
λ_{r}	Noncompact/slender slenderness limit from ANSI/AISC 360
$\sigma_{0.05}$	0.05% proof stress of material
ϕ	Resistance factor

Chapter 6: Future Work

This research presents a first step towards: (1) understanding the structural and architectural advantages of direct-formed RHS; and (2) quantifying the changes of residual stress properties and structural behaviours of cold-formed steels as a result of post-production hot-dip galvanizing. Future research can be performed on the following topics:

(i) Direct-formed regular- and high-strength RHS under combined compression and bending at cross-section level

(ii) Design of direct-formed regular- and high-strength RHS beam columns

(iii) Design of statically indeterminate direct-formed regular- and high-strength RHS continuous beams

(iv) Behaviour and design of connections made of direct-formed high-strength RHS

(v) Effect of post-production galvanizing on the above

References

[1] J.A. Packer, S.P. Chiew, R. Tremblay, G. Martinez-Saucedo, Effect of material properties on hollow section performance, Proc. Inst. Civ. Eng. - Struct. Build. 163 (2010) 375–390.

[2] M. Sun, J.A. Packer, Hot-dip galvanizing of cold-formed steel hollow sections: a state-of-the-art review, Front. Struct. Civ. Eng. 13 (2019) 49–65.

[3] M. Sun, Z. Ma, Effects of heat-treatment and hot-dip galvanizing on mechanical properties of RHS, J. Constr. Steel Res. 153 (2019) 603–617.

[4] G. Shi, X. Jiang, W. Zhou, Y. Zhang, Experimental study on overall buckling behavior of Q420 high strength welded galvanized tubes under axial compression, J. Harbin Inst. Technol. 45 (2013) 75–80.

[5] G. Shi, X. Jiang, W. Zhou, T.-M. Chan, Y. Zhang, Experimental investigation and modeling on residual stress of welded steel circular tubes, Int. J. Steel Struct. 13 (2013) 495–508.

[6] K. Tayyebi, M. Sun, Stub column behaviour of heat-treated and galvanized RHS manufactured by different methods, J. Constr. Steel Res. 166 (2020) 105910.

[7] ASTM, Standard Specification for Cold-Formed Welded Carbon Steel Hollow Structural Sections (HSS), ASTM A1085/A1085M-15, American Society for Testing and Materials, West Conshohocken, PA, USA, 2015.

[8] CSA, General requirements for rolled or welded structural quality steel / Structural quality steel, CSA G40.20-13/G40.21-13, Canadian Standards Association, Toronto, Canada, 2013.

[9] M.A. Serrano-López, C. López-Colina, J.J. Del Coz-Díaz, F.L. Gayarre, Static behavior of compressed braces in RHS K-joints of hot-dip galvanized trusses, J. Constr. Steel Res. 89 (2013) 307–316.

[10] S. Daneshvar, M. Sun, K. Karimi, Galvanized RHS X-Connections. I: Effects of vent and drain holes on SCFs, J. Constr. Steel Res. 167 (2020) 105854.

[11] S. Daneshvar, M. Sun, Stress concentration factors of RHS T-connections with galvanizing holes under in-plane bending, J. Constr. Steel Res. 169 (2020) 106039.

[12] CSA, Limit States Design in Structural Steel, CSA S16-19, Canadian Standard association, Toronto, ON, Canada, 2019.

[13] M. Sun, J.A. Packer, Charpy V-notch impact toughness of cold-formed rectangular hollow sections, J. Constr. Steel Res. 97 (2014) 114–126.

[14] ASTM, Standard practice for safeguarding against embrittlement of hot-dip galvanized structural steel products and procedure for detecting embrittlement, ASTM A143/A143M-07, American Society for Testing and Materials, West Conshohocken, PA, USA, 2014.

[15] S.H. Li, G. Zeng, Y.F. Ma, Y.J. Guo, X.M. Lai, Residual stresses in roll-formed square hollow sections, Thin-Walled Struct. 47 (2009) 505–513.

[16] L. Tong, G. Hou, Y. Chen, F. Zhou, K. Shen, A. Yang, Experimental investigation on longitudinal residual stresses for cold-formed thick-walled square hollow sections, J. Constr. Steel Res. 73 (2012) 105–116.

[17] J.L. Ma, T.M. Chan, B. Young, Experimental investigation of cold-formed high strength steel tubular beams, Eng. Struct. 126 (2016) 200–209.

[18] T.M. Chan, X.L. Zhao, B. Young, Cross-section classification for cold-formed and built-up high strength carbon and stainless steel tubes under compression, J. Constr. Steel Res. 106 (2015) 289–

295.

[19] J.L. Ma, T.M. Chan, B. Young, Design of cold-formed high strength steel tubular beams, Eng. Struct. 151 (2017) 432–443.

[20] J.L. Ma, T.M. Chan, B. Young, Design of Cold-Formed High-Strength Steel Tubular Stub Columns, J. Struct. Eng. 144 (2018) 04018063.

[21] X. Lan, J. Chen, T.M. Chan, B. Young, The continuous strength method for the design of high strength steel tubular sections in compression, Eng. Struct. 162 (2018) 177–187.

[22] X. Lan, J. Chen, T.M. Chan, B. Young, The continuous strength method for the design of high strength steel tubular sections in bending, J. Constr. Steel Res. 160 (2019) 499–509.

[23] L. Gardner, N. Saari, F. Wang, Comparative experimental study of hot-rolled and cold-formed rectangular hollow sections, Thin-Walled Struct. 48 (2010) 495–507.

[24] M. Sun, J.A. Packer, Direct-formed and continuous-formed rectangular hollow sections — Comparison of static properties, J. Constr. Steel Res. 92 (2014) 67–78.

[25] ASTM, Standard Specification for Cold-Formed Welded High Strength Carbon Steel or High-Strength Low-Alloy Steel Hollow Structural Sections (HSS) in Rounds and Shapes, ASTM A1112/A1112M - 18, American Society for Testing and Materials, West Conshohocken, PA, USA, 2018.

[26] ASTM, Tension Testing of Metallic Materials, ASTM E8/E8M-16a, American Society for Testing and Materials, West Conshohocken, PA, USA, 2016.

[27] CEN, Eurocode 3—design of steel structures—Part 1-1: General rules and rules for buildings, BS EN-1993-1-1, British Standards Institution, London, UK, 2005.

[28] CEN, Eurocode 3—design of steel structures—Part 1-12: Additional rules for the extension of EN 1993 up to steel grades S 700, BS EN-1993-1-1, British Standards Institution, London, UK, 2007.

[29] ANSI/AISC, Specification for structural steel buildings, ANSI/AISC 360-16, American Institute of Steel Construction, Chicago-Illinois, Chicago, IL, USA, 2016.

[30] ASTM, Standard Specification for Cold-Formed Welded and Seamless Carbon Steel Structural Tubing in Rounds and Shapes, ASTM A500/A500M - 13, American Society for Testing and Materials, West Conshohocken, PA, USA, 2013.

[31] R.D. Ziemian, Guide to stability design criteria for metal structures, John Wiley & Sons, Hoboken, USA, 2010.

[32] Y.B. Wang, G.Q. Li, S.W. Chen, The assessment of residual stresses in welded high strength steel box sections, J. Constr. Steel Res. 76 (2012) 93–99.

[33] H.X. Yuan, Y.Q. Wang, Y.J. Shi, L. Gardner, Residual stress distributions in welded stainless steel sections, Thin-Walled Struct. 79 (2014) 38–51.

[34] G.W. Li, Y.Q. Li, J. Xu, X. Cao, Experimental investigation on the longitudinal residual stress of cold-formed thick-walled SHS and RHS steel tubes, Thin-Walled Struct. 138 (2019) 473–484.

[35] R.B. Cruise, L. Gardner, Residual stress analysis of structural stainless steel sections, J. Constr. Steel Res. (2008).

[36] J.L. Ma, T.M. Chan, B. Young, Material properties and residual stresses of cold-formed high strength steel hollow sections, J. Constr. Steel Res. 109 (2015) 152–165.

[37] B. Somodi, B. Kövesdi, Residual stress measurements on cold-formed HSS hollow section columns, J. Constr. Steel Res. 128 (2017) 706–720.

[38] AGA, Hot-dip galvanizing for corrosion protection: A specifier's guide, American Galvanizers Association Centennial, CO, USA, 2017.

[39] M. Sun, J.A. Packer, High strain rate behaviour of cold-formed rectangular hollow sections, Eng. Struct. 62–63 (2014) 181–192.

[40] X.-L. Zhao, A. Heidarpour, L. Gardner, Recent developments in high-strength and stainless steel tubular members and connections, Steel Constr. 7 (2014) 65–72.

[41] J.L. Ma, T.M. Chan, B. Young, Experimental Investigation on Stub-Column Behavior of Cold-Formed High-Strength Steel Tubular Sections, J. Struct. Eng. 142 (2016) 04015174.

[42] J. Wang, S. Afshan, N. Schillo, M. Theofanous, M. Feldmann, L. Gardner, Material properties and compressive local buckling response of high strength steel square and rectangular hollow sections, Eng. Struct. 130 (2017) 297–315.

[43] B. Somodi, B. Kövesdi, Flexural buckling resistance of cold-formed HSS hollow section members, J. Constr. Steel Res. 128 (2017) 179–192.

[44] K. Tayyebi, M. Sun, Design of direct-formed square and rectangular hollow section stub columns, J. Constr. Steel Res. 178 (2021) 106499.

[45] Y. Huang, B. Young, The art of coupon tests, J. Constr. Steel Res. 96 (2014) 159–175.

[46] W.M. Quach, B. Young, Material Properties of Cold-Formed and Hot-Finished Elliptical Hollow Sections, Adv. Struct. Eng. 18 (2015) 1101–1114.

[47] B.. B. Schafer, T. Peköz, Computational modeling of cold-formed steel: characterizing geometric imperfections and residual stresses, J. Constr. Steel Res. 47 (1998) 193–210.

[48] E. Ellobody, B. Young, Structural performance of cold-formed high strength stainless steel columns, J. Constr. Steel Res. 61 (2005) 1631–1649.

[49] L. Gardner, D.A. Nethercot, Numerical Modeling of Stainless Steel Structural Components—A Consistent Approach, J. Struct. Eng. 130 (2004) 1586–1601.

[50] R.G. Dawson, A.C. Walker, Post-buckling of geometrically imperfect plates, J. Struct. Div. 98 (1972) 75–94.

[51] J. Roorda, K.R. Venkataramaiah, Analysis of Local Plate Buckling Experimental Data, in: 6th Int. Spec. Conf. Cold-Formed Steel Struct., St. Louis, Missouri, 1982.

[52] AISI, North American Specification for the Design of Cold-Formed Steel Structural Members, AISI S100-16, American Iron and Steel Institute, Washington, DC, 2016.

[53] S.P. Timoshenko, J.M. Gere, Theory of elastic stability, 2. ed., McGraw-Hill, Auckland, 1963.

[54] G. Winter, Commentary on the 1968 Edition of the Specification for the Design of Cold-formed Steel Structural Members, AISI-Specifications Des. Cold-Formed Steel Struct. Members. (1970).

[55] K. Tayyebi, M. Sun, K. Karimi, Residual stresses of heat-treated and hot-dip galvanized RHS cold-formed by different methods, J. Constr. Steel Res. 169 (2020) 106071.

[56] ABAQUS, Dassault Systèmes, ABAQUS Version 6.14 [Computer software], (2014).

[57] X. Yun, L. Gardner, Stress-strain curves for hot-rolled steels, J. Constr. Steel Res. 133 (2017) 36–46.

[58] L. Gardner, X. Yun, Description of stress-strain curves for cold-formed steels, Constr. Build. Mater. 189 (2018) 527–538.

[59] M. Ashraf, L. Gardner, D.A. Nethercot, Finite element modelling of structural stainless steel cross-sections, Thin-Walled Struct. 44 (2006) 1048–1062.

[60] T.G. Singh, K.D. Singh, Structural performance of YSt–310 cold–formed tubular steel stub columns, Thin-Walled Struct. 121 (2017) 25–40.

[61] X. Meng, L. Gardner, Testing of hot-finished high strength steel SHS and RHS under combined compression and bending, Thin-Walled Struct. 148 (2020) 106262.

[62] B.W. Schafer, Review: The Direct Strength Method of cold-formed steel member design, J. Constr. Steel Res. 64 (2008) 766–778.

[63] B.W. Schafer, S. Ádány, Buckling analysis of cold-formed steel members using CUFSM: conventional and constrained finite strip methods, in: Eighteenth Int. Spec. Conf. Cold-Formed Steel Struct. Orlando, FL, Citeseer, 2006.

[64] T. Wilkinson, G.J. Hancock, Tests to examine compact web slenderness of cold-formed RHS, J. Struct. Eng. 124 (1998) 1166–1174.

[65] X. Zhao, G.J. Hancock, Square and Rectangular Hollow Sections Subject to Combined Actions, J. Struct. Eng. 118 (1992) 648–667.

[66] J. Wang, S. Afshan, M. Gkantou, M. Theofanous, C. Baniotopoulos, L. Gardner, Flexural behaviour of hot-finished high strength steel square and rectangular hollow sections, J. Constr. Steel Res. 121 (2016) 97–109.

[67] J.A. Yura, M.K. Ravindra, T. V Galambos, The bending resistance of steel beams, J. Struct. Div. 104 (1978) 1355–1370.

[68] K. Tayyebi, M. Sun, K. Karimi, R. Daxon, B. Rossi, Experimental investigation of direct-formed square and rectangular hollow section beams, J. Constr. Steel Res. (2021) (in preparation).

[69] H.-T. Li, B. Young, Cold-Formed High-Strength Steel Tubular Structural Members under Combined Bending and Bearing, J. Struct. Eng. 145 (2019) 04019081.